
REACTION AND SEPARATION OPPORTUNITIES WITH MICROFLUIDIC DEVICES
Ruben C. Kolfschoten

REACTION AND SEPARATION OPPORTUNITIES WITH MICROFLUIDIC DEVICES

RUBEN C. KOLFSCHOTEN

Thesis committee

Thesis supervisor

Prof. dr. ir. R.M. Boom

Professor of Food Process Engineering

Wageningen University

Thesis co-supervisor

Dr. ir. A.E.M. Janssen

Assistant professor, Food Process Engineering Group

Wageningen University

Other members

Prof. dr. ir. A.B. de Haan, Eindhoven University of Technology

Prof. dr. J.G.E. Gardeniers, University of Twente

Prof. dr. J.T. Zuilhof, Wageningen University

Dr. ir. P.J.T. Bussmann, TNO, Zeist

This research was conducted under the auspices of the Graduate School of Food Technology, Agrobiotechnology, Nutrition, and Health Sciences (VLAG).

REACTION AND SEPARATION OPPORTUNITIES WITH MICROFLUIDIC DEVICES

RUBEN C. KOLFSCHOTEN

Thesis

submitted in fulfillment of the requirements for the degree of doctor
at Wageningen University
by the authority of the Rector Magnificus
Prof. dr. M.J. Kropff,
in the presence of the
Thesis Committee appointed by the Academic Board
to be defended in public
on Friday 25 February 2011
at 4 p.m. in the Aula.

Ruben C. Kolfschoten

Reaction and separation opportunities with microfluidic devices,
168 pages.

Thesis, Wageningen University, Wageningen, NL (2011)
With references, with summaries in Dutch and English

ISBN 978-90-8585-864-5

TABLE OF CONTENTS

1

INTRODUCTION

This thesis research was carried out within the Dutch research initiative "Process on a Chip" (PoaC), part of the framework Advanced Chemical Technologies for Sustainability (ACTS). ACTS is a public private partnership between Dutch government, universities, research institutes, and industry in the field of sustainable chemical technologies. The PoaC program aims to support fundamental and applied research in which new microtechnological concepts are developed for the initiation of novel production processes that exploit these benefits.

The PoaC projects "Massive Parallelization of Multi-Chamber Reaction and Separation Microreactors" and "Precise Control of Selectivity in Multi-Route Enzyme Systems" were combined in August 2004. This thesis research involves the extension of the first project.

1.1 MICROFLUIDICS

In our daily lives, we may come into contact with several microfluidic devices (Figure 1.1). An inkjet printer prints a photograph by propelling variably sized droplets of liquid material (ink) onto a page. A portable analyzer for a diabetic determines blood glucose levels by contacting with a droplet of blood. An electric motor powers a hydrogen car by reacting hydrogen with oxygen in a fuel cell. All these apparatus have at least one thing in common: they contain microfluidic devices.

Figure 1.1 Illustrations of microfluidic devices: ink-cartridges (left), portable blood sugar monitor (center), and hydrogen fuel cell (right).

Microfluidic devices contain one or more channels with characteristic dimensions at the scale of a human hair, and typical volumes in the sub-microliter scale. The substances flowing through such microchannels appear as gases, liquids and solids – and combinations thereof. Microfluidics is defined as the science and technology of systems that process or manipulate sub-microliter amounts of such substances in microchannels (Whitesides 2006).

1.1.1 A SHORT HISTORY OF MICROFLUIDICS

References to microfluidic devices have appeared as early as the 1940s (Long 1949). Even inkjet printing, perhaps the most matured microfluidic technology, was already invented in 1968 (Sweet and Cumming). However, extensive

exploitation of microfluidics had to wait for what Reyes et al. (2002) called the "microfluidic renaissance" in the 1990s, when Manz et al. (1990) proposed the concept of miniaturized total analysis systems (μTAS). These systems are an integration of many components, such as fluid control elements, sensors, reactors, mixers, and separators. The first applications of these microfluidic devices were in the field of analytical chemistry, and much of the research on microfluidics initially focused on small-scale reactions. After a decade of innovation, Ehrfeld et al. (2000) called microtechnology the new technology for modern chemistry. Nowadays, due to the continuous development of μTAS or "labs-on-a-chip", many microfluidic platforms are available that enable the miniaturization, integration, and automation of a large variety of biochemical assays (Haeberle and Zengerle 2007).

Microfluidics has also advanced to many other fields, including process intensification. Hessel and Löwe (2003a; 2003b) analyzed possible plant concepts for microreactors and reviewed whether these constituted a sensible option. One of the reasons for the interest in microfluidics is the need for alternatives to traditional large vessel batch processing. This conventional approach to large scale production has many inherent disadvantages, including long production cycle times, production of unwanted byproducts, inefficient use of energy and material resources, safety hazards due to the large volumes, and complex up-scaling to higher production volumes. Many of these issues may be solved by using microfluidic devices that also enable continuous production (Hartman and Jensen 2009; Stitt 2002).

1.1.2 MICROFABRICATION

Several microfabrication technologies have made the development of microfluidic devices possible. The semi-conductor industry developed some of these technologies, such as photolithography and etching, and consequently facilitated spectacular advances. Some of the earliest fabrications of microfluidic devices were closely related to the field of micro electro mechanical systems (MEMS), and

were therefore constructed of silicon and glass (Harrison et al. 1993). The main microreactor supplier in the Netherlands – Micronit Microfluidics – fabricates microfluidic devices from mainly these materials.

Soft lithographic fabrication methods, such as micromolding and microcontact printing, have appeared as a possible replacement of some of the silicon and glass materials by organic polymers such as polydimethylsiloxane (PDMS) and polycarbonate (PC) (Xia and Whitesides 1998). These polymers provide many favorable characteristics with regard to the permeability, rigidity, costs, and ease of fabrication (Duffy et al. 1998; Whitesides and Stroock 2001). Polymers may also enable feasible production of low cost, disposable microfluidic devices – which for example are useful for in-the-field diagnostics.

Another fabrication method involves high precision microstructuring in polymers, metals, and ceramics. These materials are selected for properties including chemical compatibility and physical robustness that may be desired for industrial applications (Friedrich and Vasile 1996; Knitter and Liauw 2004; Liu et al. 2005; Xiang et al. 1999). Mechanical structuring generally implies the use of larger microchannel diameters, which consequently results in reduced surface to volume ratios and increased diffusion times. However, for industrial purposes, relatively larger microchannels are frequently desired for reduced pressure drops and higher throughput.

A large range of technologies is available to further enhance the microstructures in microfluidic devices. Such enhancements can include integration of electrodes, surface modification, and particle packing. The broad availability of fabrication methods and materials enables tailor made fabrication of many microfluidic devices.

1.1.3 ENZYMES IN MICROFLUIDIC DEVICES

In the 1990s, enzymes in microfluidic devices kept a proverbial low profile. The first comprehensive book on microreactors did not even include examples of enzymatic microreactors (Ehrfeld et al. 2000). Initially, microfluidic devices with enzymes were predominantly used for enzyme assays. For example, Hadd et al. (1997) assayed the enzyme β-galactosidase in a microreactor and reported four orders of magnitude reduction of reagent consumption. Furthermore, Zhao et al. (1998) reported enhanced enzymatic reactivity at lower analyte concentrations with a microreactor using capillary electrophoresis. Moreover, Cohen et al. (1999) reported a prototype assay of an enzymatic reaction with in-situ separation in a microreactor and demonstrated its usefulness for high-throughput screening of chemical libraries against enzymes of interest. In these and later references (Guijt-van Duijn et al. 2003), the many possibilities of future automation, rapid assessment, and highly parallel assays were imagined or suggested.

Microfluidic applications that focus on organic synthesis and analysis have also used enzymes. For instance, Watts et al. (2001) reported the first application of multi-step synthesis within a microreactor. Tanaka et al. (2001) reported another application with the goal of an acceleration of an enzymatic reaction with horseradish peroxidase in a microreactor. Furthermore, Lee et al. (2003) reported more complex microfluidic structures with multi-enzyme or cascaded enzyme reactions. Besides advances in assays and biocatalytic processes, microfluidics has also strongly fueled the field of protein and nucleic acid analysis, which extends to nanotechnology (Salieb-Beugelaar et al. 2009; Urban et al. 2006).

1.1.4 WHY MICROFLUIDIC DEVICES?

The strong claims with regard to microfluidics stem from several advantageous characteristics of this technology. One such advantage is that physical phenomena – such as viscous forces – become dominant on microscale (Purcell 1976). In contrast to macro-scale technology, flows in microfluidic devices generally have

low Reynolds numbers as a result of these viscous forces dominating inertial forces. The resulting laminar flow is therefore predictable and controllable.

The surface to volume ratio is inversely proportional to the channel diameter, which can be advantageous in surface-related processes. Due to the small sizes, the distance over which transfer of mass and heat takes place is small. As a result, the driving forces involved are high. Microfluidic devices therefore also yield faster heat and mass transfer. Another advantage is that up-scaling of these microfluidic devices can be achieved by simply connecting multiple microreactors in parallel. In general, such up-scaling does not affect the characteristics of the microreactor.

Miniaturization also has many other inherent advantages, such as safety and low reagent consumption due to small volumes. Microreactors enable the continuous on-site and on-demand processing of possibly toxic chemicals. Integration of reaction with downstream processing in microfluidic devices is expected to further reduce processing volumes. The small volumes and fast heat transfer reduce the risk of thermal runaways, for example. In addition, the reduced need for storage of large volumes of these chemicals imply that only small amounts of chemicals and energy are released in case of failure. Furthermore, scarce and/or environmentally hazardous reagents for analytical purposes are only needed in small volumes.

Microfluidics clearly offers many advantages, Whitesides (2006) wrote that it seems almost too good to be true. However, one of the most crucial disadvantages of miniaturization is that the reduced dimensions cause a considerable increase in pressure drop (Chovan and Guttman 2002), which is inversely proportional to the fourth power of the channel diameter. Another issue is up-scaling. While up-scaling of individual microreactors may appear simple, many challenges remain due to manufacturing tolerances and channel blockages that may affect the flow distribution and therefore complicate reliable up-scaling (Amador et al. 2004). For microreactors to be used in chemical production, they must also be integrated with sensors and actuators (Thorsen et al. 2002). As a result, a growing number of reactors becomes increasingly complex in the areas of reactor monitoring and

control (Jensen 2001). In addition, the volume of the supporting matrix is commonly much larger than the volume of the microstructures. Hence, the complete system, including macro-fluidic connections, can grow much too large in volume and material usage.

1.1.5 GUIDELINES FOR DESIGN OF MICROFLUIDIC DEVICES

Microfluidic devices have grown more complex over the years. As physical phenomena manifest in different degrees in the miniaturized world, existing design rules for macro-scale devices may not be applicable to their microfluidic alternatives. Because of this, and the large variety of these devices, engineers lack many tools to estimate the performance of microfluidic devices. A relatively small amount of researchers has nevertheless come up with methodologies for parameter estimation and optimal design of some microfluidic devices.

Most microfluidic devices commonly use the coflow configuration to contact fluid flows. This common way of contacting fluid flows has fueled interests in methodologies for parameter estimation and optimal design of coflow microreactors. Holl et al. (1996) used such a coflow configuration in a method for optimal design of diffusion-based extraction. The development of such methods has been continued by many researchers such as Kamholz et al. (1999), Stepánek et al. (1999), and Ismagilov et al. (2000). In the field of biocatalysis, correlations and design guidelines have been established that concern the initial enzyme activity. For example, Ristenpart et al. (2008) have established scaling relations for Michaelis-Menten reactions to estimate the initial concentration of product as a function of the distance along the microchannel.

In brief, microfluidics has advanced from the field of analytical chemistry to the fields of chemical engineering, combinatorial chemistry, and biotechnology. However, many opportunities have yet to be discovered, as there are virtually endless possibilities for the use of materials, the integration of reaction steps, and the application of microfluidic devices. In particular, researchers have abundantly

studied microfluidics for analytical and sensory applications. In contrast, microfluidics for preparative processes – e.g. fractionation and production, and integration thereof – is still in its infancy.

1.2 RESEARCH AIM

In the literature review of our introduction, we concluded that, although microfluidics has advanced to many fields, it lacks similar developments in the field of process engineering. The purpose of this thesis is filling parts of that gap between high-tech microfluidics for analytical purposes, and conventional large-scale process engineering. This thesis will therefore focus on enzymatic reactions and downstream processes on microscale. In this thesis, we will describe parallelization of microfluidic channels and separation of components by diffusive processes. Furthermore, we present the effect of diffusion on enzymatic production in microreactors. Lastly, we will provide and discuss design guidelines for such microreactors. This research may lead to a better understanding of preparative processes on microscale. As a result, it will enable researchers to better develop process intensifications by means of microfluidic devices.

1.3 THESIS OUTLINE

This thesis covers four core subjects: parallelization, separation, enzymatic reactions, and microreactor design. These subjects will be discussed in Chapter 2 to 6, with a general discussion in Chapter 7.

In Chapter 2, we present a multilayer microfluidic device that enables the simultaneous performance of distinct experiments. The concept for this parallelization is the decoupling of pressure drop from residence time. We demonstrate this by a microfluidic membrane separation from which the characteristic membrane permeability can be determined.

In Chapter 3, we present a novel separation process based on the concept of mass diffusion. Differences between diffusivities of the components drive this separation, while membranes, in particular nanofiltration membranes, can enhance such a separation. We demonstrate this by the use of a membrane microfluidic device for the separation of small molecular weight components.

In Chapter 4, we present a method for diffusion-based enrichment of components in liquid mixtures. We use membrane sieves to accomplish the diffusive process. These membranes are much thinner than conventional membranes – we can therefore reduce diffusion times. This chapter describes separation of sugars that have diffusivities with the same order of magnitude. We show that the presented concept can be useful for pre-concentration or downstream processes such as fractionation and enrichment.

In Chapter 5, we present a method to estimate and circumvent diffusion limitation effects in microfluidic devices. Enzyme based assays in microfluidic devices have stimulated research on the effect of diffusion limitation on enzyme activity in a microreactor. We show that initial reaction rate determination may significantly underestimate the maximum enzyme reaction rate.

In Chapter 6, we present a methodology that yields design spaces for the optimal design of coflow enzyme microreactors. Here, we consider the microfluidic device as a production system without resorting to the approximation of initial enzyme activity. This chapter provides an elaborated view on the effects of diffusion on the productivity, and addresses correlations and guidelines for this.

Chapter 7 concludes the thesis. It reflects upon the previous chapters and provides a broader perspective on the subjects discussed. In addition, this chapter extends some of the research presented in the previous chapters, and contains suggestions for future research.

2

HIGH-THROUGHPUT SEPARATION IN MICROCHANNELS

ABSTRACT

We present a multilayer microfluidic device to conduct distinct experiments simultaneously. The concept was based on the decoupling of pressure drop from residence time. The device was fabricated by micromilling in two polystyrene layers, which were stacked with a hydrophilic membrane between them. The milled structures in one layer were partially aligned to the milled structures in the other layer. This generated channels with multiple contacting regions, separated by the membrane. The length of the contacting region and the velocity of the liquid determined the contact time of a liquid flowing through the channel. The contact time distinguished the channels. We show that the device was useful for separation. As examples, we used the separation of hydrochloric acid and glucose visualized by pH-sensitive dyes or measured by HPLC respectively. The conducted experiments showed a good correlation between contact time and mass transport. First, visualization by pH-sensitive dyes of hydrochloric acid separation confirmed the differences in contact time for each separation region in the device. Second, analysis of HPLC measurements confirmed glucose separation for different contact times as well. Furthermore, the derived membrane permeability approximated the value found in literature, which suggested a quantitative proof of concept. With the reported device, we could perform separation experiments with a three times higher throughput compared to devices with a single separation region.

Parts of this chapter have been published as: Kolfschoten RC, Janssen AEM, Boom RM. 2009. High-throughput separation in a microfluidic device with multiple contacting regions. New Biotechnology 25(Supplement 1):S164-S164.

2.1 INTRODUCTION

Developments in microfluidics, lab-on-a-chip technology and the production of microscale devices are revolutionizing chemical and biochemical research (Ramsey 1999). Down scaling of reactor equipment to the sub millimeter level creates microreactors that have several advantages such as inherent safety and low reagent consumption due to the small volumes, faster heat and mass transfer due to the small dimensions, and up-scaling by parallelization (Jensen 2001; Losey et al. 2001). The possibility of integration with fluid control elements, sensors, and separators means that microreactors offer additional functionality. In combination with information technology, sophisticated microsystems can be created (van den Berg 1995).

The developments in microtechnology have resulted in well documented advantages for many chemical and biochemical reactions (Reyes et al. 2002). For example, acceleration of reaction (Tanaka et al. 2001), as well as successful in situ separation (Zhao and Gomez 1998) have both been reported using enzymes in microreactors. Due to the small sizes involved, no elaborate mixing or special thermal energy transfer strategies are required in microreactors because diffusion is often fast enough (Purcell 1976). This reduced complexity makes the integration of several unit operations such as reaction and separation more feasible.

The integration of reaction and separation processes can for example reduce product inhibition by continuously extracting the reaction product. This is desired in many applications in order to enhance selectivity and/or yields. Membranes incorporated in microfluidic devices offer such possibilities. For fabrication of membrane microreactors, many different approaches have been reported (de Jong et al. 2006) such as direct incorporation of (unsupported) membranes, membrane preparation as part of the chip fabrication process, in-situ preparation of membranes, and use of membrane properties of bulk chip material. Conventional membrane modules usually provide adequate control of the mass transport at the feed side, however mass transfer at the permeate side is often not well defined.

This is especially important in processes such as osmosis, dialysis, and electrodialysis. In a microfluidic device, both sides of a membrane can be subjected to similar conditions and still be effective. For example, a membrane can control diffusive addition and removal of components while avoiding (instantaneous) mixing of co-currently flowing product and substrate streams.

Scaling-up of microreactors is achieved by increasing their quantity while leaving their characteristics intact – a multiple of reactors is then connected in parallel. Commonly, this multiple of reactors consists of exactly the same reactors (Kikutani et al. 2002). However, such a multiple of reactors can also consist of different microreactors that are for example distinguished by separation capacity. As a result, such parallelized microreactors can be subjected to the same input conditions while yielding a different output. Hence, distinct experiments can be performed at the same time, and in the same device – yielding faster and more accurate acquisition of information. Certain analytical applications may benefit from this relatively unexplored concept, such as kinetic parameter estimations based on experimental data, which may require many experiments. Another application is the determination of membrane properties, which requires a multiple of experiments under different conditions.

In this article, we will describe a microfluidic device with three different microcontactors connected in parallel. The purpose is to explore the concept of parallelization of multiple different microreactors. We will describe several liquid-liquid separation experiments in such a device, and discuss its performance, advantages, and potential.

2.2 MATERIALS AND METHODS

2.2.1 MATERIALS

Bromocresol Green was obtained from Sigma-Aldrich (Milwaukee, USA), all other chemicals from Merck (Darmstadt, Germany). Demineralized water was obtained from a Millipore Milli-Q water system (Billerica, USA).

2.2.2 DEVICE FABRICATION

The device was fabricated in polymethylmethylacrylate (PMMA) and polystyrene (PS) layers (Vink Kunststoffen, Didam, the Netherlands). Hydrophilic UF cellulose membranes (Cuprophan, 15 µm thick when swollen) were supplied by ENKA Membrana AG (Arnhem, the Netherlands). The nuts, tubing and adapters were obtained from Upchurch Scientific (Westchester, USA) and the syringes from SGE (Austen, Australia).

Four structures of 45.0 cm length, 500±10 µm width and 100±10 µm depth were milled on one side of two 2.00 mm thick polystyrene layers of 15 × 15 cm (Figure 2.1a) using a computer controlled numerical control mill (MAHO MH 800 E with HOLEX cutter 20 1640 of 500 µm, Pfronten, Germany). Holes with a diameter of 1.5 mm were drilled through the layers to serve as inlet or outlet channel perpendicular to the channels in the device.

From the described approaches for integrating membranes into microreactors, we chose direct incorporation of the membrane by stacking layers (Mair et al. 2007). The polystyrene layers were stacked with a hydrophilic UF membrane between them (Figure 2.1b). The milled structures in a layer were partially aligned to the milled structures in the other layer. This generated channels with multiple contacting regions, separated by the membrane.

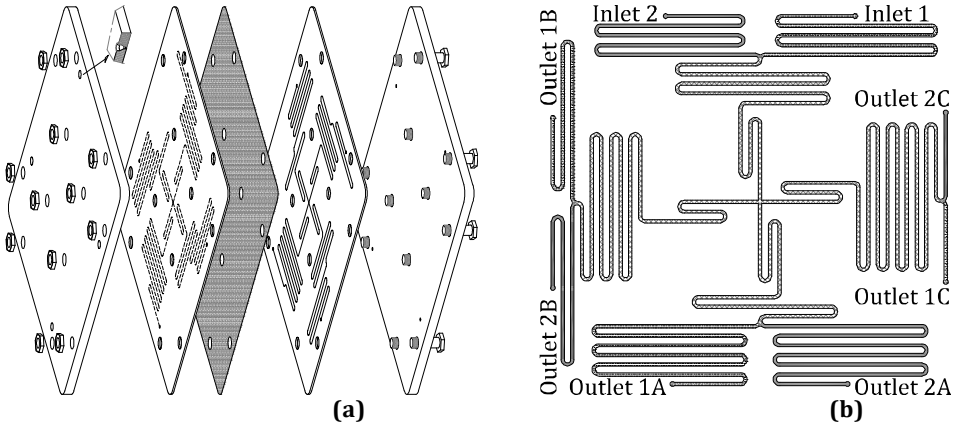

Figure 2.1 Drawing of the structures in the two polystyrene layers (a) and drawing of the overlaid layers (b). The dotted channels indicate contacting regions. The contacting region after Inlet 1 and 2 was shared by all three channels and had a length of 24.6 cm. The remaining contacting regions had a length of 15.8 cm (A), 33.4 cm (B), and 42.2 cm (C) respectively.

The length of the contacting region and the velocity of the liquid determined the contact time of a liquid flowing through the channel. In this device, three channels were used as outlets and one as inlet. All channels had an equal length – to ensure equal residence time and pressure drop in the channel – but a different contact time. Hence, the pressure drop and contact time were decoupled. Therefore, we could perform separation experiments with three different contact times simultaneously, and in one device.

The polystyrene layers were held in position by 16 screws, which went through the drilled screw holes in the two layers. The layers were clamped by two 1.0 cm thick polymethylmethylacrylate bottom and top layers respectively to seal the device. After sealing, the adapters labeled Inlet 1 and 2 were used to connect to a syringe pump (Harvard Apparatus Pump 33, Holliston, USA).

2.2.3 EXPERIMENTAL SETUP

In the conducted experiments, the color response of the pH-indicator and the concentration of glucose corresponded to this amount, which enabled us to

analyze quantitatively and qualitatively separations in the device. Demineralized water was degassed in a Branson 5210 sonification bath from the Branson Sonic Power Company (Danbury, USA) for 30 min at 30 °C. In all experiments, steady state was assumed after five times the residence time in the whole module and tubing volume at a constant flow rate.

2.2.3.1 SEPARATION OF HCL AND NAOH

Inlet 1 was connected to a syringe containing Bromocresol Green in HCl (1 mM) and water. Inlet 2 was connected to a syringe containing NaOH (1 mM) and water. Both inlets had equal flow rates. After steady state conditions were reached, photographs were taken with a digital camera (Sony DSC-S75) at set flow rates. The photographs were used for visual analysis of a color response by the pH-indicator.

2.2.3.2 SEPARATION OF GLUCOSE

Inlet 1 was connected to a syringe containing water. Inlet 2 was connected to a syringe containing a glucose solution (90 mM to 100 mM). Both inlets had equal flow rates. Samples from each channel were collected from their respective outlets. The high flow rate experiments (400 µl min^{-1}) were repeated twice, the others were repeated four times. The glucose measurement made a quantitative analysis possible. A diffusion model was derived for the setup and correlated to the measured values.

2.2.4 DIFFUSION MODEL

The experimental data was used for a proportional least squares fit of a first order diffusion model described by:

$$\frac{dc_P(L)}{dL} = \frac{dc_R(L)}{dL} = \frac{k_{ov} \cdot h}{\varphi} \cdot \left(c_R(L) - c_P(L)\right), \qquad \text{Equation 2.1}$$

where c_R and c_P are the concentrations (mol m^{-3}) of the retentate and permeate respectively, L the length (m) of the contacting region, h the height (m) of the

rectangular channel (equal at both sides), and φ the flow rate ($m^3\ s^{-1}$) at the contacting region, equal at retentate and permeate sides. It was assumed that the flow rate was constant, that the solution was dilute and that the transport of water through the membrane due to an osmotic pressure difference over the membrane could be neglected. From this model, the overall mass transfer coefficient for glucose k_{ov} ($m\ s^{-1}$) was determined. The mass transfer coefficients of the retentate (k_R), membrane, and permeate (k_P) respectively, contributed to this overall mass transfer coefficient as resistances in series by:

$$k_{ov} = \left(\frac{1}{k_R} + \frac{1}{k_m} + \frac{1}{k_P}\right)^{-1}, \qquad \text{Equation 2.2}$$

where k_m is the membrane permeability (Wesseling and Krishna 2000). The membrane was assumed to be the dominating limiting factor for the overall mass transfer.

2.2.5 ANALYSIS

The concentration of glucose in each channel was determined by isocratic HPLC (Thermo Separation Products, Hertz, UK). The HPLC was equipped with an amino column at a temperature of 40 °C (Alltech Luna 5 µm NH2 100A, Deerfield, USA), which was eluted with 80 volume% acetonitrile and 20 volume% water at a flow rate of 1.5 ml min^{-1}. A refractive index detector (Shodex, Munich, Germany) was used for detection.

2.3 RESULTS AND DISCUSSION

In this section, we demonstrate the use of the microfluidic device with several integrated parallelized microcontactors. We conducted experiments to collect both qualitative and quantitative data. Firstly, we visualized the result of transport of hydrochloric acid and sodium hydroxide by pH-sensitive dyes. Secondly, we quantified the diffusion of glucose by HPLC. Lastly, we derived the membrane permeability based on the data of the glucose separation experiment.

2.3.1 SEPARATION OF HCL AND NAOH

The flow rate and channel configuration determined the area of the separation region and thus the membrane contact time in each channel. The pH at the outlets was a result of the pH at the inlets and this contact time. When the pH was higher than the transition range of Bromocresol Green, a change in color was observed near the outlet of the channel (Figure 2.2).

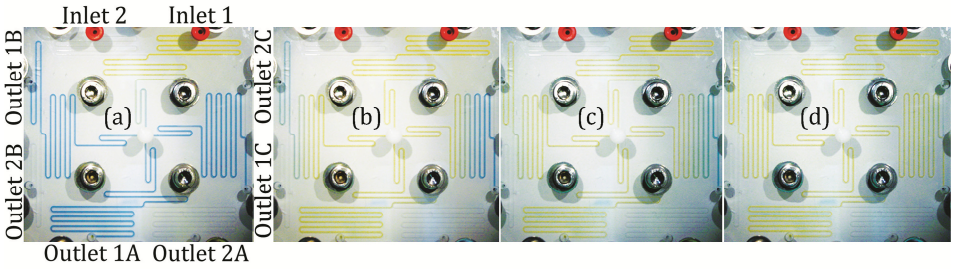

Figure 2.2: Photographs of the model. which were taken during the experiment. Inlet 1 was fed with pH-indicator Bromocresol Green in acidic water (pH 3.0), Inlet 2 with alkaline water (pH 10). The indicator had a transition range from yellow at pH 3.8 to blue–green at pH 5.4. The photographs show steady state conditions at flow rates of 0.4 ml min^{-1} (a), 1.2 ml min^{-1} (b), 2.0 ml min^{-1} (c), and 2.4 ml min^{-1} (d).

At a flow rate of 0.4 ml min^{-1}, the NaOH and HCl diffused fast enough through the membrane to have increased the pH at each outlet to the transition range of the pH-indicator. This did not occur at a flow rate of 1.2 ml min^{-1}, as shown by the yellow color at the outlet of channel A. Further increasing the flow rate, thus decreasing the contact time, eventually caused the pH-indicator to remain yellow

in all channels. At this flow rate, even in the channel with the longest contact time, the flux of the components was still too low to increase the pH to the transition range of the pH-indicator.

2.3.2 SEPARATION OF GLUCOSE

Similar to the pH-indicator experiments, the flow rate and channel configuration determined the contact time in each channel for the glucose separation. The samples of one batch of syringes corresponded to the output of a separation with three different contact times. With increasing contact time, the glucose had more time to diffuse through the membrane and the concentrations in the retentate and permeate came closer to the equilibrium value of 50 mM.

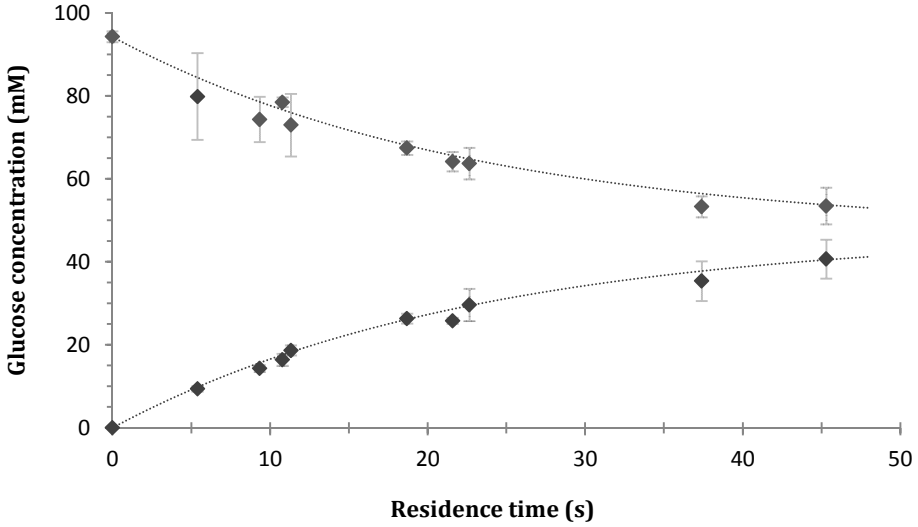

Figure 2.3 The glucose concentrations (♦) at the retentate outlet (above 50 mM) and permeate outlet (below 50 mM) as a function of the contact time. The error bars indicate the 95% confidence interval. The dotted line shows the results from the model.

The overall mass transfer coefficient for glucose k_{ov}, derived from the diffusion model, had a value of 1×10^{-5} m s^{-1}. This approximated the value found in literature (Broek 1993) for the overall membrane permeability (0.7×10^{-5} m s^{-1}).

2.3.3 DISCUSSION ON DEVICE ASPECTS

The described device not only contributed to a faster sampling but also to a possible reduction of measurement errors. When this device is used in conjunction with a device with only one separation region, errors resulting from varying flow conditions might be reduced. In such a device, contact time is dependent on flow rate only. This means the flow rate has to change in order to change the contact time. In this article, we described a decoupling of these parameters so that we could use a fixed flow rate. As a result, the microfluidics did not change. In addition, we were not dependent on the throughput linearity of the pumping system. However, with a device with only one separation region, we can obtain the same contact times, but require different corresponding flow rates. Since the boundary layer resistances depend on flow rate, results from such a device may deviate from our obtained results.

Random variations in channel throughput, due to for example temporary blockage by air bubbles, could influence the throughput in all other channels. This influence is inherent to the type of parallelization but can be detected by statistical analysis of the experimental data. Results of a single batch are always correlated, how they are correlated depends on the conditions of the channel. This means that we can predict their correlation, and possibly conclude that an, albeit undesired, variation in throughput occurred. The standard deviation of the correlation of the results in subsequent batches may quantitatively describe the occurrence of random variations.

Besides mass transfer coefficients, kinetic parameters such as enzyme conversion rates can be derived with an experimental setup as described in this article. Swarts et al. (2008) compared a lipase-catalyzed esterification on micro and bench scale. This comparison required many experiments for different substrate concentrations. Using the device described in this article would reduce the amount of required experiments and possibly improve accuracy.

With multiple separation and/or reaction regions in combination with online monitoring, many parameters can be measured simultaneously – without being limited by analysis. When the number of generated data points is sufficiently large, this technique may enable us to perform structural equation modeling for testing and estimating of causal relationships between parameters.

2.4 CONCLUSIONS

The presented microfluidic device is an efficient tool for faster acquisition of samples and determination of mass transfer coefficients. The concept of decoupling pressure drop from contact time can be used to simultaneously conduct distinct experiments. Scaling up by stacking individual devices, in combination with integrating separation regions in a single device, can be used to increase throughput. A vast amount of channels can be micromilled on a single layer, all for exposure to different conditions for simultaneous analysis of a separation or possibly a reaction and/or separation.

3

MASS DIFFUSION SEPARATION OF SUGARS IN MICROCHANNELS

ABSTRACT

Processes such as chromatographic separation and nanofiltration can remove low molecular weight sugars from liquid mixtures of oligosaccharides. We studied mass diffusion separation, which is based on differences between diffusivities of components, as an alternative for the separation of such liquid mixtures. With this separation process, there is no need for applying high transmembrane pressures. Due to the relatively small differences between the diffusivities of the components, the process requires a high separation resolution and short diffusion distances. Microfluidic membrane separation can feature such requirements with to the use of selective membranes and small microchannels. We studied several membranes for use in a microfluidic membrane separation of small sugars. Our results show that mass diffusion separation in liquids is a feasible concept. With optimized microchannel and membrane dimensions, the presented separation process can compete with currently available separation technologies.

This chapter has been submitted for publication as: Kolfschoten RC, Janssen AEM, Boom RM. Mass diffusion based separation of sugars in a microfluidic contactor with nanofiltration membranes.

3.1 INTRODUCTION

Nondigestible oligosaccharides of various types possess useful physicochemical characteristics. Most of the interest stems from their physiological properties as functional food ingredients with prebiotic properties. Prebiotics are nondigestible food ingredients that stimulate the growth and/or activity of bacterial species already resident in the colon, and hence may improve host health (Gibson and Roberfroid 1995). Since their introduction, the popularity of using oligosaccharides as health-enhancing functional food ingredients has grown rapidly (Roberfroid 2007).

Oligosaccharides are classified as glycosides containing three to ten sugar moieties. In general, food-grade oligosaccharides are not pure products, but are mixtures containing oligosaccharides of different degrees of polymerization (Crittenden and Playne 1996). Commercial products often contain low molecular weight sugars that do not contribute to the beneficial properties of the higher molecular weight oligosaccharides (Gibson et al. 2004). Such sugars can be removed from the mixtures by chromatographic separation methods and nanofiltration. Nanofiltration has been studied extensively for large scale methods of purification and concentration of oligosaccharide mixtures (Feng et al. 2009; Goulas et al. 2002; Li et al. 2004; Vegas et al. 2006). Compared to the other separation methods, nanofiltration methods require less time, less eluent, and lower energy consumption. Some challenges still remain for large scale membrane applications to among other things avoid fouling, increase lifetime, and increase resistance to chemicals (Van der Bruggen et al. 2008).

Mass diffusion separation has been examined theoretically and experimentally for the separation of gaseous mixtures (Benedict and Boas 1951; Hertz 1924; Keyes and Pigford 1957). Separation processes based on this concept are sweep diffusion (Cichelli et al. 1951), double diffusion (Schwertz 1947) and frictional diffusion (Geboers et al. 2007). The latter method was recently used for separation of a gaseous azeotropic mixture where an additional gaseous component was used as

separating agent or enhancer. The mass diffusion separation processes have been investigated for the separation of gas mixtures but may also be an option for the separation of liquid mixtures. Shuck et al. (1963) concluded from their experiments with a diaphragm diffusion cell that significant separations of the components of a miscible ternary liquid system may be achieved in the mass diffusion process. Separation of liquid mixtures may therefore also be achieved by the above mentioned separation concepts. Compared to the gaseous mixtures, the absolute diffusivities between components in the liquid mixtures are much lower due to smaller differences between the binary diffusion coefficients (Selvi et al. 2007). Consequently, a high separation resolution and short diffusion distances are desired.

We report the use of a microfluidic device with incorporated membranes for mass diffusion separation of liquid mixtures containing mono-, di-, and trisaccharides. Incorporated micro- and nanofiltration membranes mimic fluidic enhancers by acting as pseudo components to exert friction on the diffusing saccharides. These membranes and the short diffusion distances due to the small sizes of the microfluidic device enhance the separation of the liquid mixture. We compared five different membranes and different flow conditions for the separation of sugars.

3.2 THEORY

Mass diffusion separation is based on transport velocity differences in an enhancer (Breure et al. 2008). Liquid enhancers can change the density, viscosity, and polarity of a mixture. This affects the fluid dynamics in the microchannels. To avoid such issues, membranes can be used instead of liquid enhancers. Inert membranes are able to influence the transfer of the components via wall friction. In our setup, they do not completely reject any of the components but exhibit a different friction with each of the components in the mixture. Such membranes, while incorporated in microfluidic devices, enable a good definition of the permeate and retentate flows.

Mass transport in membranes is based on surface diffusion (e.g. by adsorption or charge effects), momentum diffusion, configurational diffusion (e.g. by sieving effects) and/or Knudsen diffusion (Mulder 1996). Charge effects are expected to be small because the oligosaccharides in our solutions are neutral. Our membranes function as a barrier for momentum diffusion or convective transport during coflow contact of the liquids in the microfluidic device. Due to this coflow operation, mass transport through the membranes is controlled by diffusion restriction (Deen 1987). The sugars from our setup have a relatively small variation in size with molecular weights ranging from 180 g mol^{-1} for glucose to 504 g mol^{-1} for raffinose. The molecular size of the sugars is also much smaller than the estimated membrane pore size. Configurational diffusion effects were assumed to be small for convective transport nanofiltration (Pontalier et al. 1997; Pontalier et al. 1999; Wijmans and Baker 1995) but might affect diffusive transport in nanofiltration. Knudsen diffusion in liquids can in general be neglected, as the ratio of the membrane pore sizes to the mean free path of the molecules is very large.

Conform the binary friction model the correlation of diffusion time to flow rate by Einstein's equation for Brownian motion as function of the effective diffusion coefficient is expected to determine the selectivity of the separation (Einstein

1905; Kerkhof 1996). The effective diffusion coefficient, D_{eff}, (m^2 s) for a membrane separation of a binary mixture can be described by the Bosanquet formula:

$$D_{eff,1} \propto \left(\zeta_{1,M} + \zeta_{1,2}\right)^{-1}, \qquad \text{Equation 3.1}$$

where $\zeta_{1,M}$ and $\zeta_{1,2}$ are the friction coefficients (N s mol^{-1} m^{-1}) of component 1 with the membrane and the – Maxwell-Stefan – friction coefficient in the bulk respectively. Effective diffusivities can be estimated using the porosity of the membrane and tortuosity of the pores (Whitman 1923). Differences between these diffusivities for the components in a mixture result in per membrane distinguishable fractionations. Figure 3.1 illustrates such a fractionation process. The figure shows diffusion of water to and glucose, sucrose and raffinose from the retentate flow. In the relatively large pores, the components interact with each other (intermolecular friction effects) and the membrane (membrane friction effects).

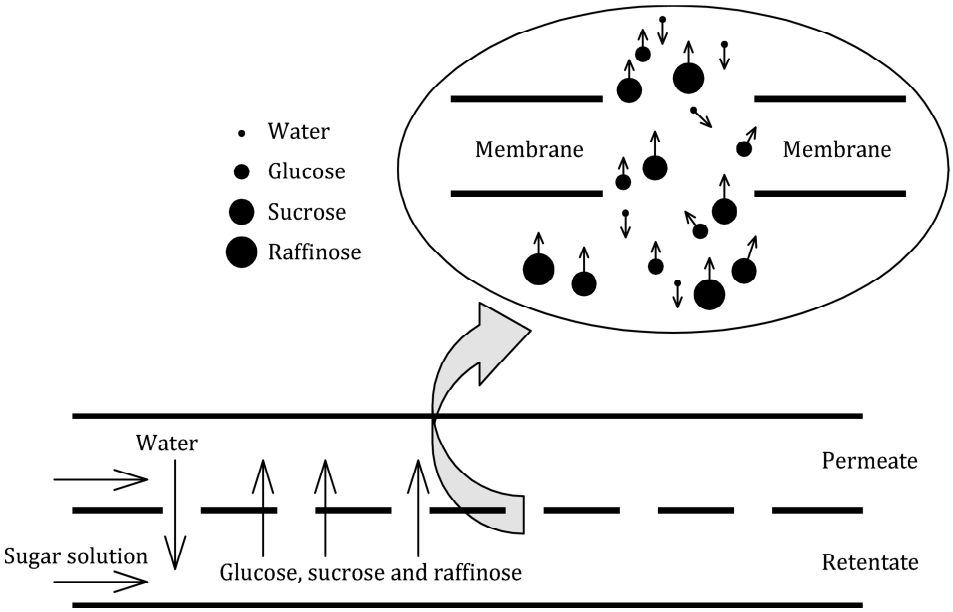

Figure 3.1 Coflow contacting of liquids that initially consist of water (permeate) and sugar with water (retentate). Water diffuses to and glucose, sucrose and raffinose diffuse from the retentate flow.

A higher flow rate causes a higher shear rate and reduces the size of the so called stagnant film layer (Whitman 1923). Concentration polarization is expected to be negligible due to low transmembrane pressures (Levich 1942). The driving force for mass transport of the sugars is the chemical potential difference over the thickness of this layer and the membrane; hence, the driving force increases with flow rate due to a decrease of the film layer. According to the film model, the thickness of the stagnant film layer in the microchannel is correlated to the channel depth d (m) (e.g. typical dimension) by the Sherwood relation (Spalding 1954). The mass transfer coefficient is inversely correlated to the thickness of this film layer and is relatively high due to the layer's small size (Brody and Yager 1997).

Overall mass transport in the microfluidic device depends on the membrane permeability (internal mass transport) and the mass transport in the film layers on

both sides of the membrane (external mass transport). The overall mass transport coefficient can be described by the resistance in series model:

$$k_{ov} = \left(\frac{1}{k_R} + \frac{1}{k_m} + \frac{1}{k_P}\right)^{-1}, \qquad \text{Equation 3.2}$$

where k_{ov} is the overall mass transport coefficient (m s^{-1}), ΔC is the concentration difference (mol m^{-3}), k_m is the membrane permeability (m s^{-1}) and k_R and k_P are the mass transport coefficients (m s^{-1}) in the retentate and permeate respectively (Kreulen et al. 1993). The overall mass transport equals the this transfer coefficient multiplied with the concentration difference, ΔC (mol m^{-3}). The membrane permeability is defined as:

$$k_m = \frac{m \cdot D_m}{\delta_m}, \qquad \text{Equation 3.3}$$

where m is the (thermodynamic) distribution coefficient (-), D_m the diffusion coefficient in the membrane (m^2 s^{-1}) and δ_m the thickness of the membrane (m) (which includes the support layer of the membrane). An optimistic estimation of the membrane permeability ($k_{m,max}$) would assume a distribution coefficient of unity between the solution inside the pores and the free solution inside the microchannels, and a membrane diffusion coefficient equal to the diffusion coefficient in water:

$$k_{m,max} = \frac{D}{\delta_m}, \qquad \text{Equation 3.4}$$

where the Maxwell-Stefan diffusion coefficients in and relative to water (D) are 6.90×10^{-10} m^2 s^{-1}, 5.60×10^{-10} m^2 s^{-1}, and 4.10×10^{-10} m^2 s^{-1} for glucose, sucrose, and raffinose respectively (Perry and Green 1997). For high separation selectivities, the difference between the membrane permeabilities of the components should be as large as possible.

The coflow liquid-liquid contacting can be described by modeling two plug flows separated by a membrane through which mass transport occurs:

$$\varphi_P \cdot dC_R = -k_{ov} \cdot \alpha \cdot \left[\left(1 + \frac{\varphi_R}{\varphi_P}\right) \cdot C_P - \frac{\varphi_R}{\varphi_P} \cdot C_I\right] \cdot dV, \qquad \text{Equation 3.5}$$

where φ_P and φ_R are the permeate and retentate flow rates ($m^3\ s^{-1}$), α is the specific area (m^2 membrane m^{-3} channels), C_P and C_R are the permeate and retentate concentrations (mol m^{-3}), C_I the initial feed concentration (mol m^{-3}) and V the combined volume of the channels (m^3). Integration of Equation 3.5 yields:

$$C_R(t) = \frac{\varphi_R \cdot C_I}{\varphi_P + \varphi_R} \cdot \varphi_P \cdot C_I \cdot e^{\frac{-\alpha \cdot k_{ov} \cdot (\varphi_P + \varphi_R) \cdot t}{\varphi_P}}, \qquad \text{Equation 3.6}$$

where t is the residence time (s). This expression gives the retentate concentration as (an exponential) function of residence time, which is also described by the integration of Fick's second law. From this equation, the rejection can be calculated by:

$$1 - (C_I - C_R)/C_P. \qquad \text{Equation 3.7}$$

3.3 MATERIALS AND METHODS

3.3.1 MATERIALS

Analytical grade purity D(+)-glucose, (D+)-sucrose and (D+)-raffinose were supplied by Merck KGaA (Darmstadt, Germany). Demineralized water was supplied by a Millipore Milli-Q water system (Billerica, USA) and degassed for 30 min at 30 °C in a Branson Sonic Power Company 5210 sonification bath (Danbury, USA).

Polyvinylchloride and polycarbonate plates were supplied by Vink Kunststoffen (Didam, the Netherlands). MF-Millipore mixed cellulose ester membranes were supplied by Millipore (Amsterdam, the Netherlands); SeIRO MPF36 polyvinylidene fluoride (PVDF) membranes were supplied by Koch Membrane Systems (Belgium); and NADIR NP010 polyethersulfone membranes were supplied by MICRODYN-NADIR (United Kingdom). Table 3.1 shows the membrane characteristics.

Table 3.1 The properties of the membranes used in this study.

Name	**Material**	**Type**	**Manufacturer**	**Pore Size / Rejection (-)**	**Thickness (µm)**
MF-Millipore	Cellulose acetate	MF	Millipore	0.025 µm	105
SeIRO MPF34	PES	NF	Koch Membrane Systems	35% NaCl 95% Glucose 97% Sucrose	200
SeIRO MPF36	PES	NF	Koch Membrane Systems	10% NaCl 30% Glucose 50% Sucrose	200
NADIR NP010	PES	NF	Microdyn-Nadir	25%-55% Na_2SO_4	230±20
NADIR NP030	PES	NF	Microdyn-Nadir	80%-90% Na_2SO_4	230±20

Before use, the membranes were cut to size and soaked in demineralized water in order to remove any preservative material. The membranes were wetted before placement in the microchannel device.

3.3.2 DEVICE FABRICATION

Structures of 80.6 cm length, 500±10 µm width were milled on one side of two 2.00 mm thick 5.0 cm by 10 cm polyvinylchloride layers using a MAHO MH 800 E computer controlled numerical control mill (Pfronten, Germany) with HOLEX cutter 20 1640 of 500 µm (Pfronten, Germany). Flat sheet membranes were directly incorporated by stacking the polyvinylchloride layers (Figure 3.2) (de Jong et al. 2006; Kralj et al. 2007; Mair et al. 2007).

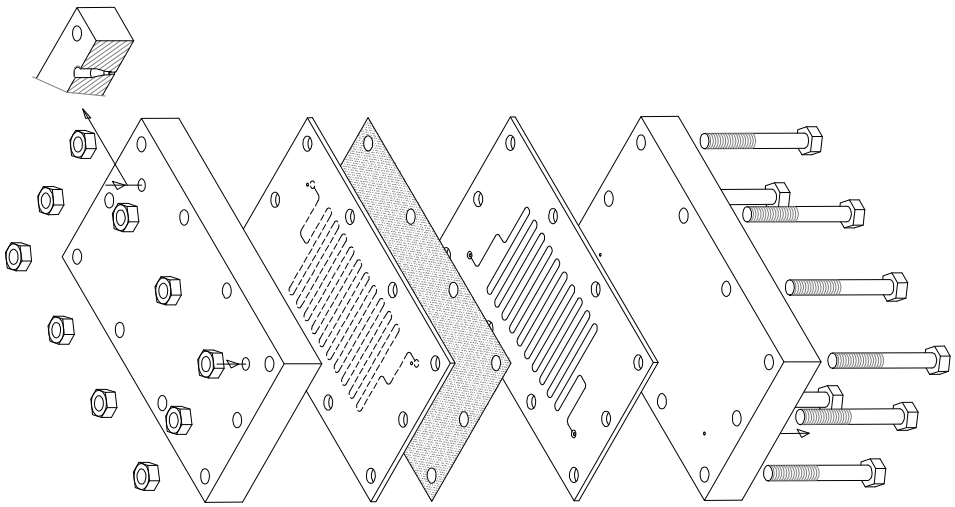

Figure 3.2 Schematic drawing of the stacked layers in the membrane microchannel device. From left to right: polycarbonate (PC) layer; polyvinylchloride (PVC) layer with microchannels; micro or nanofiltration membrane; PVC layer with microchannels; PC layer. The arrows at the left side of the left PC layer indicate Inlet 1 and Outlet 1. The arrow at the right side of the right PC layer indicates Outlet 2.

The milled structure in a layer was aligned to the milled structure in the other layer. This generated two microchannels separated by a membrane. The polyvinylchloride layers were held in position by 10 screws, which went through the drilled screw holes in the two layers. To seal the device, the layers were clamped by two 1.0 cm thick polycarbonate bottom and top layers respectively. A total of three devices were fabricated having microchannels with a depth of 50±10 µm, 100±10 µm and 200±10 µm.

3.3.3 EXPERIMENTAL SETUP

Inlet 1 and Inlet 2 of the microfluidic device were connected to SGE syringes (Austen, Australia) and a Harvard Apparatus Pump 33 syringe pump (Holliston, USA).

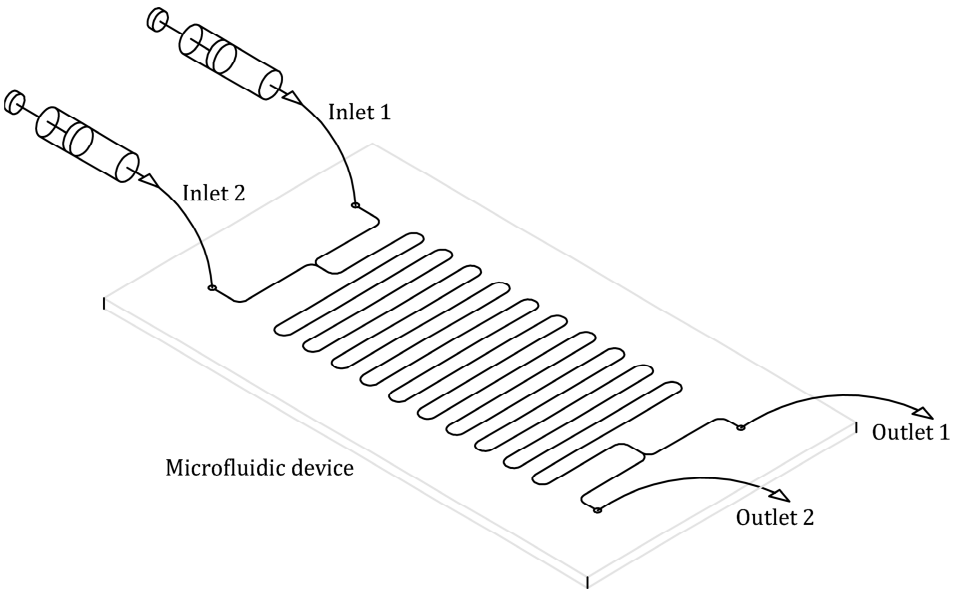

Figure 3.3 Experimental setup. Inlet 1 was fed with water, Inlet 2 was fed with an aqueous sugar solution.

Inlet 1 was fed with water and Inlet 2 was fed with an aqueous sugar solution for co-current liquid-liquid contacting (Figure 3.3). The feed contained 0.025 mol l^{-1} glucose, 0.025 mol l^{-1} sucrose, and 0.025 mol l^{-1} raffinose. Both inlets were set at equal flow rates in the range of 7.90 µl min^{-1} to 150 µl min^{-1}. All experiments were carried out at room temperature (20 °C). The microchannel depth was 100 µm unless stated otherwise.

Samples were analyzed at steady state conditions. Steady state was assumed after five times the residence time in the whole module and tubing volume at a constant

flow rate. The experiments were repeated four times. The outgoing concentration of the sugars was quantitatively analyzed by isocratic HPLC.

3.3.4 ANALYSIS

The overall mass transport coefficient (k_{ov}) was estimated by nonlinear regression of Equation 3.6 with the experimentally obtained values using the Non-Linear Least-Squares solver in Athena Visual Studio (version 14.0, Athena Visual Software, Naperville, IL).

The HPLC was supplied by Thermo Separation Products (United Kingdom) and equipped with an Alltech Lichrosphere 5 µm NH2 100A amino column (Deerfield, USA). The column was heated to 40 °C and eluted with 80 volume% acetonitrile and 20 volume% water at a flow rate of 1.5 ml min^{-1}. For detection, a Shodex refractive index detector (Munich, Germany) was used.

With the measured concentrations, we could determine the membrane rejection, selectivity, yield, and flux. This rejection was defined as:

$$1 - C_P/C_R\,; \qquad \text{Equation 3.8}$$

the selectivity of glucose or sucrose – with respect to raffinose – was defined as:

$$1 - C_{P,raffinose}/C_P\,; \qquad \text{Equation 3.9}$$

and the yield was defined as:

$$C_P/(C_P + C_R). \qquad \text{Equation 3.10}$$

The molar total flux of permeate J (mol m^{-2} h^{-1}) was expressed by:

$$J = C_P \cdot \varphi_P/A, \qquad \text{Equation 3.11}$$

where A is the membrane effective area (m^2).

3.4 RESULTS AND DISCUSSION

We studied fractionation of low molecular weight saccharides based on the concept of separation by mass diffusion. Firstly, we investigated the effects of channel depth on the rejection and selectivity. Secondly, we compared the experimentally obtained selectivities and corresponding fluxes of the membranes of our study. Thirdly, we studied the effect of rejection as function of flow rate for the nanofiltration membranes. In addition, we determined the membrane permeabilities of these membranes. Furthermore, we compared our results to conventional nanofiltration. Lastly, we estimated the mass transport by mass diffusion based on optimized microchannel and membrane characteristics.

To understand the effect of channel depth on the rejection and selectivity, we look back to our theoretical section. According to the Sherwood relation, the thickness of the film layer decreases with decreasing channel diameter. The contribution of the external mass transport to the overall mass transport (see Equation 3.2) therefore depends on the characteristic dimensions of the microchannels, and can consequently influence the selectivity. By varying the channel depth – the characteristic dimension of our system – the effects of external mass transport limitation can be studied. Figure 3.4 shows these effects on the selectivity (a) and rejection (b) as function of channel depth.

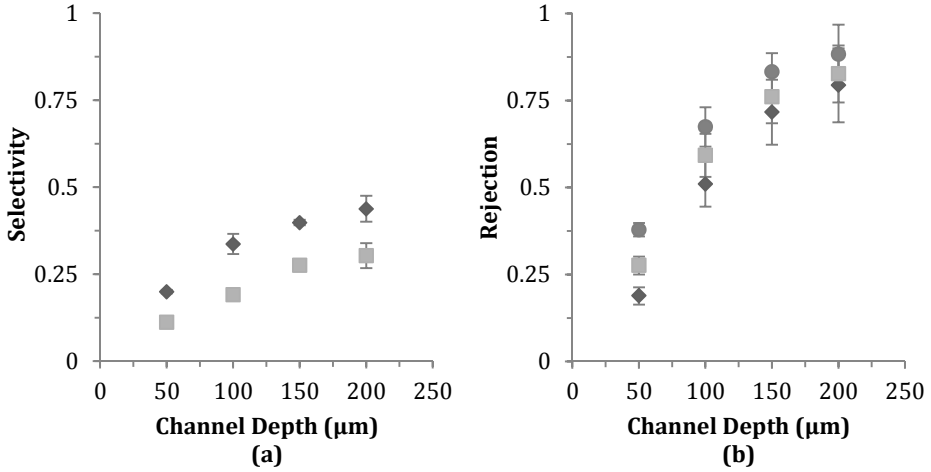

Figure 3.4 Selectivity of glucose (♦) and sucrose (■) with respect to raffinose (a), and rejection of glucose (♦), sucrose (■), and raffinose (●) (b) as function of channel depth of the membrane microchannel device with the MF-Millipore membrane at a constant residence time of 1.6 min. The error bars indicate the sample standard deviation.

Figure 3.4a & b show that the selectivity and rejection of all sugars increased as function of channel depth. Larger channel depths imply that the diffusion front shifts towards the retentate flow, smaller fractions of the sugars in the retentate can therefore reach the permeate. Figure 3.4a shows that this fraction is relatively larger for the sugars glucose and sucrose at larger channel depths. According to the theory, the external mass transfer limitation has a bigger contribution to the overall mass transfer at larger channel depths. Figure 3.4b shows increased rejections as function of channel depth accordingly. Increasingly smaller channel depths would eventually exclude external mass transfer limitations and let the selectivity solely depend on the membrane or internal mass transfer. For practical reasons we continued with channel depths of 100 µm.

In this study, we compared five different membranes – one microfiltration membrane and four nanofiltration membranes. Table 3.1 shows the pore size and rejection characteristics of these membranes. We expected to yield selectivities accordingly. Hence, the microfiltration membrane MF-Millipore was expected to yield the lowest selectivity due to its relatively large pores. Similarly, the

nanofiltration membrane SeIRO MPF36 was expected to yield the second lowest selectivity due to its relatively low specified salt rejection. Moreover, compared to the SeIRO MPF34, the SeIRO MPF36 has a lower specified glucose and sucrose rejection, thus the SeIRO MPF36 was expected to yield selectivities in agreement with this specification. Furthermore, based on the salt rejections of Na_2SO_4, the NADIR NP030 nanofiltration membrane was expected to yield higher selectivities than the NADIR NP010. However, based on the specifications as supplied by the manufacturers, it was difficult to properly estimate what the selectivity of the SeIRO-MPF34 membrane would be with respect to the NADIR membranes. All in all, the nanofiltration membranes were expected to yield relatively high selectivities. In particular, the microfiltration membrane was expected to deviate from this. Figure 3.5a shows these selectivities of glucose and sucrose with respect to raffinose for the studied membranes. The corresponding membrane fluxes are shown in Figure 3.5b.

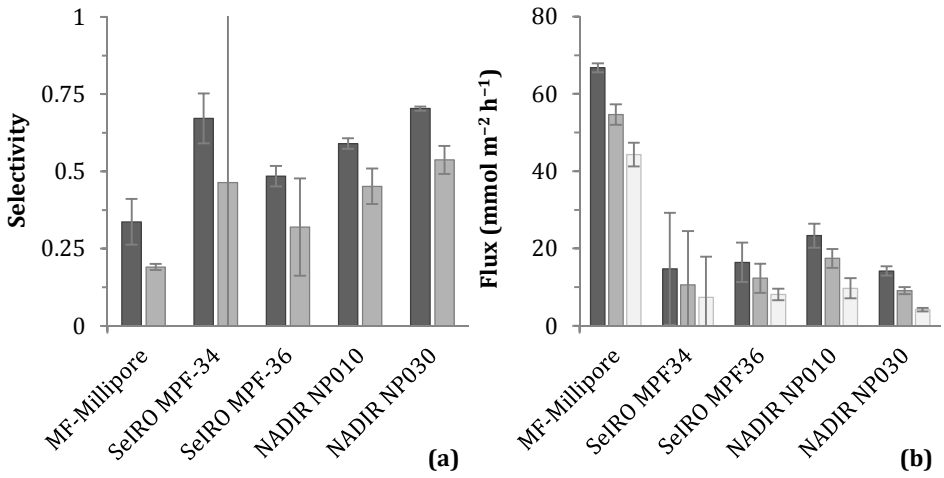

Figure 3.5 Selectivity (-) of glucose (■) and sucrose (■) with respect to raffinose (a), and membrane flux of glucose (■), sucrose (■), and raffinose (■) (b) at a flow rate of 50 µl min^{-1}. The error bars indicate the sample standard deviation.

Figure 3.5a shows that glucose consequently had a higher selectivity than sucrose - this was most probably due to the higher diffusivity of glucose. The MF-Millipore

membrane had on average the lowest selectivities, as expected. However, the results indicate that even with such a microfiltration membrane, one can obtain separation of low molecular weight components. Compared to the SeIRO MPF34 membrane, the SeIRO MPF36 membrane had lower selectivities. Likewise, the NADIR NP010 had lower selectivities than the NADIR NP030 membrane. The latter membrane had a selectivity of 0.70 for glucose, the highest selectivity of all tested membranes. In literature on nanofiltration membranes, the reported selectivities for fructose, a DP_1 sugar like glucose, were minimally 0.68 (see Table 2 in Goulas et al. (2002)). These selectivities could be obtained by applying a transmembrane pressure of at least 6.9 bar. We used a negligible transmembrane pressure and still obtained such a high selectivity.

Figure 3.5b gives an indication of the order of magnitude of the membrane fluxes. The MF-Millipore membrane, the microfiltration class membrane, yielded the highest fluxes. For the nanofiltration membranes, the NADIR NP010 had the highest fluxes. At a solute concentration of 0.03 g ml^{-1}, we obtained a solute flux of 15.9 g m^{-2} h^{-1} with this membrane. Compared to literature, a solute flux of 110 g m^{-2} h^{-1} was obtained at an equal solute concentration (see Figure 5b in Goulas et al. (2002)). Such fluxes commonly were acquired at transmembrane pressures of 5 bar to 30 bar, and usually at higher sugar mixture concentrations (Aydogan et al. 1998; Choi et al. 2007; Feng et al. 2009; Goulas et al. 2003). In nanofiltration, the high pressure actually forces solutes through the membranes. Therefore, we expected those filtration methods to yield orders of magnitude higher fluxes. However, the differences were much smaller.

The nanofiltration membranes outperformed the microfiltration membrane in terms of selectivity as indicated by Figure 3.5. However, the differences of the selectivities between the nanofiltration membranes were small. This necessitated further characterization of these membranes. The effect on rejection as function of flow rate was therefore studied. Furthermore, we fitted the diffusion model from Equation 3.6 to our experimental data. This fit would enable us to estimate the

membrane permeabilities. Figure 3.6a–d show the rejections of glucose, sucrose, and raffinose as function of flow rate, and the fitted diffusion model for the SeIRO MPF34 and SeIRO MPF36, and those of the NADIR NP010 and NADIR NP010 membranes respectively.

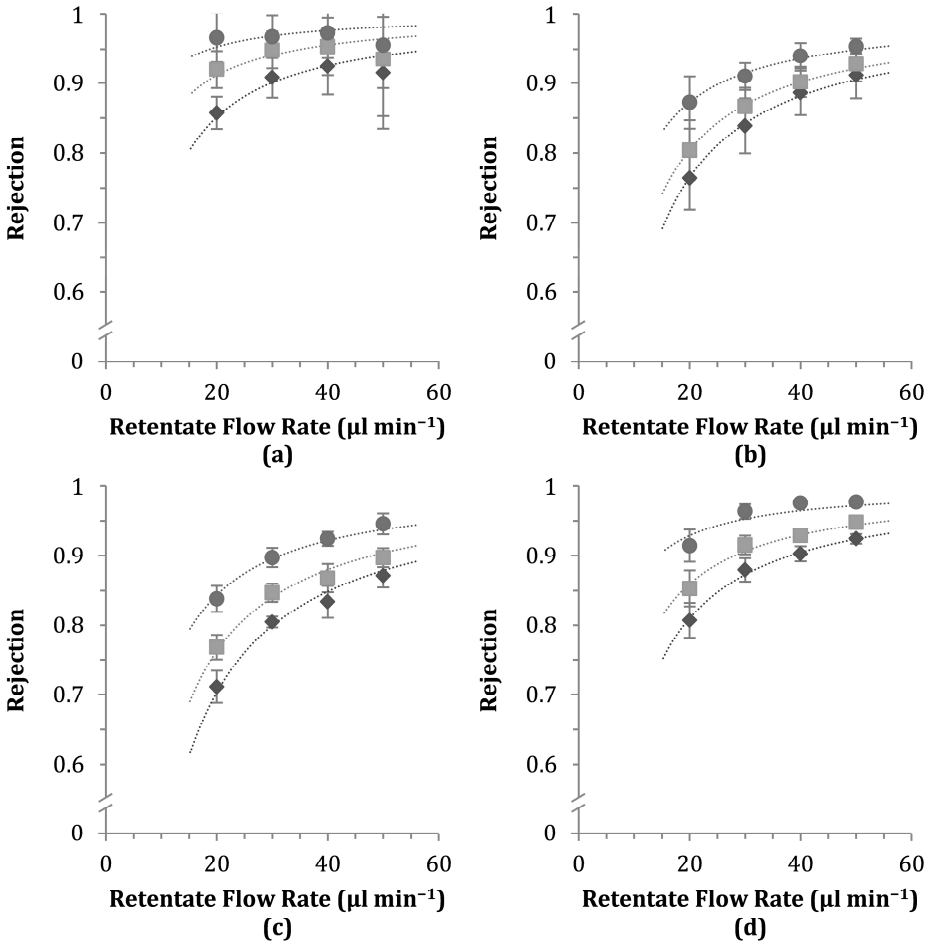

Figure 3.6 Rejection of glucose (♦), sucrose (■), and raffinose (●) as function of flow rate in the membrane microchannel device with the nanofiltration membranes SeIRO MPF34 (a), SeIRO MPF36 (b), NADIR NP010 (c) and NADIR NP030 (d). The dotted lines indicate the simulated results. The error bars indicate the sample standard deviation.

Figure 3.6a–d show the characteristic trend of rejection as function of flow rate. Overall, the rejection of raffinose was consistently higher than that of sucrose, and

likewise, the glucose consistently had a lower rejection than sucrose. This was expected since glucose had the highest diffusion coefficient, followed by sucrose, and lastly, raffinose. Based on the membrane properties, we expected the SeIRO MPF34 membrane to yield higher rejections than the SeIRO MPF36 membrane due to the higher rejections as specified by the manufacturer – Figure 3.6a & b confirm this. Likewise, these expectations are in agreement with Figure 3.6c & d that shows that NADIR NP030 membrane yielded higher rejections than the NADIR NP010 membrane.

The diffusion model confirmed the measured trend. The dotted lines in Figure 3.6a–d show the fitted results of this model. In general, the experimental results were in good agreement with the diffusion model. The results from Figure 3.6a show a slight deviation from the model at a flow rate of 50 μl min^{-1}. However, the error bars of these data points indicate a relatively large uncertainty. This was because the permeate concentration became increasingly smaller as function of flow rate, and started to reach the limitations of our HPLC analysis.

At the lowest measured flow rate of 20 μl min^{-1}, which corresponds to a residence time of 8.1 min, the rejections still remained above 0.7. Note that, if the flows are in chemical equilibrium, the rejections are zero by definition. With the diffusion model, we could predict that unfeasibly long residence times were required to obtain such a chemical equilibrium in our 100 μm deep channels with relatively thick nanofiltration membranes. Figure 3.7 shows the membrane permeabilities that were derived from this model.

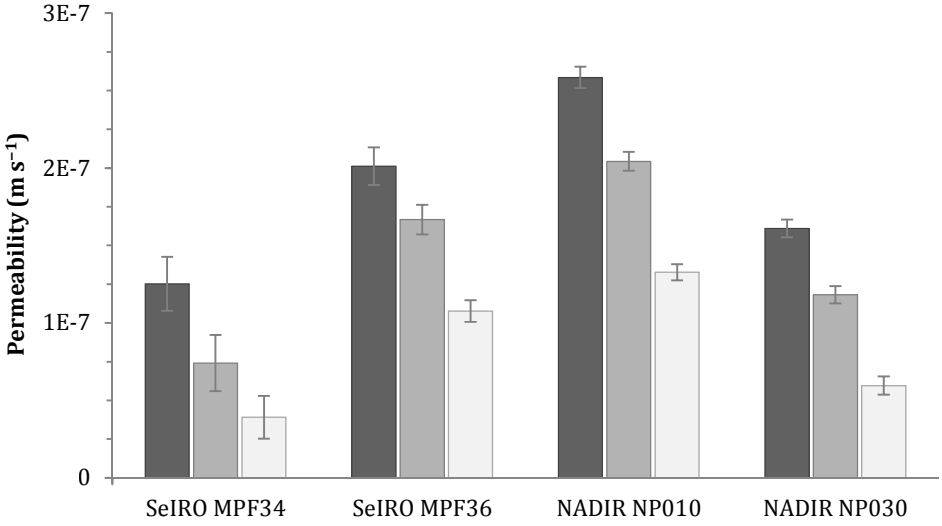

Figure 3.7 The membrane permeability, derived from the diffusion model, of glucose (■), sucrose (■), and raffinose (■) for the SeIRO MPF34, SeIRO MPF36, NADIR NP010, and NADIR NP030 nanofiltration membranes.

Figure 3.7 shows that glucose had the highest membrane permeability in all cases. In part this is due to its higher diffusion coefficient (in water), but it might also be caused by less configurational restriction effects for glucose compared to sucrose and raffinose. Figure 3.5 shows that the NADIR NP010 membrane had the lowest selectivity, followed by the SeIRO MPF36, the SeIRO MPF34, and lastly the NADIR NP030 membrane. We expected this same order with decreasing permeability. However, here the NADIR NP030 membrane switched places with the SeIRO MPF34 membrane. The NADIR NP030 would consequently be more favorable than the SeIRO MPF34, as it yields a higher selectivity and a higher permeability.

An important function of the membranes in our setup was to improve fractionation by changing the effective diffusivities of the components. From the results, it is clear that the membranes facilitated this fractionation. However, the membranes were relatively thick since they consisted of an active, selective layer, plus a much thicker support layer in which only diffusion can take place - this required long diffusion times as a result. Thinner membranes, as well as smaller channel depths,

can reduce these required times. For instance, cellulose acetate dialysis membranes of only 25 µm thick are commercially available via Fisher Scientific (Landsmeer, the Netherlands). Possibly, nanofiltration membranes can be reduced to such a thickness as well – thereby removing any support layers. Furthermore, we can fabricate microchannels with a depth of only 50 µm. An optimized membrane microfluidic device that meets these specifications would significantly increase the membrane permeability. Table 3.2 shows the potential membrane permeability, overall mass transfer coefficient, and flux of each sugar and membrane based on such altered dimensions.

Table 3.2 Simulated membrane permeability, overall mass transfer coefficient, and membrane flux of glucose, sucrose, and raffinose for the nanofiltration membranes at reduced microchannel and membrane dimensions.

	Glucose			Sucrose			Raffinose		
Membrane	k_m	k_{ov}	**Flux**	k_m	k_{ov}	**Flux**	k_m	k_{ov}	**Flux**
SelRO MPF34	1.0E-6	9.6E-7	56	5.9E-7	5.8E-7	40	3.1E-7	3.1E-7	24
SelRO MPF36	1.6E-6	1.5E-6	71	1.3E-6	1.3E-6	65	8.6E-7	8.1E-7	51
NADIR NP010	2.4E-6	2.2E-6	82	1.9E-6	1.7E-6	75	1.2E-6	1.1E-6	62
NADIR NP030	1.5E-6	1.4E-6	69	1.1E-6	1.0E-6	59	5.5E-7	5.3E-7	37

The membrane permeability k_m (m s^{-1}), the overall mass transfer coefficient k_{ov} (m s^{-1}), and flux (mmol m^{-2} h^{-1}) were calculated for a channel depth of 50 µm, flow rate of 50 µl min^{-1}, and membrane thickness of 25 µm. The reduction of a channel depth from 100 µm to 50 µm increases the external mass transfer coefficient from 2.5×10^{-5} m s^{-1} to 5.1×10^{-5} m s^{-1}.

According to Table 3.2, the membrane permeability clearly is the most significant contributor to mass transport limitation: the obtained permeabilities almost equal the corresponding overall mass transport coefficients. These coefficients in the table are a factor six to eight higher than the current values. Simulations with our diffusion model indicated that, with these transfer coefficients, the fluxes will increase with about three to six times. Compared to reported fluxes in literature (110 g m^{-2} h^{-1}, see Figure 5b in Goulas et al. (2002)), the flux of the NADIR NP010 is reasonably high with 82 g m^{-2} h^{-1}. Our results indicate that the small characteristic dimensions reduce the characteristic diffusion times significantly, and therefore increase the applicability of liquid mass diffusion separations. We

suggest therefore to further miniaturize the microfluidic contactor in order to use the mass diffusion separation as a feasible separation process for the separation of oligosaccharides in liquids.

3.5 CONCLUSIONS

We used a membrane microfluidic device to co-currently contact liquid mixtures via a membrane. In this device, a membrane acted as a pseudo component to enhance the fractionation of sugars that had comparable diffusivities – a separation concept derived from mass diffusion separation. With the nanofiltration membranes, we were able to obtain high selectivities and relatively high fluxes. In contrast to other nanofiltration processes, the transmembrane pressure in our device was negligible, which makes our separation process unique. We show that a theoretical use of even smaller microchannels and thinner membranes can increase the membrane fluxes to values with the same order of magnitude as more conventional nanofiltration processes.

4

DIFFUSION-BASED MEMBRANE SEPARATION IN A MICROFLUIDIC CONTACTOR

ABSTRACT

Diffusion-based processes have gained popularity due to the developments of microfluidic devices. These devices enable contacting of fluids on a submillimeter scale. Such close contacting of fluids of different chemical potential yields extremely high driving forces for mass transfer. Consequently, components quickly transfer over these small distances. This concept is used to separate components in liquid and gaseous mixtures. However, it commonly involves the separation of components with large differences between their diffusivities. In this article, we focus, by contrast, on small differences between diffusivities. We used a microfluidic contactor to contact liquid streams via thin membranes. In our experiments, we brought two streams – of which one contained sugars – together in either co-current or counter-current configuration. This generated a driving force for mass transfer and partially separated different sugars from each other. The function of the membrane was to ascertain a stagnant diffusion zone between the two liquid streams. We show that this separation method is useful for enrichment of a component in a liquid mixture. Moreover, the method is generally applicable to any diffusing component – regardless of its diffusivity or concentration. Our results indicate that the method can yield enough component with good selectivity for a feasible process.

This chapter will be submitted for publication as: Kolfschoten RC, Janssen AEM, Boom RM. Diffusion-based membrane separation in a microfluidic contactor.

4.1 INTRODUCTION

In the last decade, diffusion-based separation processes have appeared as a result of developments in the science and technology of microfluidics. These developments have enabled microfluidic devices to process sub-microliter amounts of substances in microchannels. At the scales that these microfluidic devices operate, viscous forces dominate over inertial forces – the region of low Reynolds numbers (Purcell 1976). As a result, turbulence hardly occurs and diffusion becomes the basic method for mixing (Brody et al. 1996). Many studies have now revealed that this concept of diffusive mixing in microchannels can also be used for the separation of components.

Most researchers working with microfluidic devices have undoubtedly encountered diffusion-based processes. Brody et al. (1997; 1996) were among the first to recognize the potential of these processes in microfluidic devices for separation of components based on their diffusivities. Earlier in the 1990s, Williams et al. (1992) reported fractionation of several proteins and sodium benzoate based on a diffusion mechanism. After Manz et al. (1990) proposed the concept of miniaturized total analysis systems, the use of such diffusion mechanisms was more and more applied to microfluidic devices. For instance, Yue et al. (1994) presented a miniature (microchannel) field-flow fractionation device for analysis of blood cell populations. Diffusion-based concepts were also used by Holl et al. (1996) to design a methodology for providing design requirements for diffusion-based extraction. For liquid mixtures, this has commonly been demonstrated for cell and protein suspensions – generally utilizing the advantageous large differences between the diffusivities of the components. Recent publications include those by Fleming Glass et al. (2008) and Mata et al. (2008), both demonstrated the use of diffusion-based separation based on the extraction of dimethyl sulfoxide from a cell suspension to a co-currently flowing wash stream. In another publication, Luo et al. (2009) reported a system for diffusion-based monolayer yeast cell culture monitoring. All in all, many of these

processes had in common that there was a clear distinction between the low and high molecular weight components – in general, diffusing versus non-diffusing particles.

Overall, the researchers mostly studied the separation of components that have diffusivities with different orders of magnitude. For separation of gaseous mixtures, this is generally the case. Consequently, diffusion-based separation of gaseous mixtures can yield considerable throughput and resolution (Breure et al. 2008; Geboers et al. 2007). However, liquid mixtures often contain low molecular weight components that do not differ that much in diffusivity. Besides, the absolute diffusivities of the components are relatively low. As a result, diffusion-based separation is considered to be a sensitive and timely process, and therefore often not recommended (Selvi et al. 2007). Furthermore, many diffusion-based separations in liquids assume a stable laminar flow at low Reynolds numbers. In general, for analytical purposes this is not an issue. This changes when higher volumetric throughputs are desired, which consequently advocates for larger microchannels, and may yield less stable flows. In this study, we try to address these conditions of less distinguishable diffusive properties and larger microchannels by incorporating facilitating membranes.

Chou et al. (1999) demonstrated that facilitating membranes had the potential to enhance a separation. They reported the use of a microfabricated membrane sieve to separate DNA molecules, providing a continuous instead of batch wise separation. Interestingly, similar membranes have already been used in the 1960s by Shuck and Toor (1963) for the diffusion-based separation of liquid mixtures – they used a stainless steel, 5 mm thick diaphragm to act as a diffusion zone. Kolfschoten et al. (2011) recently studied the diffusion-based separation of sugars with comparable diffusivities. They obtained high selectivities with the use of nanofiltration membranes, but reported that these membranes were relatively thick for the mass diffusion process. In this article, we therefore used membrane sieves that are an order of magnitude thinner than these conventional

nanofiltration membranes. However, the membrane sieves have much larger pores – as Kolfschoten et al. (2011) indicated, increasing the pore sizes of the membrane can reduce its selective properties considerably. As a result, such a membrane sieve merely acts as a diffusion zone between streams. In this article, we focus on this concept, and use it to our advantage.

The objective of our study was to ascertain the possibilities of diffusion-based separation in relatively large microchannels. In order to prevent mixing up of streams by convection, we used very thin metal and polymeric sheets to separate permeate and retentate streams. We were interested in the diffusive behavior of low molecular weight sugars that had diffusivities in the same order of magnitude. The purpose of this research was to study development a method for diffusion-based separation of low molecular weight sugars from galacto-oligosaccharide (GOS) mixtures.

4.2 THEORY

In this study we consider a microfluidic contactor in which a solution containing sugars coming from one inlet – the retentate – is contacted in coflow, and via a membrane, with a solution containing water – the permeate. The resulting separation is based on the diffusion of these sugars towards the permeate through the membrane, and transverse to the primary convective flow direction.

The flow characteristics of the fluids in microchannels can be described by the Reynolds number Re (-) (Reynolds 1883).For our microfluidic device, this number can be calculated by:

$$Re = \frac{\rho \cdot v \cdot L}{\mu}, \qquad \text{Equation 4.1}$$

where ρ is the density of the fluid (kg m^{-3}), v is the mean fluid velocity (m s^{-1}), μ is the dynamic viscosity of the fluid (Pa s), and L is the hydraulic diameter. The hydraulic diameter is defined by:

$$L = \frac{2 \cdot w \cdot d}{w + d}, \qquad \text{Equation 4.2}$$

where w is the channel width (m) and d is the channel depth (m).

When using larger microchannels, the hydraulic diameter increases and thus the Reynolds number increases. For example, for our microchannels with a depth of 50 µm and a flow rate of 10 µl min^{-1}, this number equals approximately 0.3. However, with a larger depth of 200 µm and a higher flow rate of 200 µl min^{-1}, this increases up to a value of 10. The membranes in our microfluidic device can prevent instantaneous mixing of flows due to flow disturbances at higher Reynolds numbers, in particular with counter-current flows.

The membranes of our study have large enough pore sizes to prevent exclusion of the relatively small sugars based on their sizes. In addition, surface diffusion and Knudsen diffusion (Mulder 1996) are not expected to affect the diffusion of the

sugars as well. However, the momentum diffusion does not necessarily have to be zero. For instance, this momentum diffusion can be influenced by adjusting the pressure over the membranes – thereby inducing convective transport. By setting the permeate stream to a higher flow rate than the retentate stream, this transport can be forced through the membrane. Hence, the momentum diffusion towards the retentate side of the membrane can counter the diffusion due to the chemical potential towards the permeate side. The result of such a condition would be that slower diffusion components would be retained in the retentate stream. The flow conditions would therefore determine the selectivity of such a diffusion-based separation.

With included momentum diffusion, the driving force for mass transport of the sugars through the membrane is the convective flow through plus the concentration difference – or more correctly, chemical potential – over the membrane:

$$-D_i \cdot \frac{dC_i}{dz} + v \cdot C_i = N_i, \qquad \text{Equation 4.3}$$

where D_i is the diffusion coefficient of component i ($m^2\ s^{-1}$), C_i is the local concentration of component i ($mol\ m^{-3}$), z is the position on the z-axis along the width of the channel (m), v is the convective flow through the membrane ($m\ s^{-1}$), and N_i is the flux of component i ($mol\ m^{-2}\ s^{-1}$).

Integration of the differential equation of Equation 4.3 yields:

$$N_i = \frac{v \cdot \left(C_{P,i} - C_{R,i} \cdot e^{\frac{v}{k_{m,i}}}\right)}{1 - e^{\frac{v}{k_{m,i}}}}, \qquad \text{Equation 4.4}$$

where $C_{P,i}$ and $C_{R,i}$ are the permeate and retentate concentrations of component i ($mol\ m^{-3}$). The mass transfer coefficient of the membrane or membrane permeability k_m ($m\ s^{-1}$) is defined as:

$$k_m = \frac{m \cdot D_m}{\delta_m}, \qquad \text{Equation 4.5}$$

where m is the (thermodynamic) distribution coefficient (-), D_m the diffusion coefficient in the membrane ($m^2\ s^{-1}$) and δ_m the thickness of the membrane (m).

The convective flow in the primary flow direction is zero at the microchannel surfaces. As a result, so called film layers are present near these surfaces. The amount of convection and the corresponding flow rate of the liquid mixture in the microchannels influence the shear rate and the size of this film layer (Whitman 1923). According to the film model, the thickness of this stagnant layer in the microchannel is correlated to the channel width and depth by the Sherwood relation (Spalding 1954). Consequently, the external mass transfer coefficient is inversely correlated to the thickness of this film layer, and is relatively high due to the layer's small size (Brody and Yager 1997).

The overall mass transport coefficient k_{ov} ($m\ s^{-1}$) includes both the induced diffusion within and on both sides of the membrane, and is calculated with the resistance in series model:

$$k_{ov} = \left(\frac{1}{k_R} + \frac{1}{k_m} + \frac{1}{k_P}\right)^{-1}, \qquad \text{Equation 4.6}$$

where k_R and k_P are the external mass transport coefficients ($m\ s^{-1}$) in the retentate and permeate respectively (Kreulen et al. 1993). Hence, transport through the membrane can be described by substituting this transfer coefficient in Equation 4.4:

$$N_i = \frac{v \cdot \left(C_{P,i} - C_{R,i} \cdot e^{\frac{v}{k_{ov,i}}}\right)}{1 - e^{\frac{v}{k_{ov,i}}}}, \qquad \text{Equation 4.7}$$

where the permeate and retentate concentrations now correspond to the bulk concentrations in each channel.

By altering the convective flow v through the membrane, the flux of each component changes accordingly. The degree of this change for the individual components determines the selectivity of the separation.

4.3 MATERIALS AND METHODS

4.3.1 CHEMICALS

Analytical grade purity sugars – D(+)-glucose, (D+)-sucrose, and (D+)-raffinose – were supplied by Sigma-Aldrich (Milwaukee WI, USA). Demineralized water was obtained from a Millipore Milli-Q water system (Billerica MA, USA). Acetonitrile was purchased from Biosolve (Valkenswaard, the Netherlands).

4.3.2 MEMBRANES

Two manufacturers, namely Fisher Scientific (Landsmeer, the Netherlands) and Stork Veco (Eerbeek, the Netherlands), supplied the membranes used in this study. Table 4.1 lists the membranes of this study, and their specifications.

Table 4.1 Properties of the membranes that were used in this study.

Name	Material	Manufacturer	Pore size / MWCO	Thickness
Spectra/Por 3	Cellulose	Fisher Scientific	3500 MWCO	25 µm
Veco Micro	Nickel	Stork Veco	4±0.5 µm	25 µm
Veco Micro S	Nickel	Stork Veco	0.2±0.02 µm	130 µm

4.3.3 MEMBRANE MICROFLUIDIC DEVICE

Vink Kunststoffen (Didam, the Netherlands) supplied Polyvinylchloride (PVC) and polycarbonate (PC) plates. Structures of 80.6 cm length, 500±10 µm width were milled on one side of two 2.00 mm thick 5.0 cm by 10 cm of the PVC plates. For the milling, we used a MAHO MH 800 E computer controlled numerical control mill (Pfronten, Germany) with HOLEX cutter 20 1640 of 500 µm (Pfronten, Germany).

The membranes were cut to size and soaked in demineralized water in order to remove any preservative material. The membranes were wetted and directly incorporated by stacking the PVC layers (see Figure 4.1). The milled structure in a layer was aligned to the milled structure in the other layer. This alignment created two microchannels separated by a membrane. Ten screws, which went through the

drilled screw holes in the two layers, held the PVC layers in position. Two 1.0 cm thick PC bottom and top covers, supported by a stainless steel window, clamped the layers – this sealed the device. We called this assembly a membrane microfluidic device.

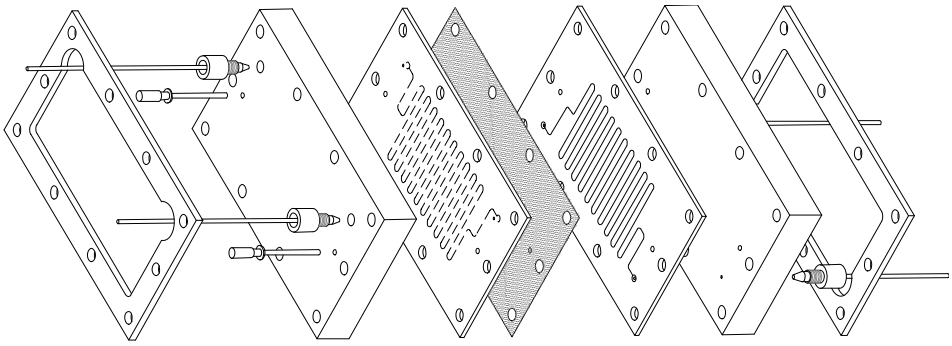

Figure 4.1 Schematic drawing of the membrane microfluidic device. From left to right: stainless steel windows, polycarbonate (PC) layer, polyvinylchloride (PVC) layer with microchannels, membrane, PVC layer with microchannels, PC layer, and stainless steel window. The arrows near the PC layers indicate the inlets and outlets.

Four devices were fabricated, having microchannels with a depth of 50±10 μm, 100±10 μm, 150±10 μm, and 200±10 μm respectively.

4.3.4 EXPERIMENTAL SETUP

The stock solution contained 25.0 mM of each of the sugars – glucose, sucrose, and raffinose – in demineralized water. Just before the experiments, the stock solution and water were degassed for 30 min at 30 °C in a Branson Sonic Power Company 5210 sonification bath (Danbury, USA). Both inlets of the microfluidic device were connected to SGE syringes (Austen, Australia), which were placed in a Harvard Apparatus Pump 33 syringe pump (Holliston, USA), see Figure 4.2. In the device, the smoothest – usually glossy – surface of asymmetrical membranes was always oriented towards the channel connected to Inlet 2. This inlet was fed with the stock solution containing the sugars, whereas Inlet 1 was fed with demineralized water. The feeds were either co-currently brought together, as depicted in Figure 4.2, or

counter-currently brought together – which means that Outlet 1 and Inlet 1 were switched.

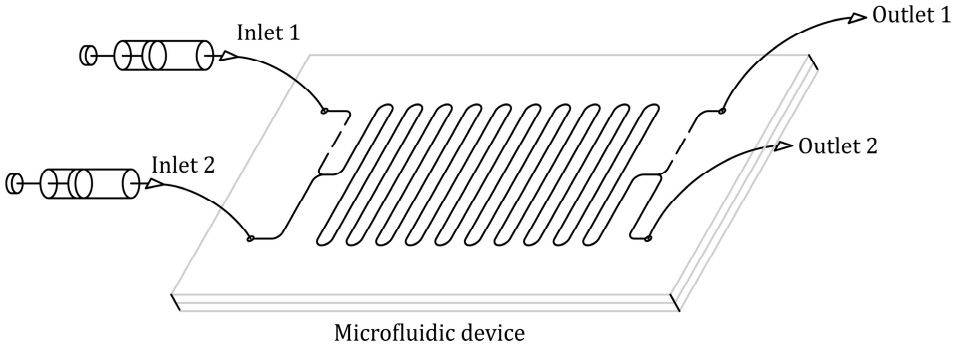

Figure 4.2 Schematic representation of the experimental setup. For co-current flow, Inlet 1 was fed with water, and Inlet 2 was fed with the stock solution containing the sugars. For counter-current flow, Inlet 1 and Outlet 1 were switched.

Both inlets were set at equal flow rates in the range of 5 µl min^{-1} to 100 µl min^{-1}. However, in some experiments, the permeate to retentate flow rate was, instead of one, set up to a ratio ranging from 0.25 to 3. Unless stated otherwise, we used a channel depth of 100 µm. Furthermore, all experiments were carried out at a room temperature of 25 °C to 30 °C and repeated three times.

4.3.5 SAMPLING AND ANALYSIS

For each experiment, we collected the samples after flushing the reactor at 500 µl min^{-1} for 0.5 min, and subsequently at the corresponding flow rate. The concentration of each of the sugars was quantitatively determined by isocratic HPLC from Thermo Separation Products (United Kingdom). The HPLC was equipped with an Alltech Lichrosphere 5 µm NH2 100A amino column (Deerfield, USA). At 40 °C and a flow rate of 1.5 ml min^{-1}, the column was eluted with 80 volume% acetonitrile and 20 volume% demineralized water. For detection, we used a Shodex refractive index detector (Munich, Germany).

With the measured concentrations, we could determine the membrane rejection, selectivity, and yield. The rejection was defined as:

$$1 - C_P/C_R\,; \qquad \text{Equation 4.8}$$

the selectivity of glucose or sucrose with respect to raffinose was defined as:

$$1 - C_{P,raffinose}/C_P\,; \qquad \text{Equation 4.9}$$

and the yield was defined as:

$$C_P/(C_P + C_R). \qquad \text{Equation 4.10}$$

4.4 RESULTS AND DISCUSSION

We used three key parameters to illustrate and compare the results of our diffusion-based separation experiments – these were rejection, selectivity, and yield. Firstly, we investigated the effects of flow rate on these parameters at different channel depths. Secondly, we compared these effects with those obtained with the more commonly used Spectra/Por dialysis membrane. Furthermore, we studied how the ratio of permeate to retentate flow rate could affect the results of our experiments. Lastly, we conducted a counter-current diffusion-based separation with the Spectra/Por membrane.

In this first section, Figure 4.3 to Figure 4.5 show the values of our key parameters as function of flow rate at channel depths of 100 µm and 200 µm for the Veco Micro membrane. Figure 4.3, the first figure, shows the rejection of the sugars glucose, sucrose, and raffinose as function of retentate (or equal permeate) flow rate. Figure 4.3a shows that the rejection was almost zero for glucose at the lowest flow rate of 10 µl min^{-1}, and reached a maximum of 0.47 for raffinose at the highest flow rate of 50 µl min^{-1}. However, Figure 4.3b shows a minimum rejection of 0.11 for glucose and maximum rejection of 0.78 for raffinose at the corresponding flow rates for a channel depth of 200 µm. Nota bene, a twice as high flow rate in a 200 µm deep channel compared to the flow rate in a 100 µm deep channel yielded the same residence time in the channel. The fact that the rejection increased with increasing flow rate, and thus decreasing residence time, confirmed that the retentate and permeate streams were kept – at least partially – separated by the membrane – which thereby allowed for diffusion-based separation.

The pores of the Veco Micro membrane had a diameter of 4 µm, which was large enough to allow each sugar to pass unhindered – which means that diffusion could occur rapidly at these small dimensions. Hence, the differences between Figure 4.3a and Figure 4.3b can mostly be ascribed to diffusion effects in the fluid channels itself, and probably less to the membrane.

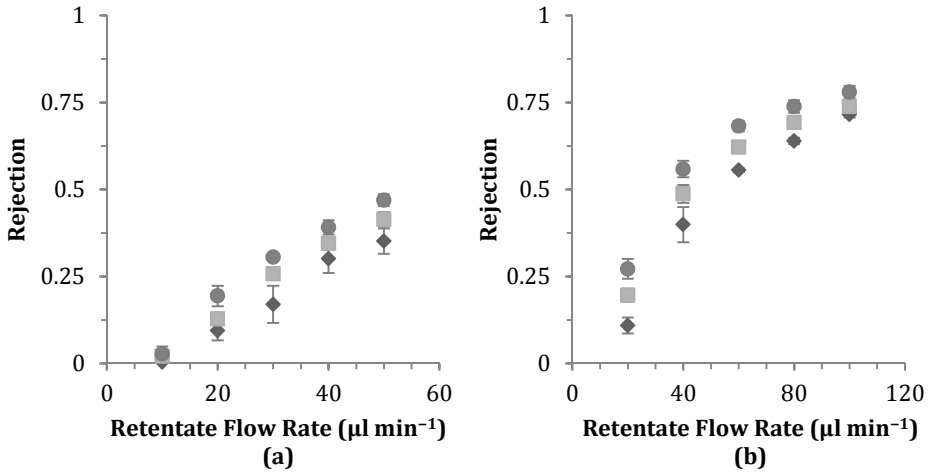

Figure 4.3 Rejection of glucose (♦), sucrose (■), and raffinose (●) as function of flow rate in the membrane microchannel device with Veco Micro membrane at 100 µm (a) and 200 µm (b) channel depth. The error bars indicate the sample standard deviation.

Interestingly, the channel depth also affected the selectivity of glucose and sucrose with respect to raffinose, see Figure 4.4. As mentioned earlier, the membrane was not expected to be responsible for diffusion restriction due to its large pores. Consequently, this figure shows the maximum obtainable selectivity with diffusion-based extraction alone. Note that we could still obtain a remarkable selectivity. For instance, the selectivity for glucose at a channel depth of 100 µm was between 0.04 and 0.13, whereas for a channel depth of 200 µm this selectivity was between 0.12 and 0.20. Such selectivities will yield at least an enrichment of glucose in a solution containing glucose and raffinose. How much glucose in effect can be obtained in such an enrichment step is indicated by the yield parameter. Figure 4.5 shows the values for each sugar for this parameter as function of flow rate with our separation.

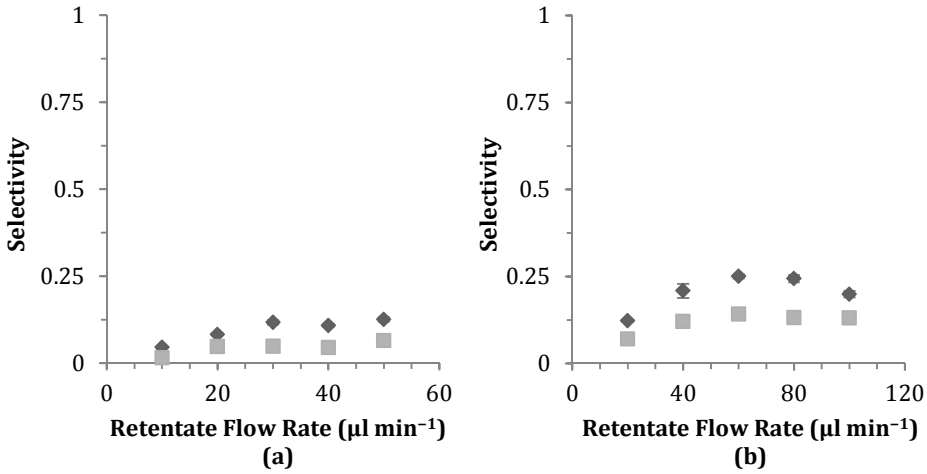

Figure 4.4 Selectivity of glucose (♦) and sucrose (■) with respect to raffinose as function of flow rate in the membrane microchannel device with Veco Micro membrane at 100 µm (a) and 200 µm (b) channel depth. The error bars indicate the sample standard deviation.

According to the definition in the Materials and Methods section, the yield can reach a maximum of 0.5 at permeate flow rates equal to the retentate flow rates. At low flow rates, this theoretical maximum was almost obtained. Thus, the permeate and retentate flows were almost at chemical equilibrium. Figure 4.5b shows that at a channel depth of 200 µm, the yields were slightly lower than those obtained at a channel depth of 100 µm. Due to the decreasing residence time, and the dependence of the amount of molecular diffusion on this residence time, the yield decreased as function of flow rate.

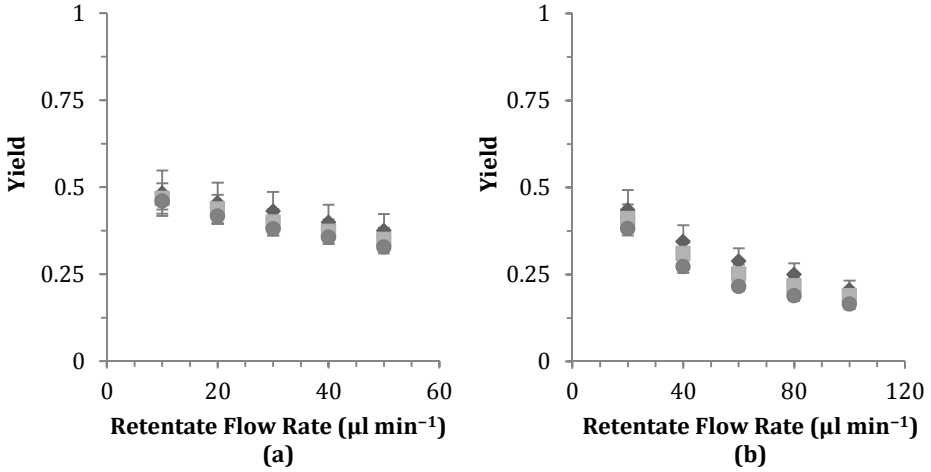

Figure 4.5 Yield of glucose (♦), sucrose (■), and raffinose (●) as function of flow rate in the membrane microchannel device with Veco Micro membrane at 100 µm (a) and 200 µm (b) channel depth. The error bars indicate the sample standard deviation.

Although we obtained high yields with the thin Veco Micro membrane, the rejections were marginal, especially at the smallest channel depth of 100 µm. The relatively large pores of this membrane allowed for convective transport to easily occur – thereby mixing up permeate and retentate streams. The Spectra/Por membrane had the same approximate thickness as the Veco Micro membrane (25 µm), but it had a higher resistance to convective mass transport. The Spectra/Por was therefore an interesting membrane to compare with. Figure 4.6 shows the rejection and yield as function of flow rate for this membrane at a channel depth of 200 µm.

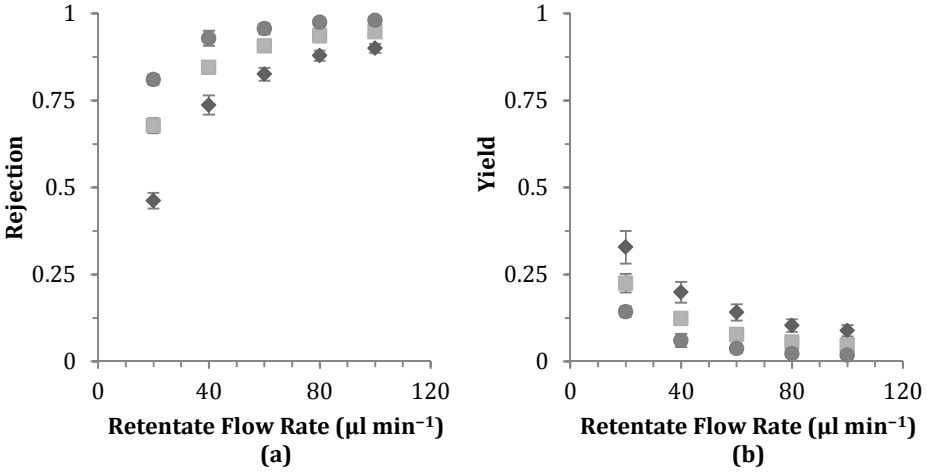

Figure 4.6 Rejection (a) and yield (b) of glucose (♦), sucrose (■), and raffinose (●) as function of flow rate in the membrane microchannel device with Spectra/Por 3 membrane at 200 µm channel depth. The error bars indicate the sample standard deviation.

Similar to Figure 4.3b, Figure 4.6a shows that the rejection increased as function of flow rate. However, the rejections obtained with the Veco Micro membrane were consequently lower at corresponding flow rates. The rejection of raffinose in Figure 4.6a almost approaches the theoretical limit of one – meaning that no raffinose diffused through this membrane towards the permeate side. Theoretically, increasing the flow rate even more would asymptotically yield rejections of one for all sugars. Of course, the yield as indicated by Figure 4.6b will be dramatically low as a result. Even at the lowest flow rate, the yield of glucose was only 0.33 – approximately 66% of the maximum.

It is apparent that the rejection, selectivity, and yield are coupled. However, how these are affected by the flow rate depends on the properties of the membrane. In particular, the selectivity was an interesting parameter to optimize against yield. Changing the ratio of permeate to retentate flow rate provided insight in the convection-diffusion process occurring in our membrane microchannel device. Figure 4.7 to Figure 4.9 show how the rejection, yield, and selectivity depended on

this ratio. The first of these figures shows that the rejection as function of ratio enabled us to obtain similar trends as with rejection as function of flow rate.

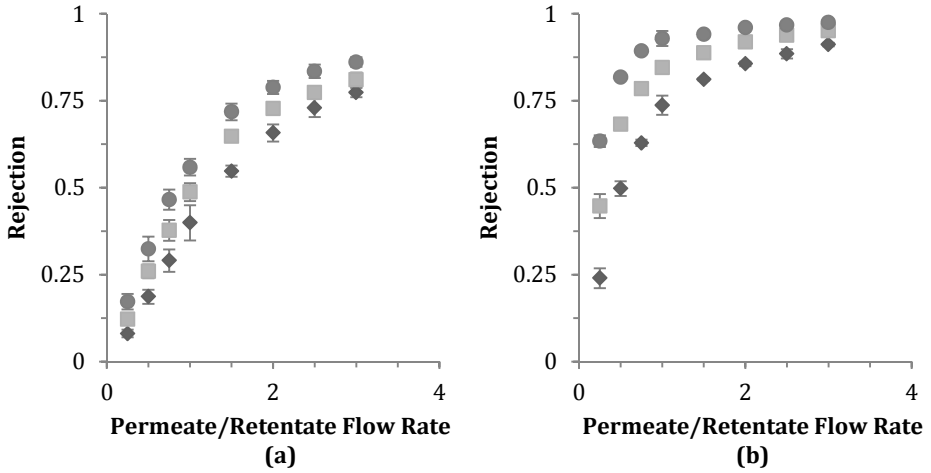

Figure 4.7 Rejection of glucose (◆), sucrose (■), and raffinose (●) as function of the ratio of permeate to retentate flow rate in the membrane microchannel device with Veco Micro membrane (a) and Spectra/Por 3 membrane (b) at 200 µm channel depth. The error bars indicate the sample standard deviation.

Figure 4.7a shows that with the Veco Micro membrane, we could almost cover the complete theoretical range of rejection values from zero to one by varying the ratio of permeate to retentate flow rate from 0.25 to 3.0 µl min^{-1}. Figure 4.7b shows that this was also the case with the Spectra/Por membrane. With this membrane, the obtained rejections varied from 0.24 for glucose to 0.97 for raffinose.

As with the rejection as function of ratio, any desirable yield could also be obtained as function of ratio. Both Figure 4.8a and Figure 4.8b show that the yield decreased as function of ratio. After all, increasing the ratio also dilutes the permeate flow, thus the yield decreased correspondingly to its definition. More important was the effect on the selectivity, see Figure 4.9. In this figure, we could observe distinguishable trends between the Veco Micro and the Spectra/Por membrane.

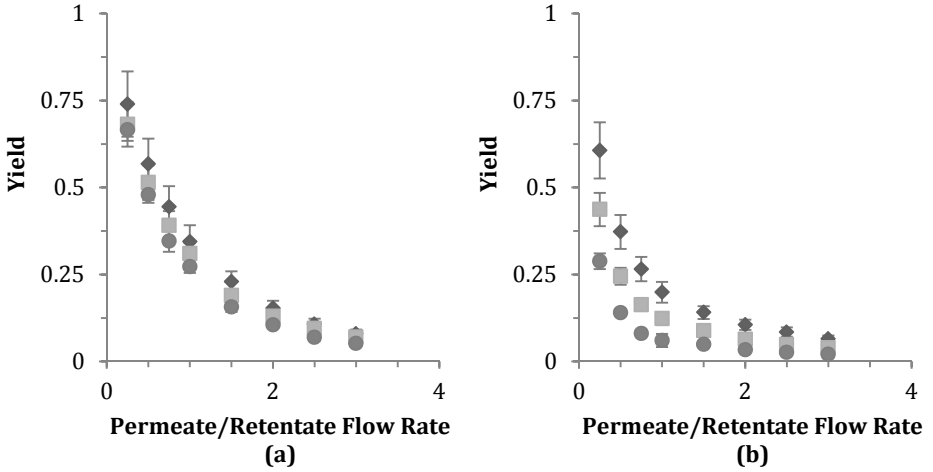

Figure 4.8 Yield of glucose (♦), sucrose (■), and raffinose (●) as function of the ratio of permeate to retentate flow rate in the membrane microchannel device with Veco Micro membrane (a) and Spectra/Por 3 membrane (b) at 200 µm channel depth. The error bars indicate the sample standard deviation.

Figure 4.9a shows that increasing the ratio of permeate to retentate flow rate yielded an increasingly higher selectivity. This selectivity ranged from a minimum of 0.10 to a maximum of 0.35. We could observe a similar trend with the Spectra/Por 3 membrane, as shown in Figure 4.9b. However, the difference between the minimum and the maximum of the selectivity was significantly smaller: from a minimum of 0.52 to a maximum of 0.62. Moreover, from a ratio of one and higher, the selectivity remained rather constant for the latter membrane.

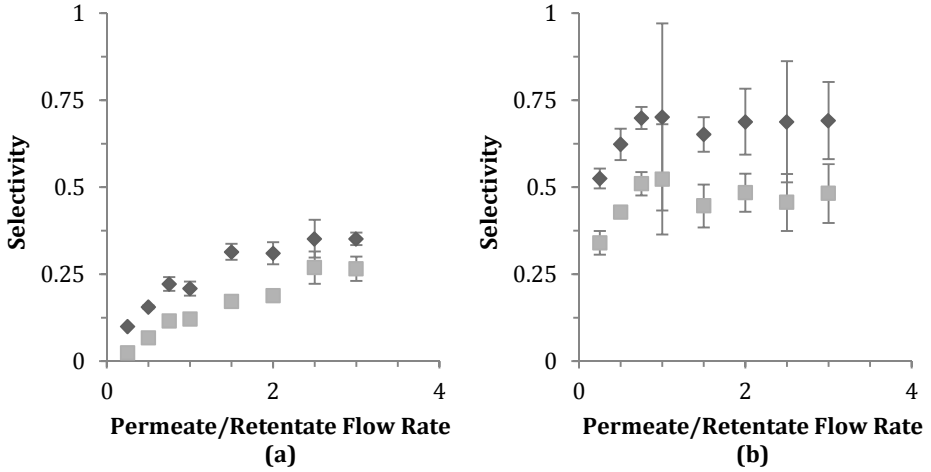

Figure 4.9 Selectivity of glucose (♦) and sucrose (■) with respect to raffinose as function of the ratio of permeate to retentate flow rate in the membrane microchannel device with Veco Micro membrane (a) and Spectra/Por 3 membrane (b) at 200 µm channel depth. The error bars indicate the sample standard deviation.

The cause of the differences between Figure 4.9a and Figure 4.9b can be ascribed to what extent convective transport was limited by the membranes. In particular, this convective transport is quite fundamental to diffusion-based membrane separations. When the membrane virtually blocks convective transport, higher ratios will only dilute the permeate flow. As a result, the yield will decrease as shown by Figure 4.8b. If, however, the membrane only partially limits – thus allows for a small amount of – convective transport, slowly diffusing components will at a point not be able to reach the permeate flow due this momentum diffusion in the opposite direction. In our case, this meant that raffinose could almost be excluded from the permeate flow. Figure 4.9a would in that situation show a selectivity that asymptotically reaches one. Although our experiments show that such an asymptote was not reached, compared to the maximum selectivity of 0.21 for glucose at a ratio of one, we managed to increase the selectivity up to 0.35 for glucose at a ratio of three. Furthermore, the ratio can be altered to obtain acceptable selectivities with acceptable yields by optimizing the selectivity against yield (see Figure 4.9a and Figure 4.8a). In such a way, depending on the

requirements, this separation method can enrich streams with desired components.

We used the fact that convective transport was limited by the Spectra/Por 3 to conduct a rather uncommonly used flow configuration on microscale: microfluidic counter-current separation. Contrary to co-current flow, we can maintain a constant chemical potential difference between the retentate and permeate flows over the entire length of the microchannel with counter-current flow. While a yield of maximum 50% can be obtained with a co-current flow, this counter-current flow can theoretically yield 100%. Figure 4.10a & b show the rejection and yield as function of flow rate for the counter-current contacting of the retentate and permeate streams. Note that, while the flows had opposite directions, they had equal velocities.

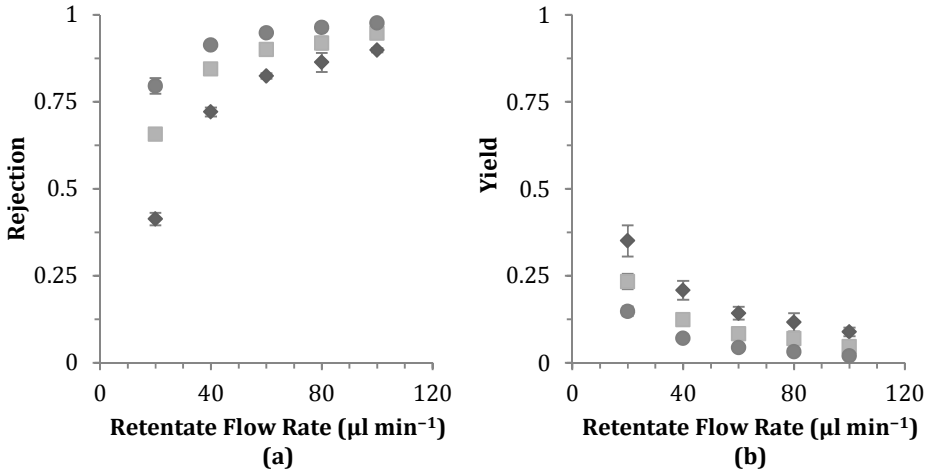

Figure 4.10 Rejection (a) and yield (b) of glucose (♦), sucrose (■), and raffinose (●) as function of flow rate in the membrane microchannel device with Spectra/Por 3 membrane at 200 µm channel depth in counter-current configuration. The error bars indicate the sample standard deviation.

Similar to Figure 4.6, Figure 4.10 shows the characteristic increase of rejection and decrease of yield as function of flow rate. The differences between both figures are marginally visible. However, the yield, as shown in the latter figure, was

structurally higher. For instance, at a flow rate of 20 µl min^{-1}, the maximum yields of glucose, sucrose, and raffinose were 0.33±0.047, 0.22±0.022, and 0.14±0.015 with the co-current, and 0.35±0.045, 0.23±0.016, and 0.15±0.013 with the counter-current separation. These results support the notion that counter-current flow maintains a higher averaged chemical potential difference over the length of the microchannel device, and therefore we obtained higher yields.

The results from the counter-current experiment suggest that counter-current flow can be successfully performed when the appropriate membrane is selected. For example, the Veco Micro membrane was as well tested for counter-current separation. However, the high transmembrane pressure due to this type of separation resulted in convective transport through the large pores of this membrane – consequently, the flows were immediate mixed. Hence, the rejection was always zero. By using the Veco Micro S membrane with smaller pores, we thought that we could reduce this effect. After all, this membrane had pores of only 0.2 µm – a factor 20 reduction of the pore size. However, in contrast to the Veco Micro, this Veco Micro S membrane had rectangular pores instead of round ones. The consequence was that, due to capillary motion, fluids moved transverse to the flow direction out of the membrane microchannel device. Thus, the desired data could not be collected. As a conclusion, we suggest to further investigate counter-current separation with Veco Micro sheets, which have smaller but round pores. The Veco Micro sheets are extremely thin, inert, and rigid, which makes them good candidates for diffusion based separation.

4.5 CONCLUSIONS

The presented separation of sugars was based on the differences between their diffusivities. These differences were only marginal – all sugars had a diffusion coefficient of the same order of magnitude. The performance of this separation was quantified by the parameters rejection, selectivity, and yield. These parameters were affected by the use of different membranes. By disallowing convective transport, the selectivity could be decoupled from the ratio of permeate to retentate flow. However, in cases when higher selectivities were desired, coupling of the selectivity to the ratio by allowing convective transport increased the selectivity significantly. We concluded that an appropriate membrane for diffusion-based membrane separation should balance the requirements of convective and diffuse transport and corresponding yields and selectivities, but be thin enough to allow for fast diffusion. We show that, when the membrane limits convective transport, counter-current diffusion-based separation is perfectly possible, as opposed to such a separation in a microcontactor without a membrane. Based on these results, we suggest to further investigate the use of the Veco Micro membranes with smaller pores for a counter-current diffusion-based separation process.

Our results show that even with membranes that have pore sizes orders of magnitude larger than the components to separate, we could achieve single step enrichment of a component. Although we specifically aimed at sugars in our study, diffusion-based separation is generally applicable to any diffusing component – regardless of its diffusivity or concentration. In particular, this separation technique is interesting for enrichment of streams – having good selectivities and high enough yields.

5

EFFECT OF DIFFUSION ON ENZYME ACTIVITY IN A MICROREACTOR

ABSTRACT

To establish general rules for setting up an enzyme microreactor system, we studied the effect of diffusion on enzyme activity in a microreactor. As a model system, we used the hydrolysis of *ortho*-nitrophenyl-β-D-galactopyranoside by β-galactosidase from *Kluyveromyces lactis*. We found that the Michaelis-Menten kinetic parameters were similar at the microscale and bench scale. With residence times below a few seconds, diffusion effects limited the reaction rate and therefore reduced the conversion per volume of enzyme microreactor. The critical residence time where diffusion limits the conversion increased quadratically with channel width, increased with enzyme concentration, and decreased with substrate concentration. These general rules can be used for choosing parameters when setting up an enzyme microreactor system. To use an enzyme microreactor efficiently, diffusion effects should be taken into account.

This chapter has been published as: Swarts JW, Kolfschoten RC, Jansen MCAA, Janssen AEM, Boom RM. 2010. Effect of diffusion on enzyme activity in a microreactor. Chemical Engineering Journal 162(1):301-306. Elsevier has granted permission to reproduce the material of this publication.

5.1 INTRODUCTION

Over the years, microreactors have been credited with many advantages over conventional systems. Due to their small internal dimensions, the diffusion of heat and mass can be very rapid. Furthermore, their limited use of chemicals and energy can reduce cost and lessen environmental impact.

Enzymes have been used in microfluidic systems to catalyze the production of very specific molecules. In the 1990s, enzyme microreactors were first used for enzyme assays (Cohen et al. 1999; Hadd et al. 1997). Enzyme microfluidic systems were also used to determine enzyme kinetics (Lee et al. 2003; Ristenpart et al. 2008; Srinivasan et al. 2002; Swarts et al. 2008), screen enzymes in droplets (Song and Ismagilov 2003; Zheng and Ismagilov 2005), and to investigate temperature effects on enzyme activity (Arata et al. 2005; Mao et al. 2002) and study cascaded enzymatic reactions (Lee et al. 2003; Mao et al. 2001; Wang et al. 2001).

The reaction rate of an enzyme is determined by its activity and the availability of the substrate at the enzyme's active site. In a system where the substrate has to bridge a large distance to the active site, the effective reaction rate could be limited. Due to the small dimensions, typically 10 μm to 100 μm , microreactors could reduce these diffusional limitations of enzymes.

The effect of diffusion on enzyme activity was studied as early as in the 1960s by Lilly and co-workers (Hornby et al. 1968; Lilly and Hornby 1966; Sharp et al. 1969). That work focused on the effect of diffusion on the enzyme activity of β-galactosidase and ficin immobilized on membranes. The effect of diffusion on enzyme activity in microreactors was discussed in some papers. The diffusion limitation on the effective enzyme activity was hinted by Kanno et al. (2002), but was not investigated. Maruyama et al. (2003) did investigate the effect of diffusion, but they used an excess of enzyme to make diffusion dominant. More recently, Ristenpart et al. (2008) investigated enzyme kinetics in a microsystem with both diffusion and reaction limitation. Their article focused on the rapid extraction of

kinetic data from experimental results, rather than on estimating the effect of the limitation.

In our research, we investigated the effect of diffusion limitation on the β-galactosidase catalyzed cleavage rate of *ortho*-nitrophenyl-β-D-galactopyranoside (*o*-NPG) in a microreactor. We chose this reaction as a model system; it results in *ortho*-nitrophenol (*o*-NP), a yellow substance, and galactose, which is colorless. First, the kinetics of this reaction were determined at the bench scale and microscale and were compared. Second, the reaction was tested under diffusion limiting circumstances in a microreactor. Finally, the effect of diffusion combined with a reaction was studied using computer models and theoretical parameters. The results from this research show the conditions under which the short diffusion paths in microreactors eliminate diffusion limitation in an enzymatic reaction.

5.2 THEORY

In the enzyme microreactor discussed in this paper, a Y-shaped junction brings a substrate and an enzyme solution into a single laminar flow reaction channel. Figure 5.1 depicts this reaction channel schematically. A flow with enzyme and a flow with substrate enter the left side of the rectangle. Even though the two laminar streams in the microchannel do not mix by convection, there is molecular diffusion between them. Substrate and enzyme start to diffuse over the boundary between the two aqueous flows. The substrate is a smaller molecule, so it diffuses more quickly into the enzyme stream. The enzyme diffuses much more slowly into the substrate stream. The curved lines indicate the theoretical fronts of the diffusing molecules.

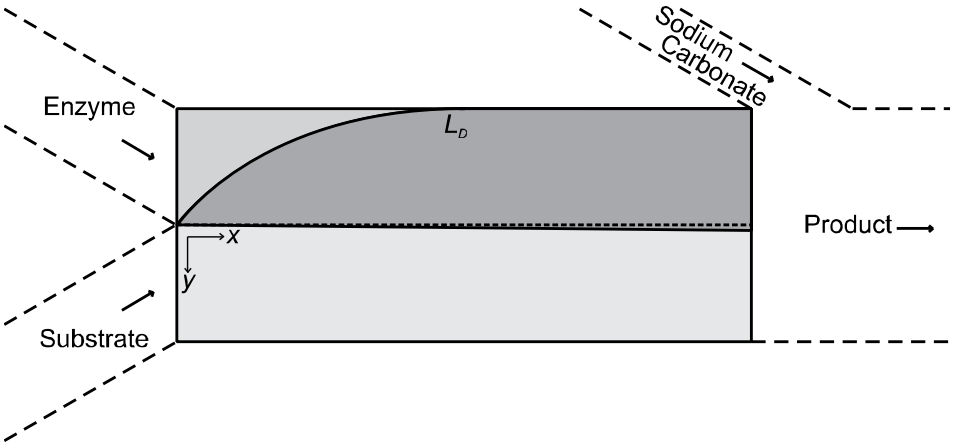

Figure 5.1 Schematic diffusion profiles of substrate (bottom to top) and enzyme (top to bottom) in the microreactor. The dotted line indicates the original position of the interface; L_D indicates the position in x-direction where diffusion of substrate is complete. Dashed lined indicate the supplying and exiting channels not taken into consideration for calculations.

The reaction takes place at locations where both substrate and enzyme are present, indicated by the dark gray area in Figure 5.1. From position L_D onwards in the x-direction, the substrate has distributed more or less evenly over both streams and the enzyme reaction should be at its kinetically determined rate over

the whole width of the channel. The position of L_D relative to the total reaction channel length is an indication of the importance of diffusion limitation, resulting in a significantly lower product concentration at the exit of the channel. In the extreme case that diffusion is very fast compared to the other processes (i.e. the reaction mixture is ideally mixed at $t = 0$ s); the analytical solution, shown in Equation 5.1, should apply:

$$K_m \cdot \ln \frac{[S]_0}{[S]_0 - [P]_t} + [P]_t = V_{max} \cdot [E] \cdot t. \qquad \text{Equation 5.1}$$

In this equation, K_m is the Michaelis-Menten constant (mM), $[S]_0$ is the initial substrate concentration (mM), $[P]_t$ is the product concentration at residence time t (mM), V_{max} is the maximum enzyme reaction rate (µmol s^{-1} g $enzyme^{-1}$), $[E]$ is the enzyme concentration (g enzyme m^{-3}), and t is the residence time (s).

The second Damköhler number (Da_{II}), a dimensionless number, is often used to express the ratio of diffusion time to reaction time. Although the use of this number has been proposed for enzyme microreactor systems (Kockmann et al. 2004), it is not used extensively:

$$Da_{II} = \frac{t_D}{t_r} = \frac{y^2}{D} \cdot \frac{v_0 \cdot [E]}{[S]_0}, \qquad \text{Equation 5.2}$$

$$t_D = \frac{y^2}{D}, \qquad \text{Equation 5.3}$$

$$t_r = \frac{[S]_0}{v_0 \cdot [E]}. \qquad \text{Equation 5.4}$$

In Equation 5.2, t_D is the characteristic time needed for diffusion (s), t_r is the characteristic reaction time (s), y is the diffusion distance (m), v_0 is the initial reaction rate (µmol s^{-1} g $enzyme^{-1}$), and D is the diffusion coefficient (m^2 s^{-1}). Equation 5.2 is composed of the parts of Equation 5.3 and Equation 5.4. Equation 5.2 assumes that the reaction will continue at a zero-order initial rate. By inserting the Michaelis-Menten kinetic equation in the Damköhler number we obtain:

$$Da_{II} = \frac{t_D}{t_r} = \frac{y^2}{D} \cdot \frac{v_{max} \cdot [S] \cdot [E]}{(K_m + [S]) \cdot [S]} = \frac{y^2}{D} \cdot \frac{V_{max} \cdot [E]}{(K_m + [S])}. \quad \text{Equation 5.5}$$

Equation 5.5 is again built up from the characteristic diffusion times (Equation 5.3) and reaction times:

$$t_r = \frac{(K_m + [S])}{V_{max} \cdot [E]}. \quad \text{Equation 5.6}$$

The calculations of the characteristic diffusion times (Equation 5.3) and reaction times (Equation 5.6) indicate how parameters influence the ratio between the two. For instance, a high enzyme concentration leads to a low characteristic reaction time and consequently to less kinetic limitation.

Over the course of a reaction, conversion progresses, and the substrate concentration decreases. As a result, the value of Da_{II} calculated using Equation 5.5 is not constant as opposed to the value calculated using Equation 5.2. With very low substrate concentrations, the reaction rate approaches zero. A full conversion, as assumed in the Da_{II} number, will only be reached after an infinitely long time.

To avoid complication due to the 100% conversion assumption, we propose a critical time as an alternative to the Da_{II} number. We calculated the ratio of the product concentration exiting the microreactor including diffusion (from numerical models) to the concentration without diffusion limitation (from Equation 5.1) at various residence times. For the critical time, we chose the residence time at which this ratio is 0.9. This critical time is an indicator of the effect of diffusion on reactor efficiency.

5.3 MATERIALS AND METHODS

5.3.1 CHEMICALS

The β-galactosidase from *Kluyveromyces lactis* (in solution, ≥ 3000 U mL^{-1}), *ortho*-nitrophenol (*o*-NP, 98%), potassium phosphate (99%), and sodium carbonate (99%) were purchased from Sigma-Aldrich (Milwaukee, WI). The *ortho*-nitrophenyl-β-D-galactopyranoside (*o*-NPG) was obtained from Fluka (Steinheim, Germany). The cobalt (II) chloride (hexahydrate) was purchased from ICN Biomedicals Inc. (Aurora, OH). Milli-Q water (Millipore, Billerica, MA) was used for the experiments discussed in this study.

5.3.2 EXPERIMENTS ON BENCH SCALE

At 23 °C, two 150 mL buffer solutions were mixed in a 500 mL stirred vessel with baffles and a 3-blade propeller type stirrer at 350 rpm. Both buffers contained 25 mM of sodium phosphate, 15 µm cobalt chloride, and were set to pH 7.3 using sodium hydroxide. One buffer contained β-galactosidase at a concentration of 0.2 g L^{-1}. The other buffer contained *o*-NPG at concentrations varying from 1 mM to 20 mM. During the first 2 min to 4 min, 0.5 mL samples were taken and mixed with 0.5 mL 1% (w/w) sodium carbonate. Addition of sodium carbonate resulted in a hundredfold lower activity (results not shown), which ensured no significant reaction after sampling. The concentration of *o*-NP was measured with a spectrophotometer at 420 nm. The linear part of the *o*-NP concentration vs. time plots (9 to 11 samples, $R^2 > 0.995$) was used to calculate the initial enzyme activity.

5.3.3 EXPERIMENTS ON MICRO SCALE

The micro scale enzymatic reaction was carried out at room temperature (20 °C to 22 °C). The two aqueous streams were combined on-chip. The microchannels were on average 83 µm wide and 40 µm deep and were isotropically etched in a microchip by Micronit (Enschede, The Netherlands). A schematic view of the chip

is shown in Figure 5.2. The total microchannel volume on-chip was 0.113 µL. An in-house constructed PEEK chip holder facilitated the connections between the chip and capillaries, which supplied the fluids. These fused silica capillaries from Bester (Amstelveen, the Netherlands) have a 50 µm diameter and were connected to SGE 1 mL luer lock syringes (Austin, TX). The syringes were placed in Harvard Apparatus Pico Plus 11 syringe pumps (Holliston, MA).

The enzyme solution (approximately 0.2 g L^{-1}) and the substrate solution (*o*-NPG concentration varying from 1 mM to 20 mM) were prepared with a 25 mM potassium phosphate buffer with 15 µm Co^{2+} set to pH 7.3. The two solutions were placed on the same syringe pump and consequently pumped at the same rate. The solutions (shown at the left in Figure 5.2) were combined at a 1:1 volumetric ratio. Just before exiting the chip, this stream was joined by a 1% (w/w) sodium carbonate in Milli-Q stream (top-right in Figure 5.2). The combined enzyme and substrate flow was matched with this carbonate solution in a 1:1 volumetric ratio. Due to the inhibiting effect of sodium carbonate (even at fairly low concentrations) and the relatively fast diffusion (shorter diffusion distance due to the compressing of streams and the small molecule), reaction stoppage was assumed to be instantaneous. The enzyme diffuses into the substrate domain much more slowly than the substrate into the enzyme domain, and in almost every case, an enzyme molecule would move from an area with both enzyme and substrate to another area with both enzyme and substrate. Therefore, the net effect on activity was negligible.

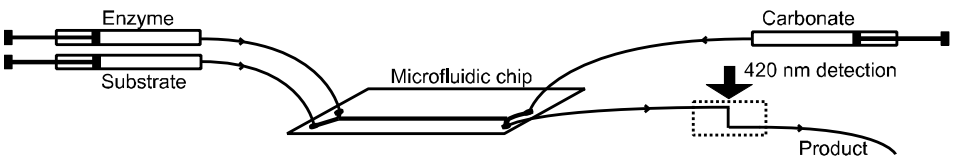

Figure 5.2 Schematic representation of the experimental set-up; enzyme and substrate are combined on-chip, at the end of the reaction channel, sodium carbonate is added to stop the reaction. All fluids exit the channel and pass through a *z*-shaped cell for detection at 420 nm.

In most cases, the Reynolds number of the fluid was below unity. Depending on the flow rates and position in the system, it varied from approximately 0.02 to 25. With these values, laminar flow could be assumed. Therefore, the dominant type of mixing was by means of molecular diffusion. In practice, there are some limitations to using very high flow rates. For instance, the pressure in the system could become very high. This could result in leakage at connections. Furthermore, depending on the size of the channels and the viscosity of the more gas-like fluids, the Reynolds number could become too high to assume laminar flow and simple mixing by diffusion. However, this latter case is very unlikely for fluids.

The reaction mixture exited the chip through a fused silica capillary, which was connected to a LC Packings U-Z View capillary flow cell (Sunnydale, CA). The total post-chip volume until detection was 0.8 µL to 1.2 µL. This flow cell was placed in an UltiMate UV-VIS detector from Dionex (Sunnydale, CA) and had a 10 mm light path for accurate measurements. The measured absorbance at 420 nm was correlated to the o-NP concentration. The *o*-NP concentration was plotted against the residence time (inversely proportional to the flow rate), and from the linear part of this graph the initial activity was calculated.

Two methods were used to investigate the effect of diffusion limitation on enzyme reactions in practice. In the first method, the original 83 µm wide microchannel was used, but both the enzyme concentration and the flow rates were increased by a factor of 10. A second method was to increase the time needed for diffusion by using a wider microchannel. The same fluids as with the kinetic experiments were pumped through microchannels with effective channel widths of 183 µm and 283 µm.

5.3.4 COMPUTER MODELS

Two-dimensional numerical models were constructed to calculate the concentration of all components at any position in the channel. The models were constructed with COMSOL Multiphysics from COMSOL (Burlington, MA). Similar to

Figure 5.1, two rectangular shapes sharing one long side were used to represent the domains of the two aqueous streams. As both streams were laminar and had the same flow rate, we could assume that the fluids would stay in their initial domains. All other components (*o*-NPG, *o*-NP, galactose, and β-galactosidase) were free to diffuse over the interface between the two domains.

The two rectangular fluid domains were 41.5 μm wide (equal to the real effective diffusion distance) and 2 mm long. The real length of the channel was 34 mm. Assuming constant volumetric flow rate, the superficial fluid velocity was scaled proportionally to the ratio between the real length and the model length. The diffusion coefficients *D* of all diffusing components in water were calculated using the Wilke-Chang equation (Wilke and Chang 1955). These coefficients were 0.64×10^{-9} m^2 s^{-1} for *o*-NPG, 0.94×10^{-9} m^2 s^{-1} for *o*-NP, 0.85×10^{-9} m^2 s^{-1} for galactose, and 0.047×10^{-9} m^2 s^{-1} for β-galactosidase.

The reaction was modeled using Michaelis-Menten kinetics and parameters from microscale experimental results. Combinations of substrate concentration and initial activity were fitted to Michaelis-Menten kinetics using Athena Visual Studio V12.0 (Athena Visual Studio, Naperville, IL).

5.4 RESULTS AND DISCUSSION

5.4.1 ENZYME KINETICS

Kinetic experiments were conducted at room temperature at both bench scale and microscale. Microscale experiments were conducted at slightly lower temperatures than at bench scale (by approximately 2 °C). As the results will show, this did not affect the enzyme activity very much. Figure 5.3 shows the initial activities from experiments and the fitted model on microscale (Figure 5.3a) and bench scale (Figure 5.3b). The activity is expressed as the number of micromoles produced per second per gram of the original enzyme solution. The kinetic parameters obtained from these fitted models are summarized in Table 5.1.

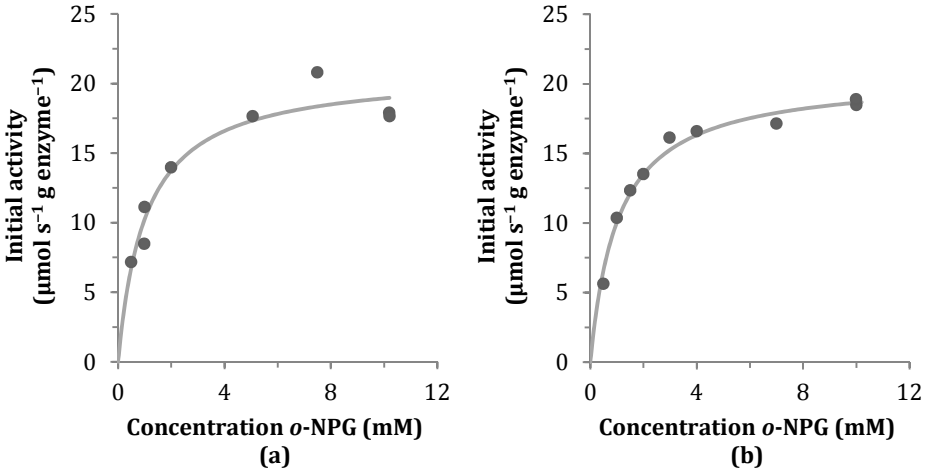

Figure 5.3 Initial β-galactosidase activity as function of the *o*-NPG concentration on (a) microscale and (b) bench scale, symbols indicate experimental findings, drawn lines indicate model based on fitted kinetic parameters.

Figure 5.3 shows that for increasing substrate concentrations, the enzyme activity increases. The initial steep slope of the activity vs. substrate curve and the subsequent leveling off is consistent with Michaelis-Menten kinetics. The values for K_m are somewhat lower, but in the same range as those from the literature; Cavaille and Combes (1995) and Dickson et al. (1979) both reported a K_m of about

1.7 mM. The values for the kinetic parameters as presented in Table 5.1 are very close for both experimental scales.

Table 5.1 Kinetic parameters and 95% confidence interval determined from microscale and bench scale experimental results.

Parameter	Microscale	Bench scale
V_{max}	20.9±2.3 μmol s^{-1} g $enzyme^{-1}$	20.6±1.0 μmol s^{-1} g $enzyme^{-1}$
K_m	1.04±0.45 mM	1.05±0.21 mM

Figure 5.4 shows the product concentration in the microchannel with increasing residence times. The results from the numerical COMSOL model were compared to the analytical solution of Equation 5.1. Figure 5.4 shows that the numerical results generally correspond to the analytical solution. With increasing residence times, the product concentration increases. Eventually, the *o*-NP concentration levels off at 3 mM, which corresponds to 100% conversion. Only at residence times below 10 s, the two models give different results, due to diffusion limitation. The results from experiments to determine the kinetic parameters in Figure 5.3a, were typically obtained at residence times of around 30 s. Figure 5.4 shows that ignoring the effect of diffusion limitation at these concentrations yields a 2% overestimation of the conversion. At these residence times, this overestimation is negligible, but it becomes significant at higher flow rates (i.e. smaller residence times).

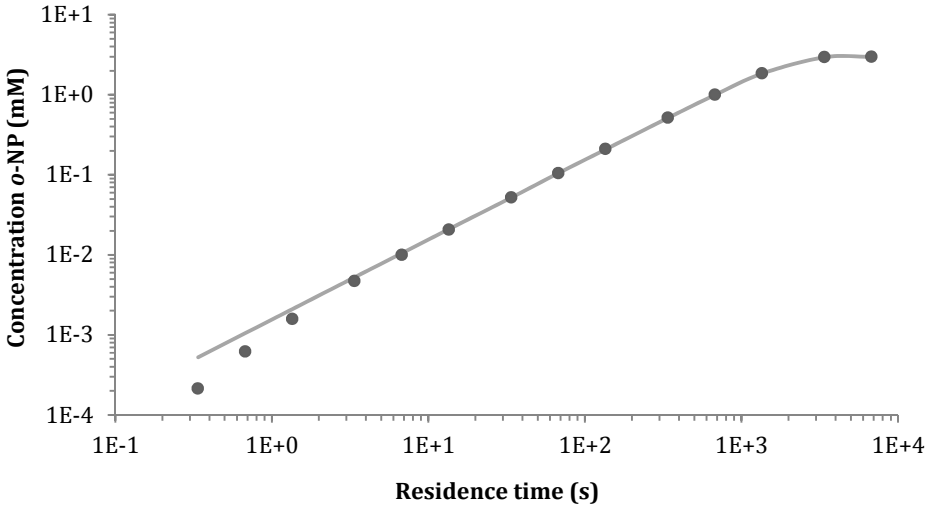

Figure 5.4 Concentration of *o*-NP from the numerical COMSOL model (symbols) and the analytical equation (line) at different residence times.

5.4.2 DIFFUSION LIMITATION IN ENZYME MICROREACTORS

Two methods were employed to investigate the effect of diffusion on product concentration: the use of wider micro channels and the combination of a high enzyme concentration with high flow rates. Figure 5.5 shows the effect of micro channels of 183 µm (Figure 5.5a) and 283 µm (Figure 5.5b). Figure 5.5a & b show the increasing product concentration with increasing residence times, as obtained from the analytical solution (Equation 5.1), the numerical model, and experiments. The analytical solution yields much higher product concentrations than either the experiments or the numerical solution, indicating diffusion limitation in the latter two cases. The numerical and experimental results are in agreement, indicating that the lower concentrations are indeed caused by diffusion limitation. The models can therefore be used to investigate the effect of diffusion.

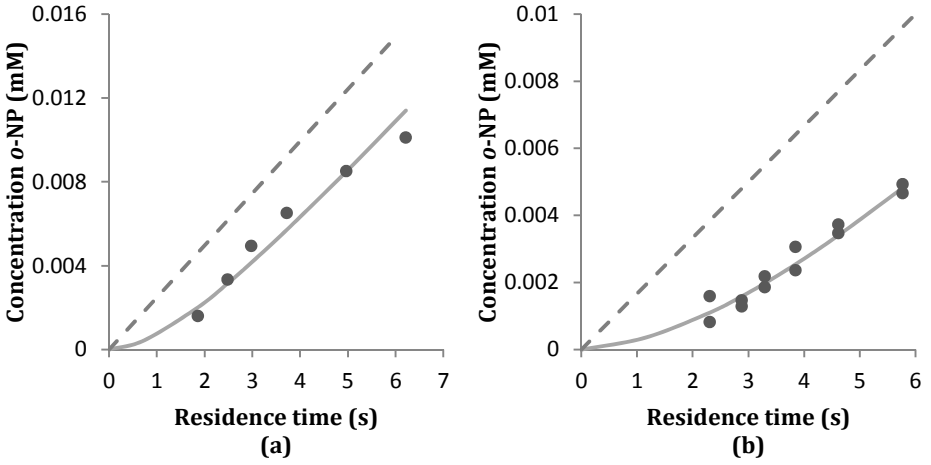

Figure 5.5 The *o*-NP (product) concentration as function of the residence time; the dashed line represents the analytical solution, the solid line the numerical solution, and the symbols are the experimental results. The widths of the microchannels are: (a) 183 μm and (b) 283 μm.

As shown in Figure 5.5a & b, diffusion limitation clearly increased with wider channels, which was expected. The maximum diffusion distance in this microchannel is half the channel width. By increasing the channel width from 83 μm to 183 μm and 283 μm, the characteristic diffusion time increased by a factor of 4.9 and 11.6 (quadratically, according to Equation 5.3), while the total reaction volume increased linearly by factors of 2.2 and 3.4, respectively.

Similar results were obtained by using the original 83 μm wide channels with a tenfold higher flow rate and enzyme concentration. This means that in the right-hand term of Equation 5.1, V_{max} is constant, $[E]$ is 10 times higher, and t is 10 times lower. In absence of diffusion limitation, the product concentration should be the same. However, Figure 5.6 shows that diffusion limitation is important at all residence times (albeit relatively more important at lower residence times). This effect was predicted by the numerical model, which shows that diffusion limitation indeed is the cause of the reduction in product concentration.

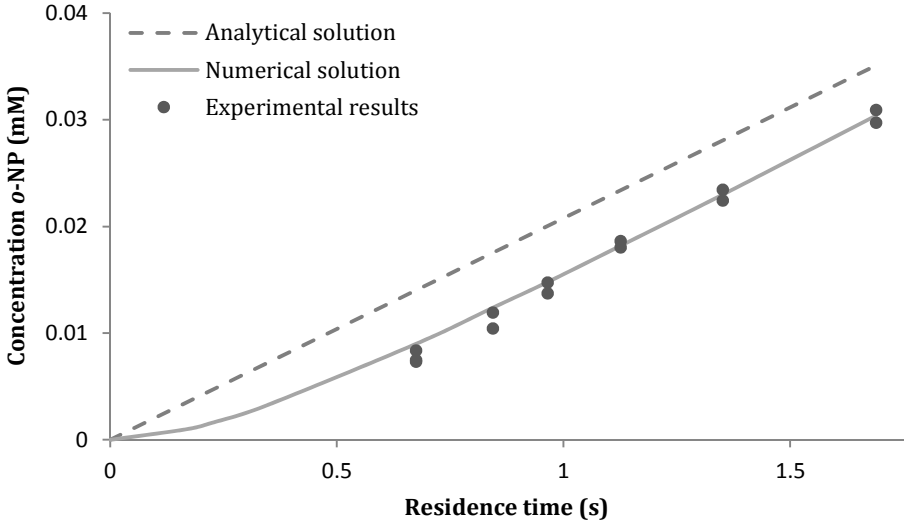

Figure 5.6 The *o*-NP (product) concentration as function of residence time; dashed line for analytical solution, solid line for numerical solution, and symbols for experimental results. Microchannel with a width of 83 μm. The enzyme concentration is 10 times higher than in the experiments shown in Figure 5.4 and Figure 5.5.

The numerical models correspond well with experimental results, as was shown in Figure 5.5 and Figure 5.6. We could therefore use these models to study the effect of the system parameters on the critical time, where diffusion caused a 10% reduction in product concentration. The enzyme reaction was kept the same, but parameters such as channel width and enzyme and substrate concentrations were varied to investigate the contribution of diffusion under these circumstances. Figure 5.7 shows the results of variation of the model parameters.

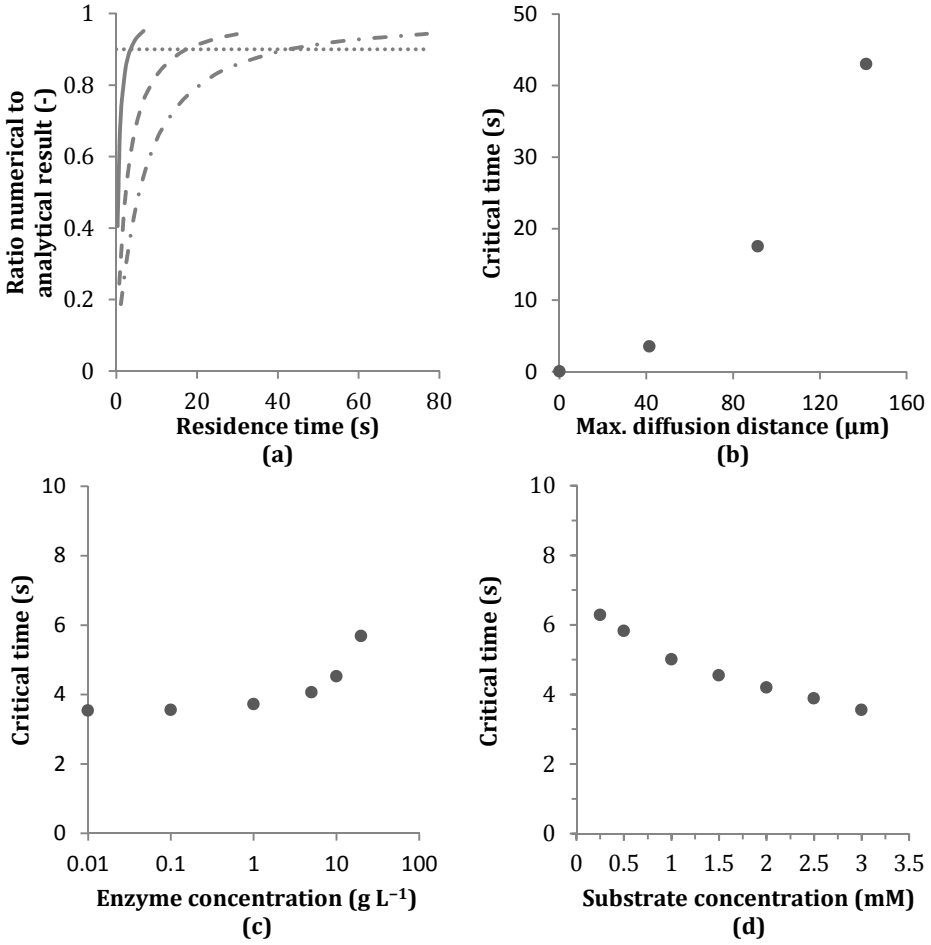

Figure 5.7 Standard reaction conditions of 83 µm wide channel, 1 g L^{-1} enzyme, and 1 mM substrate were varied, one parameter each time. (a) Effect of different channel widths; the ratio of product concentration from numerical models to analytical solution is plotted against the residence time for different channel widths (solid line is 83 µm, dashed line is 183 µm, dash-dot-dashed line is 283 µm), (b) effect of different channel widths; critical time at which this ratio is 0.9 vs. maximum diffusion distance (equal to half the channel width), (c) critical time vs. enzyme concentration on a logarithmic scale, and (d) critical time vs. substrate concentration.

Figure 5.7a shows the efficiency of the system (the ratio is from numerical and analytical calculations; it is an indicator of diffusion limitation). As a residence time approaches 0 s, the substrate and enzyme are completely separated, and the efficiency is zero. At longer times, a uniform distribution of all components is

obtained, and the actual reaction rate becomes equal to the intrinsic reaction rate. The efficiency therefore approaches one.

Figure 5.7a shows that with increasing channel widths it takes longer to approach the analytical result. To illustrate this, Figure 5.7b shows the critical time, when the numerical result is 90% of the analytical result. This is shown as a gray dotted line in Figure 5.7a. Here, diffusion effects caused a 10% limitation on the effective reaction rate. This critical time was plotted against the maximum diffusion distance in the micro channel, which is the distance the substrate has to travel to the enzyme (equal to half the channel width).

The effect of a wide range of enzyme concentrations on the critical time is shown Figure 5.7c. The critical time is fairly constant at 3.5 s to 4 s up to an enzyme concentration of 1 g L^{-1}. At higher enzyme concentrations, the critical time slightly increases to about 6 s. At low enzyme concentrations (< 1 g L^{-1}), diffusion is apparently fast enough to supply the enzyme with substrate. At higher enzyme concentrations, the reaction is faster, leading to local depletion of substrate. At very high enzyme concentrations (100 g L^{-1} and higher), any substrate would be converted very quickly. The analytical solution gives a 99% conversion in slightly more than 2 s. Consequently, the critical time would no longer be an expression of diffusion limitation.

Figure 5.7d shows the effect of substrate concentration on the critical time. At low substrate concentrations, the critical time was high; with increasing concentrations, the critical time decreased. When we only looked at diffusion of the substrate, different substrate concentrations did not change the shape of the theoretical diffusion front (curved line in Figure 5.1). At the diffusion front, the concentration started to become non-zero, reaching the bulk concentration towards the original substrate channel. This concentration profile is similar to an error function. When we included reaction, the shape of the front changed, depending on this reaction.

Comparing the results of Figure 5.7b-d with the Da_{II} number from Equation 5.2, and its corresponding characteristic diffusion and reaction time from Equation 5.3 and Equation 5.6, we can see similarities and differences. Figure 5.7b shows that with increasing diffusion distances, the critical time increases quadratically, as does the Da_{II} number due to the increased diffusion time (Equation 5.3). The Da_{II} number thus also predicts more diffusion limitation with an increased channel width.

According to Equation 5.6, the enzyme concentration should correspond inversely to the extent of diffusion limitation. However, numerical studies (Figure 5.7c) showed an increase of the critical time, i.e. an increase in diffusion limitation, after a nearly constant level at the beginning. Initially, the enzyme concentration and the total reaction rate were so low that the critical time was purely diffusion driven. With increasing enzyme concentrations, substrate was depleted around the enzyme and caused a lower reaction rate per gram of enzyme due to Michaelis-Menten kinetics.

Again, according to Equation 5.5, the Da_{II} should scale inversely with the term $(K_m + [S])$. A low $[S]$ in Equation 5.6 will result in a lower limit for the characteristic reaction time. When $[S]$ is significant relative to K_m, the characteristic reaction time will be higher. Thus, diffusion limitation at higher substrate concentrations is less likely. Similarly, the critical time from numerical studies (Figure 5.7d) decreased with increasing substrate concentrations.

As the Da_{II} number assumes zero-order kinetics and one-dimensional Fickian diffusion, we expected deviations, with more complex cases. The enzyme we used followed Michaelis-Menten kinetics and diffusion results in a concentration gradient rather than a propagating substrate front with a uniform substrate concentration behind it. The effect of varying parameters on the Da_{II} number corresponded with our numerical findings regarding the channel width and the substrate concentration, but differed regarding the enzyme concentration. The numerical model was a valuable tool added to the use of dimensionless numbers,

as it can deal with non-ideal systems, demonstrated by the variation of the enzyme concentration.

Even though this study focused on Michaelis-Menten kinetics, and some of the relations are only valid for this type of kinetics, we suggest that the approach can be adapted to other kinetics such as ternary-complex or Ping-Pong mechanisms. The approach for both the mathematical derivation and the experimental work will be similar to the work described in this article.

We studied a microreactor under laminar (creep) flow conditions, which implies that mixing by convection does not take place. Many mixing methods have been proposed in microfluidic technology, which would enhance mass transfer. We can however extract general lessons from Figure 5.7b-d. However, we can draw general conclusions from Figure 5.7b to d.

When the goal of using an enzyme microreactor is converting the substrate to products, diffusion limitation is not desirable, as it reduces volumetric productivity (conversion per volume). When the residence time is much higher than the critical time given in this article, the reduction in the efficiency is very small. In contrast, when the residence time is lower than the critical time, the reduction in reactor efficiency is significant (> 10%). Such a significant efficiency reduction is most likely to occur with wide microchannels (Figure 5.7b), high enzyme concentrations (Figure 5.7c), and low substrate concentrations (Figure 5.7d).

5.5 CONCLUSIONS

The hydrolysis of *ortho*-nitrophenyl-β-D-galactopyranoside catalyzed by β-galactosidase from *Kluyveromyces lactis* was shown to follow Michaelis-Menten kinetics on bench scale and microscale. The kinetic parameters on both scales were the same. With the time scales applied during the experiments, the reaction seemed to be unaffected by diffusion limitation. Diffusion limitation was observed with experimental residence times below a few seconds. At these short residence times, the volumetric efficiency of the enzyme microreactor (conversion per volume) decreased. The critical residence time, where diffusion significantly the conversion, increased quadratically with channel width, increased with enzyme concentration, and decreased with substrate concentration. Estimations based on numerical calculations rather than the Da_{II} number can be used in wider range of conditions; it can be used in non-ideal situations. An enzyme microreactor can be run most efficiently when these factors receive appropriate attention.

6

GUIDELINES FOR OPTIMAL DESIGN OF ENZYME MICROREACTORS

ABSTRACT

Enzyme microreactors are used as research tools because of many advantages including low reagent consumption and the general notion that mass transfer restrictions are reduced. The use of microchannels can indeed shorten the characteristic mass transfer time but may also affect the productivity of the microreactor. To what extent mass transfer restrictions affect the reaction rate and the productivity is determined by parameters such as the enzyme properties, operating conditions, and dimensions of the microreactor. This article provides the correlations between these parameters for coflow enzyme microreactors obeying Michaelis-Menten kinetics. These correlations outline the design space based on reduced mass transfer restrictions and maximum productivity respectively. The methodology that yields the design space provides a generic hands-on approach to optimally design coflow enzyme microreactors. This is demonstrated by an example in which a selection should be made between enzymes with different properties.

This chapter has been submitted for publication as: Kolfschoten RC, Swarts JW, Janssen AEM, Boom RM. Guidelines for optimal design of enzyme microreactors.

6.1 INTRODUCTION

In order to reduce mass and heat transfer restrictions in a reactor, its characteristic diffusion distances can be decreased. In large stirred tank reactors this is done by, for example, adjusting the impeller speed and type to reduce the Kolmogorov scale of mixing (Kolmogorov 1941). Miniaturization of reactors in essence achieves the same result by increasing the surface to volume ratios and hence decreasing diffusion distances (Brody and Yager 1997). In general, continuous microreactors, which can be divided into coflow and segmented (Taylor-Couette) flow reactors, are used for this purpose. These miniaturized reactors enable the development of new reactor types and configurations.

The applications of microreactors are broad but can be covered by a limited number of reactor types. Many enzyme microreactor applications use a coflow configuration to contact fluid flows. Commonly such microreactors are referred to as T-sensors, T-shaped microchannels, Y-junction microreactors, and Y-shaped junction microreactors. In order to design these microreactors according to desired characteristics, methodologies for parameter estimation and optimal design have been studied and reported. Holl et al. (1996) reported a method for optimal design for diffusion-based extraction; Kamholz et al. (1999) have developed an analytical model that predicts device behavior from the diffusion coefficients of the reacting components and from the reaction kinetics; Stepánek et al. (1999) studied optimal design and operation of a separating monolith microreactor; Ismagilov et al. (2000) found a scaling relation for the width of the reaction-diffusion zone as function of the axial distance down the microchannel; and Ristenpart et al. (2008) established a scaling relation for Michaelis-Menten reactions to estimate the initial concentration of product as function of the distance along the microchannel.

The referred articles stress the necessity of guidelines for optimal design of microreactors. This article provides a generic design methodology for elaborated parameter estimation of coflow enzyme microreactors from a productivity

perspective. Constraints are provided that enable determination of what can be considered as optimal conditions. Within the design space, optimal microreactor dimensions and operating parameters can be found that correspond to the desired constraints.

6.2 THEORY

We consider microreactors in which a solution containing reactant coming from one inlet, is contacted in coflow with a solution containing an enzyme. Hence, the (low molecular weight) reactant has to diffuse into the stream containing the enzyme, before being converted into the product. In order to overcome mass transfer restrictions, the mass transfer rate of this reactant should be equal to or higher than the maximum enzymatic reaction rate. The ratio of the reaction rate to the mass transfer rate is expressed in the dimensionless second Damköhler number, Da_{II} (-), which is defined by:

$$Da_{II} = \frac{\tau_d}{\tau_r}, \qquad \text{Equation 6.1}$$

where τ_r is the reaction time (s) and τ_d is the characteristic diffusion time (s).

Kockmann et al. have proposed a Da_{II} number for zero-order kinetics enzyme microreactors (Kockmann et al. 2004). Swarts et al. (2010) proposed to include Michaelis-Menten kinetics in this Da_{II} number. Swarts et al. concluded that complete conversion is assumed in the Da_{II} number proposed by Kockmann et al., which will only be reached after an infinitely long time. To avoid complications due to the assumption of complete conversion, Swarts et al. (2010) proposed a critical time as an alternative to the Da_{II} number. They defined the critical time as the residence time at which the ratio of the observed reaction rate to the reaction rate without mass transfer restrictions equals 0.9. This ratio is known as the effectiveness η (-):

$$\eta = \frac{observed\ reaction\ rate}{reaction\ rate\ without\ mass\ transfer\ restrictions}. \qquad \text{Equation 6.2}$$

In the case of an ideal microreactor, mass transfer restrictions do not affect the reaction time. Hence, Equation 6.2 ideally equals one, meaning that there are no mass transfer restrictions.

When there are no mass transfer restrictions transverse to the flow direction, the flow type of the coflow microreactor corresponds to plug flow. The unsteady-state mass balance of a plug flow microreactor obeying Michaelis-Menten kinetics is described by:

$$\frac{dS}{dt} = -\frac{V_{max} \cdot E + S}{K_M + S}, \qquad \text{Equation 6.3}$$

where S is the substrate concentration (mol m^{-3}), t the time (s), V_{max} the maximum enzyme reaction rate (mol s^{-1} kg enzyme^{-1}), E the enzyme concentration (kg enzyme m^{-3}) and K_M the Michaelis-Menten constant (mol m^{-3}) (Doran 2000; Michaelis and Menten 1913). Many enzyme reactions are reasonably well characterized by Michaelis-Menten kinetics. By assuming that the substrate concentration is much higher than the Michaelis-Menten constant, the characteristic reaction time may be estimated by assuming zero-order kinetics. An expression for the whole substrate conversion range with the complete Michaelis-Menten kinetics (being in between zero and first order) can be obtained by integration of Equation 6.3:

$$\tau_r = \frac{S_0 - S + K_M \cdot \ln\frac{S_0}{S}}{V_{max} \cdot E} = \frac{S_0 \cdot \theta_s + K_M \cdot \ln\left(\frac{1}{1-\theta_s}\right)}{V_{max} \cdot E}, \qquad \text{Equation 6.4}$$

where τ_r is the reaction time (s), S_0 is the initial substrate concentration (mol m^{-3}), and θ_s is the conversion of the substrate (-) defined by $(S_0 - S)/S_0$. This expression yields the reaction time when there are no mass transfer restrictions.

The effectiveness is determined by many parameters that relate to diffusional effects in the microreactor. These effects can be described by a general expression for convection parallel to the channel length and diffusion transverse to the convection:

$$v_x \frac{\partial S}{\partial x} = D_s \frac{\partial^2 S}{\partial y^2} - \frac{V_{max} \cdot E \cdot S}{K_M + S}, \qquad \text{Equation 6.5}$$

where v is the fluid velocity (m s^{-1}) and x and y denote values on their respective Cartesian coordinate axes (Bird et al. 1960). Hereby we assume that diffusion of the enzyme is negligible due to its relatively high molecular weight. In dimensionless form, Equation 6.5 can be expressed as:

$$\frac{\partial \sigma}{\partial \xi} = \frac{\partial^2 \sigma}{\partial \zeta^2} - C^2 \cdot \frac{\sigma}{1 + \sigma}, \qquad \text{Equation 6.6}$$

where σ is the dimensionless substrate concentration defined by S/K_M; and ζ is the dimensionless width defined by y/d where d is the channel width (m). The parameter C is a dimensionless constant which is a measure of the width of the channel allowed without having diffusive mass transfer limitation. The parameter is defined as the dimensionless reaction-width:

$$C = \sqrt{\frac{V_{max} \cdot E}{K_M \cdot D_s}} \cdot d. \qquad \text{Equation 6.7}$$

The parameter ξ is a dimensionless spatial coordinate. Taken over the whole channel, the parameter is defined as the dimensionless length of the microchannel:

$$\xi = \frac{D_s}{d^2 \cdot v_x} \cdot L, \qquad \text{Equation 6.8}$$

where L is the channel length (m).

The effectiveness at each conversion can be quantified by calculating the reaction time with Equation 6.4 and by deriving the corresponding observed reaction time from a numerical convection-diffusion model. The correlations between the effectiveness, the dimensionless reaction-width, and the dimensionless length provide the design space for coflow enzyme microreactors. This design space

provides values for C and ξ from which subsequently the optimal values for channel width, residence time, and throughput can be obtained.

The required microchannel width can be calculated by rewriting Equation 6.7:

$$d = \sqrt{\frac{K_M \cdot D_s}{V_{max} \cdot E}} \cdot C. \qquad \text{Equation 6.9}$$

The required residence time, τ_{res} (s), for selected conditions in the design space can be calculated by rewriting Equation 6.8:

$$\tau_{res} = \frac{L}{v_x} = \frac{\xi \cdot d^2}{D_s}. \qquad \text{Equation 6.10}$$

The throughput, T ($m^3\ s^{-1}$) of the microreactor can be calculated by:

$$T = v_x \cdot A \cdot \theta_s = \Phi \cdot \theta_s, \qquad \text{Equation 6.11}$$

where A is the cross sectional area of the microchannel (m^2) and Φ is the volumetric flow rate of both inlets (enzyme solution and substrate solution) combined ($m^3\ s^{-1}$). The throughput is considered to be proportional to the volumetric productivity.

6.3 MATERIALS AND METHODS

The β-galactosidase catalyzed cleavage of *ortho*-nitrophenyl-β-D-galactopyranoside (*o*-NPG) in the coflow microreactor was chosen as a model reaction. The numerical model simulated the two flows that were brought together at a 1:1 volumetric ratio at a Y-shaped junction of a microreactor to flow adjacently in a microchannel (Figure 6.1). One flow contained β-galactosidase at concentrations varying from 1 kg m^{-3} to 10 kg m^{-3}. The other flow contained *o*-NPG at concentrations varying from 1.04 mol m^{-3} to 10.4 mol m^{-3}. The enzymatic reaction in the microreactor yielded the products *ortho*-nitrophenol (*o*-NP) and galactose.

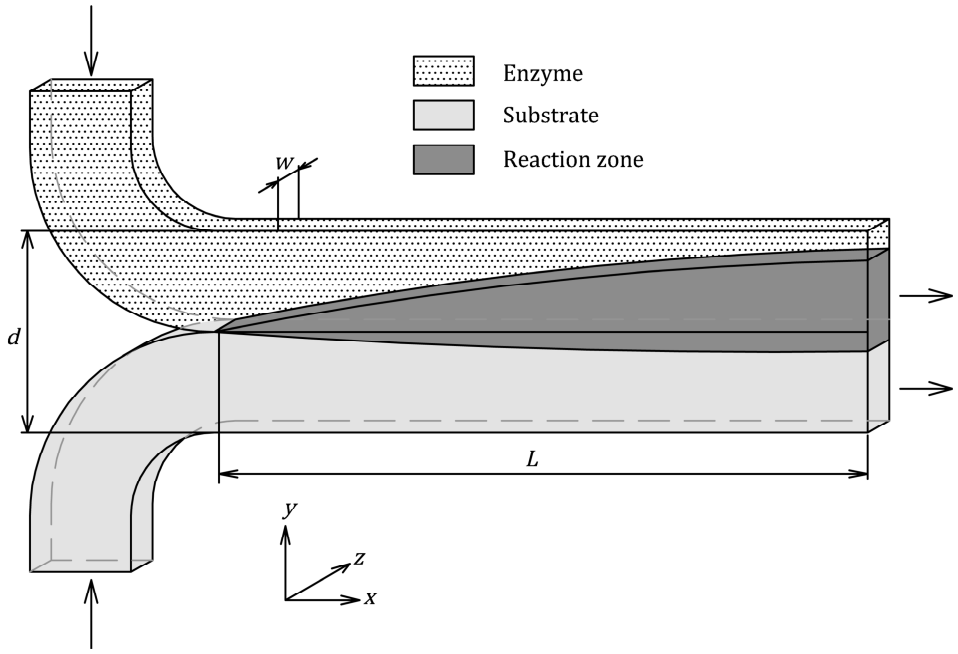

Figure 6.1 Microreactor with Y-shaped junction for co-current flow where the enzyme and substrate solution are brought together into a microchannel. The symbol *d* denotes the microchannel width, *L* the microchannel length, *w* the microchannel depth.

The kinetic parameters of the enzymatic reaction were obtained from research by our group under conditions that eliminated effects of diffusion limitation (Table 6.1).

Table 6.1 Kinetic parameters and 95% confidence interval of micro and bench scale experiments with the β-galactosidase catalyzed cleavage of *o*-NPG. The data is obtained from Swarts et al. (2010).

Parameter	Microscale	Bench scale
V_{max}	20.9±2.3 μmol s^{-1} g $enzyme^{-1}$	20.6±1.0 μmol s^{-1} g $enzyme^{-1}$
K_m	1.04±0.45 mM	1.05±0.21 mM

The numerical model was created using the Chemical Engineering Module of COMSOL Multiphysics (version 3.5a, Burlington, MA). The Incompressible Navier-Stokes and Convection and Diffusion application modes were used to simulate the fluid flows and diffusional transport respectively.

Two rectangular subdomains of 2.75 mm length and 125 μm width represented the microchannel of 34 cm length, 83 μm width, and 40 μm depth, in which the fluids flowed adjacently. The aspect ratio of the microchannel (width divided by length) was ~1:410. To achieve a more favorable meshing, the model was scaled to an aspect ratio of 1:11. The flow regime was laminar according to the low Reynolds numbers, convection could therefore be scaled by scaling the inlet velocity. Diffusion was anisotropically scaled to the corresponding aspect ratio. Convective transport across the interface of the two subdomains was excluded. Diffusional transport was included for *o*-NPG, *o*-NP, galactose and β-galactosidase. Their diffusion coefficients in water were estimated using the Wilke-Chang equation (Wilke and Chang 1955) and yielded 6.4×10^{-10} m^2 s^{-1} for *o*-NPG, 9.4×10^{-10} m^2 s^{-1} for *o*-NP, 8.5×10^{-10} m^2 s^{-1} for galactose, and 0.47×10^{-10} m^2 s^{-1} for β-galactosidase (Swarts et al. 2010).

The simulations by the numerical model were in good agreement with the experimentally obtained results from Swarts et al. (2010) and therefore corroborated the model's validity.

6.4 RESULTS AND DISCUSSION

The design of a coflow enzyme microreactor depends on among other things the activity of the enzyme and the substrate availability. In general, faster reactions require smaller typical system dimensions such as the reactor width, resulting in faster diffusion. A smaller reactor width generally yields reduced mass transfer restrictions and therefore an increased effectiveness. Figure 6.2 shows the effectiveness as function of channel width at 95% substrate conversion with β-galactosidase.

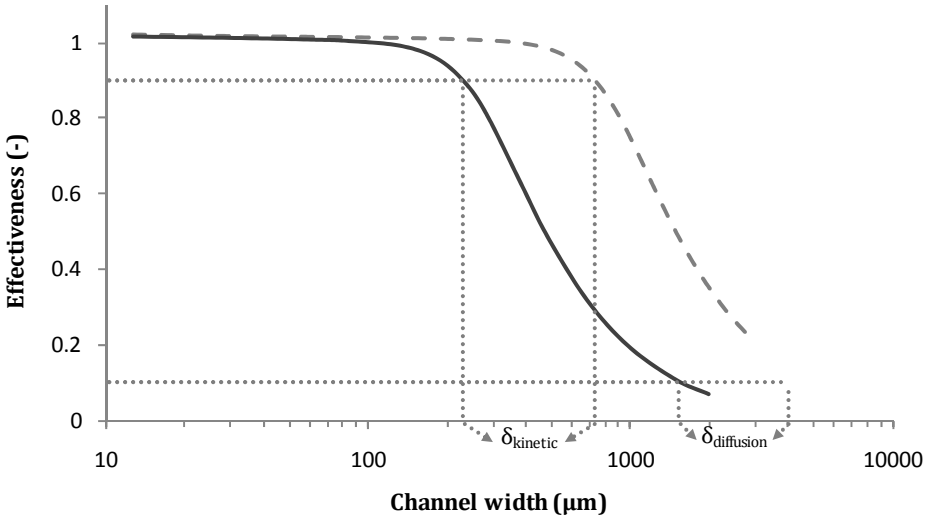

Figure 6.2 Effectiveness as function of channel width at 95% substrate conversion and $S_0/K_M = 10$ in the coflow microreactor with enzyme concentrations of 1 kg m^{-3} (– –) and 10 kg m^{-3} (—) respectively. The dotted lines (···) that intersect with the graph lines indicate an effectiveness of 0.1 and 0.9 and the corresponding diffusion and kinetic limitation widths respectively.

Both lines in Figure 6.2 have a distinctive sigmoid shape and mathematically resemble a Gauss error function. The low enzyme concentration (1 kg m^{-3}) line shows that the effectiveness factor reaches a value of one below a channel width of ~400 μm. The other line of the high enzyme concentration (10 kg m^{-3}) reaches this value below a channel width of ~100 μm. According to Equation 6.2 this means

that there are no mass transfer restrictions that affect the conversion below these channel widths. The characteristic width at an effectiveness of 0.9 resembles the critical time and is defined as the kinetic limitation width ($\delta_{kinetic}$). These widths are depicted in the figure for the low and high enzyme concentration lines and equal ~740 µm and ~230 µm respectively. The kinetic limitation width forms the right boundary of the first out of three regions. In this first region, the reaction is dominated by kinetic limitation: $d \leq \delta_{kinetic}$. Microfluidic devices are interesting because they can operate in this kinetically limited region to overcome mass transfer restrictions.

In the second region, a decline of the effectiveness can be observed. The right boundary of this region at an effectiveness of 0.1 is defined as the diffusion limitation width ($\delta_{diffusion}$). This region is characterized by mixed diffusion and kinetic limitations: $\delta_{kinetic} \leq d \leq \delta_{diffusion}$. For the low enzyme concentration line, the second region starts at a channel width of ~740 µm and ends above ~4.50 mm. For the high enzyme concentration line, this region starts at a channel width of ~230 µm and ends at the diffusion limitation width of ~1.50 mm. The diffusion limitation width marks the end of the second region and the beginning of the third and latter region, which is characterized by dominating diffusion limitation: $d \geq \delta_{diffusion}$.

At extremely short residence times and therefore low substrate conversions, the effectiveness can be lower than 0.9 at channel widths even much lower than the kinetic limitation width. Figure 6.3 shows the effectiveness as function of the substrate conversion with β-galactosidase in a microchannel having a width of 83 µm.

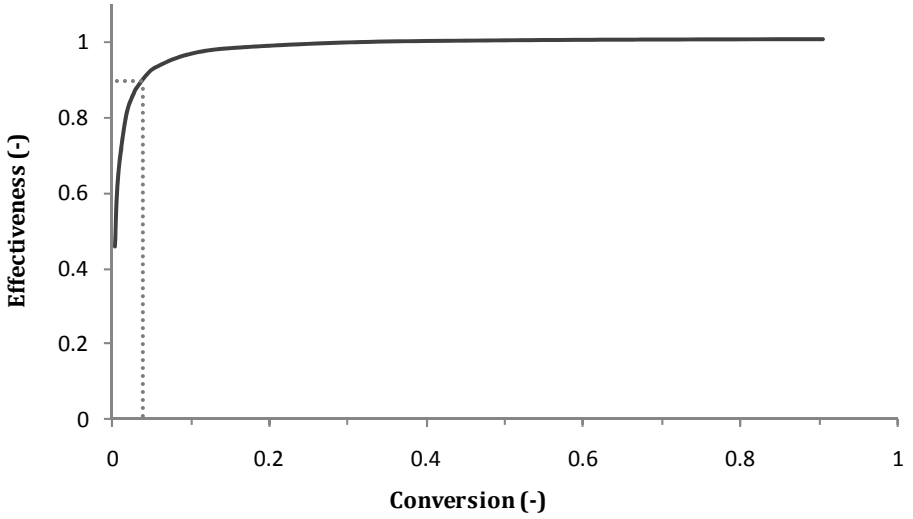

Figure 6.3 Effectiveness as function of substrate conversion in 83 μm wide channel for an enzyme concentration of 10 kg m^{-3} and $S_0/K_M = 10$ (—).The dotted lines (···) that intersect with the graph line indicate an effectiveness of 0.9 and the corresponding substrate conversion from which kinetic limitation is dominating.

Figure 6.3 shows that the effectiveness reaches a value of 0.9 for a large range of substrate conversions from ~4% and higher (indicated by the intersection of the dotted line with the horizontal axis of the figure). This is due to the use of a channel width much smaller than the kinetic limitation width ($d \ll \delta_{kinetic}$). However, the figure shows much lower values for the effectiveness at substrate conversions up to ~4%. Initial rate experiments in microreactors are usually in this conversion range and may therefore significantly underestimate the maximum enzyme reaction rate.

The correlations shown in Figure 6.2 and Figure 6.3 are fundamental for understanding the design of an enzyme microreactor. The figures raise questions such as in what region one would want to operate the microreactor and what conversion is desirable. Hence, the kinetic limitation width and conversion are useful constraints for designing the microreactor. However, the figures show data for one specific reaction under a specific condition. For this reason, the Michaelis-

Menten kinetics in the coflow microreactor were derived in dimensionless form (Equation 6.6). Figure 6.4 shows the dimensionless reaction-width (Equation 6.7) as function of the dimensionless length (Equation 6.8) for an effectiveness of 0.9 (equal to the critical time) at various S_0/K_M ratios and conversions.

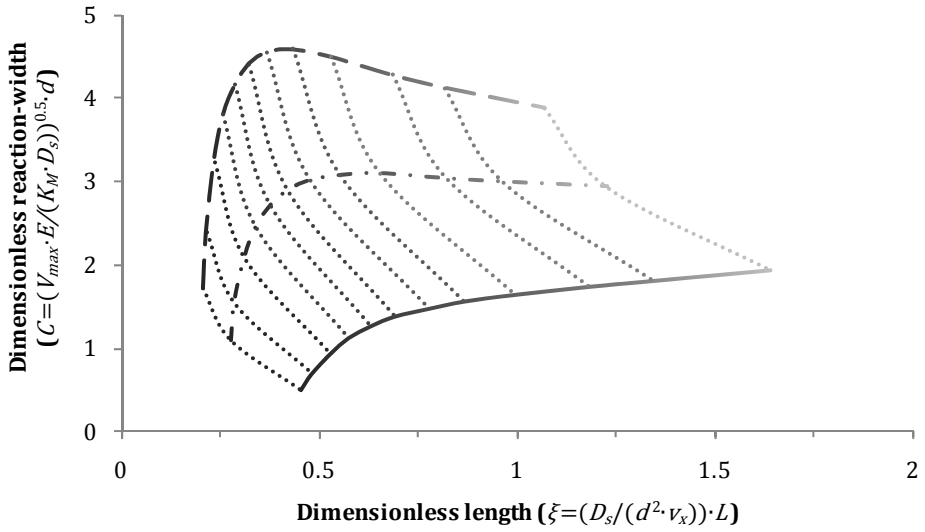

Figure 6.4 The dimensionless reaction-width as function of the dimensionless length for an effectiveness of 0.9 (equal to the critical time) at various S_0/K_M ratios of: 1 (—), 5 (– · –) and 10 (– –); and conversions (···) of (from left to right): 5%, 10%, 20%, 30%, 40%, 50%, 60%, 70%, 80%, 90%, 95% and 99% respectively. The data was acquired with the described COMSOL model.

Figure 6.4 shows three iso-S_0/K_M lines and nine iso-conversion lines. The iso-conversion lines cross the iso-S_0/K_M lines. Their intersections define the conversion ranging from 5% to 99% with an effectiveness of 0.9 at different S_0/K_M values ranging from 1 to 10. The figure provides a generic design space for an effectiveness of 0.9 with coflow enzyme microreactors that obey Michaelis-Menten kinetics within these ranges.

The dimensionless reaction-width is larger for higher S_0/K_M ratios at the same effectiveness of 0.9 as depicted by the iso-S_0/K_M lines. In addition, the figure shows that higher dimensionless lengths yield higher conversions for each iso-

S_0/K_M line. At the iso-S_0/K_M line of 10, the dimensionless reaction-width increases as function of the dimensionless length until 70% conversion; above 70% conversion, the dimensionless reaction-width decreases as function of the dimensionless length. Likewise, the iso-S_0/K_M line of 5 shows an increase of the dimensionless reaction-width as function of the dimensionless length until 80% conversion; above 80% conversion, the dimensionless reaction-width decreases as function of the dimensionless length. The iso-S_0/K_M line of 1 shows that the dimensionless reaction-width always increases as function of the dimensionless length.

The area below each iso-S_0/K_M line yields an effectiveness above 0.9 for the corresponding S_0/K_M values. The area above each iso-S_0/K_M line yields an effectiveness below 0.9 for the corresponding S_0/K_M values. A similar effect occurs with the iso-conversion lines where the area below each iso-conversion line yields lower conversions and the area above each iso-conversion line yields higher conversions. An iso-S_0/K_M line can be followed to the left or right by, for example, tuning the enzyme concentration, flow rate, and/or channel width, to obtain low or high conversions respectively.

An essential feature of Michaelis-Menten kinetics is that the enzyme becomes saturated at high substrate concentrations ($S \gg K_M$). At these concentrations, the reaction rate is zero order with respect to substrate. At low substrate concentrations ($S \ll K_M$), the reaction rate is first order with respect to substrate. Hence, the averaged reaction rate over the course of a reaction is a function of the substrate conversion with a negative direction. For the S_0/K_M value of 1, higher conversions always yield a lower averaged reaction rate. For S_0/K_M values of 5 and 10, low conversions initially yield a constant averaged reaction rate as function of conversion while high conversions yield a lower averaged reaction rate as function of conversion.

The high S_0/K_M values initially yield a high substrate mass flux due to the high driving force for mass transport, which is caused by large concentration gradients.

A higher S_0/K_M value therefore allows for a larger channel width in order to meet the effectiveness criterion of $\eta = 0.9$. A higher conversion implies a longer residence time and therefore, according to the criterion, allows for a longer diffusion time, hence a larger channel width. The initial influence of the substrate flux on the required channel width is highest for the iso-S_0/K_M line of 10, and reduces as function of conversion. This effect in combination with the proportionality between the diffusion time and reaction time, determines the development of the iso-S_0/K_M lines; in this case, this resulted in an optimum for the iso-S_0/K_M lines of 5 and 10. The design optimization of these S_0/K_M values is obtained by keeping the reaction zero order as long as possible.

The optimal microreactor dimensions with respect to the effectiveness can be obtained from the design space in Figure 6.4. In general, this implies a necessity for miniaturization down to relatively small channel widths. Unfortunately, reducing this width also reduces the volumetric flow rate. However, for industrial applications, throughput, which is defined as the volumetric flow rate multiplied with the conversion (Equation 6.11), commonly plays a key role. Microreactors have low absolute throughputs due to their small dimensions. The optimal microreactor dimensions to reach, for example, 95% substrate conversion therefore not only depend on mass transfer restrictions. Figure 6.5 demonstrates this by showing the throughput as function of channel width at 95% substrate conversion with β-galactosidase.

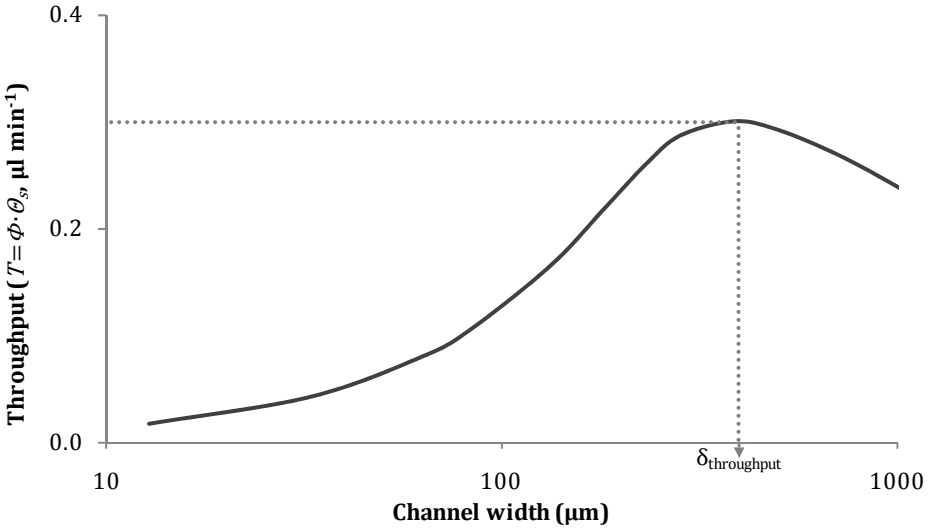

Figure 6.5 Throughput (µl min^{-1}) as function of channel width (µm) at 95% substrate conversion in a coflow microreactor with an enzyme concentration of 10 kg m^{-3} and $S_0/K_M = 10$ (—).The dotted lines (···) that intersect with the graph line indicate the maximum throughput and the corresponding width for maximum throughput.

Figure 6.5 shows that the throughput reaches an optimum at a certain channel width. This channel width is defined as the width for maximum throughput ($\delta_{throughput}$). A channel width larger than the width for maximum throughput yields a reduced throughput. The figure shows that the width for maximum throughput is ~400 µm for this specific reaction. This value is much higher than the kinetic limitation width of this reaction (~230 µm). According to Figure 6.2, the effectiveness of this reaction at the width for maximum throughput is ~0.6; meaning that compared to the kinetic limitation width, the width for maximum throughput yields a reaction with a lower effectiveness.

The optimum of Figure 6.5 can be explained by looking at the extremes of the channel width. The throughput is proportional to the channel width and residence time: $T \sim d/\tau_{res}$. According to Einstein's equation for Brownian motion, the (substrate) diffusion time is proportional to the square of the channel width (Einstein 1905). By definition, the observed reaction time, $\tau_{r,obs}$ (s), will always be

larger than the observed diffusion time, $\tau_{d,obs}$ (s), which is a function of the channel width d. Hence, $\lim_{d\to\infty} d/\tau_{r,obs} = 0$; meaning that the throughput will become zero at an infinitely large channel width. Decreasing the channel width from this extreme will therefore increase the throughput.

At infinitely small channel widths, diffusion of the substrate to the enzyme occurs instantly. However, the reaction is in that case dominated by kinetic limitation (Figure 6.2) yielding a constant observed reaction time (equal to the reaction time obtained from Equation 6.4) as function of channel width. Hence, $\lim_{d\to 0} d/\tau_{r,obs} = 0$; meaning that the throughput will become zero at an infinitely small channel width. Increasing the channel width from this extreme will increase the throughput. In between both extremes for the channel width, a certain channel width will yield an optimal throughput.

Besides the conversion and the kinetic and diffusion limitation widths, the width for maximum throughput can in terms of productivity be a useful constraint for designing the microreactor. For each reaction condition, the width for maximum throughput can be obtained. Figure 6.6 shows the dimensionless reaction-width (Equation 6.7) as function of the dimensionless length (Equation 6.8) for a maximum throughput at various S_0/K_M ratios and conversions.

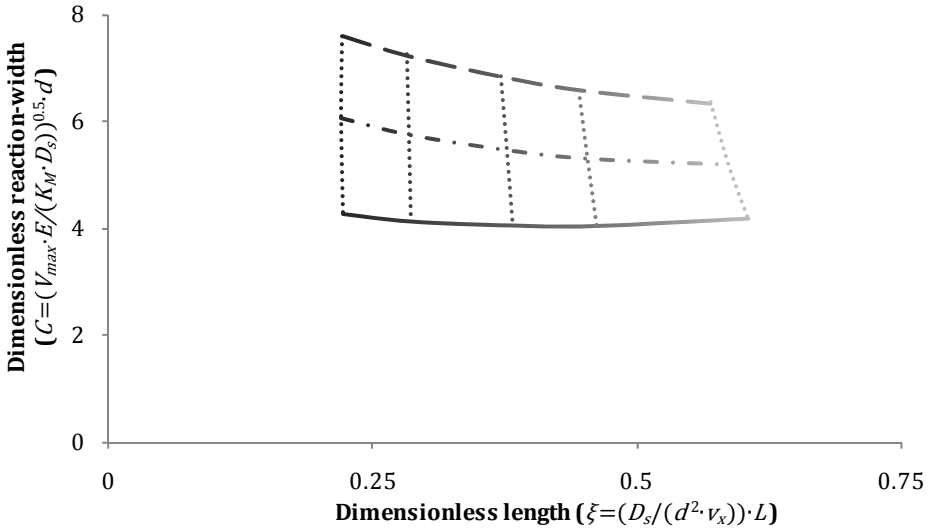

Figure 6.6 The dimensionless reaction-width as function of the dimensionless length for a maximum throughput at various S_0/K_M ratios of: 1 (—), 5 (– · –) and 10 (– –); and conversions (···) of (from left to right): 70%, 80%, 90%, 95%, and 99% respectively. The data was acquired with the described COMSOL model.

Figure 6.6 shows three iso-S_0/K_M lines and five iso-conversion lines. The iso-conversion lines cross the iso-S_0/K_M lines. Their intersections define the conversion ranging from 70% to 99% at different S_0/K_M values ranging from 1 to 10. The figure provides a generic design space for maximum throughput with coflow enzyme microreactors that obey Michaelis-Menten kinetics within these ranges.

The dimensionless reaction-width is larger for higher S_0/K_M ratios for maximum throughput as depicted by the iso-S_0/K_M lines. In addition, the figure shows that higher dimensionless lengths yield higher conversions for each iso-S_0/K_M line. At the iso-S_0/K_M lines of 10 and 5, the dimensionless reaction-width decreases as function of the dimensionless length. The iso-S_0/K_M line of 1 shows that the dimensionless reaction-width first marginally decreases as function of the dimensionless length until 95% conversion. Above 95% conversion, the dimensionless reaction-width marginally increases.

The areas below and above each iso-S_0/K_M line yield a lower throughput for the corresponding S_0/K_M values. The area at the left of each iso-conversion line yields lower conversions and the area at the right of each iso-conversion line yields higher conversions. Furthermore, each S_0/K_M value in Figure 6.6 has a different effectiveness, which ranges from: 0.64 to 0.65 at $S_0/K_M = 10$; 0.58 to 0.61 at $S_0/K_M = 5$; and 0.48 to 0.53 at $S_0/K_M = 1$ (data not shown in figure).

Figure 6.4 and Figure 6.6 show the design space with respect to the critical time and the maximum throughput respectively. The effect of adjustments to the parameters that constitute the dimensionless entities can be seen in these figures. The applicability and usability of the design space can be demonstrated by an example situation when a selection should be made between different enzymes that are able to convert the same substrate. In this example, the design space provides values for the dimensionless reaction-width C and the dimensionless length ξ based on various S_0/K_M values and the requirement of 95% substrate conversion with a coflow microreactor. The channel width d, residence time τ_{res} and throughput T can be calculated for each combination of C and ξ by using Equation 6.9, Equation 6.10, and Equation 6.11 respectively. Table 6.2 shows the correlation between kinetic parameters of different enzymes and the corresponding design and operating parameters for this example situation according to the design space of Figure 6.4 to obtain an effectiveness of 0.9.

Table 6.2 Optimal channel width (d), residence time (τ_{res}) and throughput (T, liter (L) per hour (h)) for a coflow microreactor of 34 cm length and 40 µm depth.

Enzyme	V_{max} (µmol s^{-1} g enzyme^{-1})	K_M (mol m^{-3})	S_0/K_M (-)	ξ (-)	C (-)	$d \cdot \sqrt{b/a}$ (µm)	$\tau_{res} \cdot \frac{b}{a}$ (min)	$T \cdot \sqrt{b/a} \cdot \frac{a}{b}$ (L h^{-1})
E1	a	b	10	0.82	4.13	1.6E+00	5.6E-05	2.2E-03
E1	a	b	1	1.3	1.81	1.1E+00	4.0E-05	2.1E-03
E2	a	$2 \cdot b$	10	0.82	4.13	2.3E+00	1.1E-04	1.6E-03
E2	a	$2 \cdot b$	1	1.3	1.81	1.5E+00	8.1E-05	1.5E-03
E3	$2 \cdot a$	b	10	0.82	4.13	1.1E+00	2.8E-05	3.2E-03
E3	$2 \cdot a$	b	1	1.3	1.81	7.6E-01	2.0E-05	2.9E-03

Values are shown for different enzymes with a concentration of 10 kg m^{-3}, substrate diffusion coefficient of 6.4×10^{-10} m^2 s^{-1}, 95% conversion, and variable values for V_{max} and K_M respectively to obtain an effectiveness of 0.9. The values of the dimensionless reaction-width (C) and dimensionless length (ξ) corresponding to an effectiveness of 0.9 were obtained from Figure 6.4.

Table 6.3 shows the correlation between kinetic parameters of different enzymes and the corresponding design and operating parameters for the example situation according to the design space of Figure 6.6 to obtain a maximum throughput.

Table 6.3 Optimal channel width (d), residence time (τ_{res}) and throughput (T, liter (L) per hour (h)) for a coflow microreactor of 34 cm length and 40 µm depth.

Enzyme	V_{max} (µmol s^{-1} g enzyme^{-1})	K_M (mol m^{-3})	S_0/K_M (-)	ξ (-)	C (-)	$d \cdot \sqrt{b/a}$ (µm)	$\tau_{res} \cdot \frac{b}{a}$ (min)	$T \cdot \sqrt{b/a} \cdot \frac{a}{b}$ (L h^{-1})
E1	a	b	10	0.44	6.6	2.1E+00	4.9E-05	3.3E-03
E1	a	b	1	0.46	4.0	1.6E+00	3.1E-05	4.0E-03
E2	a	$2 \cdot b$	10	0.44	6.6	2.9E+00	9.8E-05	2.3E-03
E2	a	$2 \cdot b$	1	0.46	4.0	2.3E+00	6.2E-05	2.8E-03
E3	$2 \cdot a$	b	10	0.44	6.6	1.5E+00	2.4E-05	4.6E-03
E3	$2 \cdot a$	b	1	0.46	4.0	1.1E+00	1.5E-05	5.7E-03

Values are shown for different enzymes with a concentration of 10 kg m^{-3}, substrate diffusion coefficient of 6.4×10^{-10} m^2 s^{-1}, 95% conversion, and variable values for V_{max} and K_M respectively to obtain a maximum throughput. The values of the dimensionless reaction-width (C) and dimensionless length (ξ) corresponding to a maximum throughput were obtained from Figure 6.6.

Table 6.2 and Table 6.3 show the effect of variations in V_{max} and K_M to the residence time and channel width. Both tables show that of the three different enzymes, the enzyme with the lower affinity for the substrate (E2) requires the

largest channel widths and longest residence times; this enzyme also has the lowest (volumetric) productivity according to the throughput values. The enzyme with a higher maximum reaction rate (E3) requires the smallest channel widths and shortest residence times; this enzyme also has the highest productivity. Characteristic for Table 6.3 compared to Table 6.2 is the larger values for the channel width, residence time, and throughput respectively.

In order to obtain a certain conversion, effectiveness, and/or maximum throughput with a predefined S_0/K_M ratio, only one dimensionless length and dimensionless reaction-width need to be known. The example shows that the presented methodology provides a generic hands-on approach to solve and/or clarify such optimal design issues for coflow enzyme microreactors.

Previous research among others have considered the design of coflow microreactors for use as a research tool (Kamholz et al. 1999); to quantify effects of diffusion on the reaction-diffusion zone (Ismagilov et al. 2000); and to establish correlations and design guidelines that concern the initial enzyme activity (Ristenpart et al. 2008; Swarts et al. 2010). This article considers the coflow microreactor as a production method without resorting to the approximation of initial enzyme activity, quantifies effects of diffusion on the productivity, and addresses correlations and guidelines for this.

6.5 CONCLUSIONS

The effects of mass transfer restrictions to the enzymatic reaction can be described by the effectiveness, which is defined as the ratio of the observed reaction rate to the reaction rate without mass transfer restrictions. Our results show that the effectiveness decreases as function of the channel width for coflow enzyme microreactors obeying Michaelis-Menten kinetics; meaning that indeed smaller microchannels reduce mass transfer restrictions. In contrast to the effectiveness, the throughput of these microreactors has an optimum as function of the channel width at conditions that yield significant mass transfer restrictions. The obtained correlations between parameters such as enzyme properties, microreactor dimensions, and operating conditions outline the design space for coflow enzyme microreactors. The maximum throughput and a high effectiveness respectively define boundaries of the design space. The design space provides an understanding and quantitative estimation of the correlations between the parameters based on these boundaries. Examples show a hands-on approach of the generic applicability and usability of the presented design methodology for appropriate selection of example enzymes based on the optimal and enzyme specific microreactor dimensions and operation conditions.

7

GENERAL DISCUSSION

7.1 INTRODUCTION

The goal of this thesis was to fill parts of the gap between microfluidics for analytical purposes and conventional large-scale process engineering. In particular, microfluidics for preparative processes is still in its infancy. This thesis presents microfluidics in different forms such as proofs of concept, innovative ideas, and rules of thumb, which are aimed to contribute to the maturing of micro process engineering for larger scale production. Firstly, we studied the concept of high-throughput processing for mass parallelization of microfluidics for large-scale plants. Secondly, we investigated a novel separation method for fractionation of micro-channeled streams. Next, we demonstrated the potential of miniaturized devices for enrichment of streams by diffusive processes. After that, we combined the obtained knowledge on diffusive processes on microscale with reaction kinetics. Lastly, we developed a generic design space for microfluidic systems.

The goal of this discussion is to summarize and reflect on the previous parts of this thesis. The leading thread of the following paragraphs is throughput, in particular for larger scale – thus industrially – oriented micro process engineering. Section 7.2 briefly describes how the mass parallelization concept, as presented in Chapter 2, can further exploit microfluidics for enhanced data acquisitions. Next, Section 7.3 demonstrates another branch of mass parallelization; it presents a hundred-fold up-scaling of a microextractor. Subsequently, Section 7.4 mathematically describes the advantages of surface related processes in

miniaturized devices. Furthermore, Section 7.5 shows an extension of the generic design space from Chapter 6 with an optimization for pressure drop for parallelized microfluidics. Finally, Section 7.6 will discuss what determines adoption of microfluidics by industries.

7.2 PARALLELIZATION FOR DATA ACQUISITION

Chapter 2 shows that collecting data can be convenient with miniaturized analytical devices. Due to parallelization, such devices can generate more data in less time. Another method of parallelization involves the use of multi-phase systems. For instance, each slug in a Taylor flow may function as an individual reactor. By controlling the supply of reactants to these slugs, each of them can contain different amounts of reactants, and a reaction may occur accordingly. Likewise, emulsification in microchannels can yield droplets with different composition or size that may function as individual microreactors. Hence, these multi-phase systems physically decouple parallelization from the amount of microfluidic devices. Such techniques can thus generate thousands of individual microreactors in a single channel.

Unfortunately, parallelization with and without physical decoupling has not yet been fully explored. This leaves ample opportunity for new studies. Of course, reaction monitoring and analysis becomes increasingly complex when microfluidics is extended to parallelization. For example, the amount of data to process can grow tremendously, in particular with transient state data collection. The detection system may therefore limit the throughput of such analytical systems (deMello 2006). For large datasets, data mining technologies can assist the data acquisition. Ideally, discovered patterns can characterize reactions, and determine key parameters that eventually define the whole system. Currently available automated microfluidic platforms have already taken steps towards this ideal. The proof of concept described in Chapter 2 opens a door to these methods for understanding, predicting, and optimization of system behavior.

7.3 PARALLELIZATION FOR HIGH THROUGHPUT

The parallelization of microstructures is part of the foundation of microfluidics – the inherent advantage of up-scaling by parallelization. In this section, we present an approximately hundredfold up-scaling of a microextractor. The general consent is that such a parallelization has no implications for the characteristics of the microreactor. However, due to manufacturing tolerances and possible channel blockages, the flow distribution and reliable up-scaling may be more complicated (Amador et al. 2004). Besides, pressure drops along microstructures of different dimensions, and multi-phase flows add additional complexity. A proper design of the microfluidic device can minimize such issues.

We fabricated a microextractor with parallelized microchannels for an extraction process. In this extractor, a stream of demineralized water was contacted in coflow with a stream of 0.7 M propionic acid and 0.01 M acetophenone in decane. Approximately 15 µm thick hydrophilic UF cellulose membranes from ENKA Membrana AG (Arnhem, the Netherlands) separated the streams. Similar to the fabrication of the micro-contactor in §4.3.3, structures of 6 cm length, 500±10 µm width, and 50±10 µm depth were milled on both sides of 2.0 mm thick polystyrene plates. Ten of these plates of 10 cm by 10 cm were stacked with the UF cellulose membranes in between them, but the bottom and top layer only had channels on the inner sides. This stacking generated 90 channel pairs. A PMMA bottom and top layer sealed this assembled microextractor – see Figure 7.2 for the schematic drawing and Figure 7.2a for a photograph of the assembled microextractor.

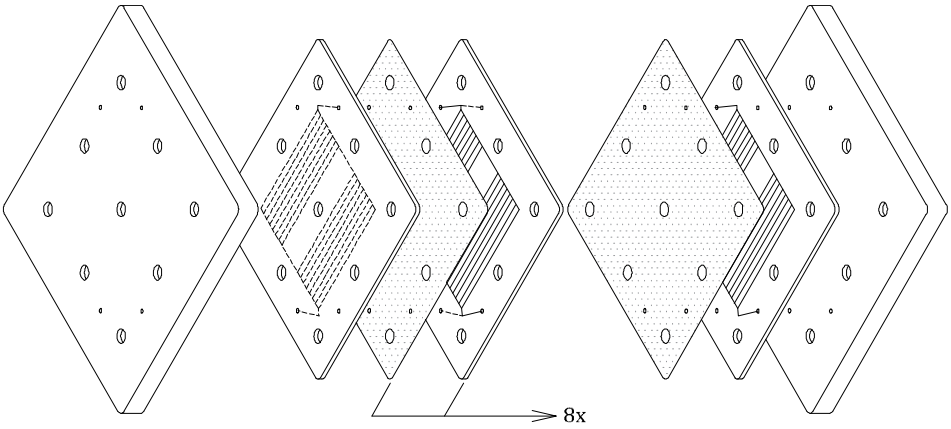

Figure 7.1 Schematic drawing of the microextractor. From left to right: polymethyl methacrylate (PMMA) cover layer, polystyrene (PS) layer with microchannels on inner (right) side, eight times membrane and PS layer with microchannels on both sides, membrane, PS layer with microchannels on inner (left) side, and PMMA cover layer.

From separate experiments, we determined that the partition coefficient of propionic acid was 3.3 (water to decane). Hence, propionic acid dissolves well in water, and the water could therefore extract the propionic acid from the decane solution. Acetophenone hardly dissolves in water, which means that the water could not extract the acetophenone. Without convective transport of water or decane through the membrane, we expected that the propionic acid concentration in decane would decrease with residence time, while the acetophenone concentration would remain constant.

Figure 7.2b shows the results that we obtained with the parallelized microextractor. The figure shows the concentration of propionic acid and acetophenone in decane as function of the residence time of decane.

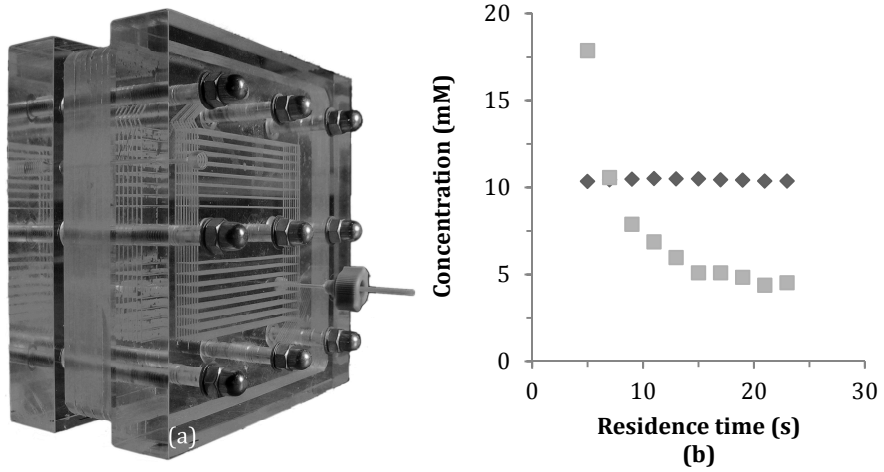

Figure 7.2 Photograph of the microextractor (a). Concentration of acetophenone (♦) and propionic acid (■) in decane, as function of residence time in the microextractor, during the extraction with water (b).

As expected, Figure 7.2b shows that the concentration of propionic acid decreased as function of the residence time. This implies that we successfully extracted the propionic acid in the water phase. Furthermore, the figure shows a constant concentration of acetophenone as function of residence time. Due to its low solvability in water, acetophenone was thus not extracted.

Subsequent resistances in series and parallel can conceptually describe the behavior in the microextractor. Based on the estimation of the pressure drop with the Poiseuille equation, one can estimate the pressure drop in each subsequent section. The inlet and outlet channels had a much larger diameter than the microchannels, which yielded a negligible pressure drop over the inlet and outlet channels. However, the pressure drop over the microchannels with decane was smaller due to the lower viscosity of decane. Equal volumetric flow rates of water and decane would consequently result in a transmembrane pressure transverse to the flow direction. Therefore, we set the decane flow rate higher than the water flow rate so that the maximum transmembrane pressure drop from the decane to

the water stream was 0.2 bar. This shows that microfluidic reactors also have their disadvantages compared to larger-volume systems.

From the samples retrieved at the outlet, we qualitatively determined that no or negligible amounts of decane or water had been transported through the membrane. If transport of decane or water through the membrane had occurred, it would have yielded a mixture of decane and water in both outlets. The design of this experimental setup, with the addition of acetophenone, enabled us to analyze possible malfunction of the microextractor. This section therefore demonstrates how to successfully exploit the inherent up-scaling advantages of microfluidics.

7.4 SURFACE REACTIONS IN MICROFLUIDIC DEVICES

For microfluidic devices, it will be important to exploit characteristics resulting from the small dimensions, beyond the high transport rates (Jensen 2001). In particular, forces associated with high surface area to volume ratios are worth exploiting. For example, reactions that occur at surfaces, such as a reaction with an immobilized catalyst, may profit from these high ratios. In this section, we discuss scaling relations between the volumetric flow rate or throughput and the channel radius for such a catalyst.

In a system with fixed dimensions, the total number of cylindrical microchannels N (-) that it can contain is inversely proportional to the cross sectional area that a channel occupies:

$$N \propto r^{-2}, \qquad \text{Equation 7.1}$$

where r is the channel radius (m). The available surface area of such a microchannel $A_{sur,channel}$ (m^2) scales to its radius as:

$$A_{sur,channel} = 2 \cdot \pi \cdot L \cdot r \propto r, \qquad \text{Equation 7.2}$$

where L is the channel length (m). This implies that the available surface area of the system $A_{sur,system}$ (m^2) scales as:

$$A_{sur,system} = A_{sur,channel} \cdot N \propto r^{-1}. \qquad \text{Equation 7.3}$$

For a zero order reaction with respect to substrate, the reaction time τ (s) only depends on the total amount of catalyst available in the system C (kg). With a constant catalyst density per surface area, this total amount of catalyst is directly proportional to the surface area of the system:

$$\tau \propto \frac{1}{C} \propto \frac{1}{A_{sur,system}} \propto r. \qquad \text{Equation 7.4}$$

The reaction time is inversely proportional to the superficial flow velocity v (m s^{-1}), as described by:

$$v \propto \frac{1}{\tau}. \qquad \text{Equation 7.5}$$

Because the described system has constant overall dimensions, the cross sectional area of the system $A_{cross,system}$ (m^2) is constant. However, the cross sectional area of a single microchannel $A_{cross,channel}$ (m^2) depends on the channel radius:

$$A_{cross,channel} = \pi \cdot r^2 \propto r^2. \qquad \text{Equation 7.6}$$

The combination of Equation 7.5 and Equation 7.6 yields the volumetric flow rate or throughput. This throughput of a single microchannel $\Phi_{channel}$ (m^3 s^{-1}) equals:

$$\Phi_{channel} = v \cdot A_{cross,channel} \propto r. \qquad \text{Equation 7.7}$$

The total throughput of the system Φ_{system} (m^3 s^{-1}) equals the throughput of a single channel multiplied with the total number of channels:

$$\Phi_{system} = \Phi_{channel} \cdot N \propto r^{-1}. \qquad \text{Equation 7.8}$$

Equation 7.7 shows that the throughput of a single microchannel is proportional to the channel radius – meaning that reducing the channel radius reduces the throughput. By contrast, Equation 7.8 shows that the *total* throughput of the system is inversely proportional to the channel radius. Thus for the described zero order reaction, decreasing the channel dimensions yields a lower throughput with a single microchannel, but yields a higher throughput with the whole system. For first and higher order reactions, decreasing these dimensions can also proportionally yield a higher throughput with a single microchannel. For example, adsorption monolith microreactors and immobilized enzyme microreactors can

achieve this, which means that the productivity of the overall system increases even more rapidly (Horvath et al. 1972; Kreutzer et al. 2005; Urban et al. 2006). Even for a zero order reaction, the results indicate that miniaturization for surface oriented reactions can still have advantages for large-scale applications that aim at productivity – it is therefore important to consider a complete microfluidic system with a parallelization of many microchannels.

7.5 DESIGN OF MICROFLUIDIC DEVICES

Counterbalancing a possible increase in pressure drop caused by the reduced dimensions may be a crucial aspect when designing microfluidic devices (Chovan and Guttman 2002). The pressure drop for laminar flow through a microchannel can be described by the Hagen-Poiseuille equation (Poiseuille 1847). According to this equation, pressure drop inversely scales with a power of four to the channel radius. Hence, miniaturization may be limited at some point by issues related to a highly increased pressure drop.

In Chapter 6, we suggested that the throughput as defined in Equation 6.11 could be a good parameter to describe overall productivity of the microfluidic device. By connecting a number of microreactors N in parallel, we can obtain the throughput of the whole system T_{tot} ($m^3\ s^{-1}$), which is linearly proportional to the throughput of an individual microreactor T:

$$N \cdot T = T_{tot}. \qquad \text{Equation 7.9}$$

Likewise, the pressure drop over the whole system corresponding to this total throughput can be estimated. The pressure drop over one microreactor ΔP (Pa) is defined by:

$$\Delta P = \frac{8 \cdot \mu \cdot L}{\pi \cdot r^4} \cdot \Phi = R \cdot \Phi, \qquad \text{Equation 7.10}$$

where μ is the fluid viscosity (Pa s), L is the length (L), r is the channel radius (m), and R is the resistance.

The total pressure drop over multiple microreactors P_{tot} (Pa) can be calculated by regarding the parallelized individual microreactors as resistances in parallel by:

$$P_{tot} = \left(N \cdot \frac{1}{R}\right)^{-1} \cdot \Phi_{tot}, \qquad \text{Equation 7.11}$$

where Φ_{tot} is the total volumetric flow rate of the whole system ($m^3\ s^{-1}$) (Amador et al. 2004).

Figure 6.5 in Chapter 6 shows the throughput for individual microreactors as function of the channel width. According to this figure, an individual microreactor of a certain width requires a distinct throughput to reach 95% conversion. The number of required individual microreactors and the related total pressure drop can be calculated by Equation 7.9 and Equation 7.11 respectively to obtain a certain total throughput. Figure 7.3 shows the number of channels (a) and the pressure drop (b) as function of the channel width at 95% substrate conversion with β-galactosidase and a total throughput equal to the maximum throughput of Figure 6.5.

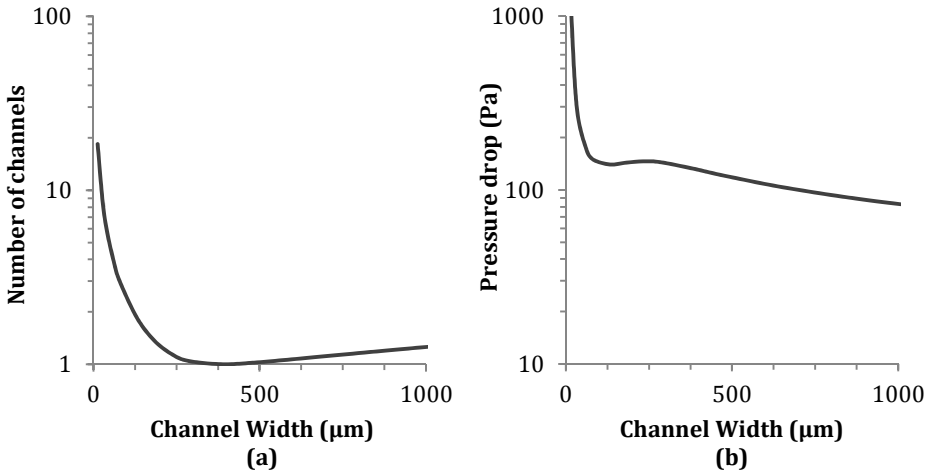

Figure 7.3 Pressure drop (Pa) as function of channel width (µm) at 95% substrate conversion in a coflow microreactor with an enzyme concentration of 10 kg m^{-3}, $S_0/K_M = 10$ (—), and total throughput of 0.3 µl min^{-1}.

Figure 7.3a shows that the total number of channels decreased as function of channel width, up to the channel width for maximum throughput ($\delta_{throughput}$, see Figure 6.5). From that point, the required number of channels increased. Note that, due to the assumption of having only one channel at the maximum obtained throughput, the total number of channels is not necessarily a discrete number. The figure illustrates that due to reduced efficiency, more microchannels are required for channel widths below and above the efficiency optimum in order to obtain a desired throughput.

Figure 7.3b shows that the pressure drop initially decreases as function of channel width up to ~100 μm. From a channel width of ~100 μm up to a channel width of ~200 μm, the pressure drop seemed almost constant as function of channel width. From a channel width of ~200 μm, the pressure drop decreased again as function of channel width.

We can make two important observations based on Figure 7.3. Firstly, from the width of maximum throughput ($\delta_{throughput}$) for this specific situation (which equals ~400 μm, see Figure 6.5), decreasing the channel width not only reduced the throughput, but also increased the amount of required microchannels and the pressure drop. Secondly, from the kinetic limitation width ($\delta_{kinetic}$) for this specific situation (which equals ~230 μm, see Figure 6.2), decreasing the channel width hardly affected the pressure drop, but increased the effectiveness of the reaction by using more parallel channels. These effects are very relevant in the design of microfluidic enzyme reactors.

Besides mass transfer restrictions described by the effectiveness, other parameters apart from the throughput and pressure drop can have a distinct optimum as function of channel width. In compliance with §7.4, we conclude that it is important to explore and exploit other characteristics of continuous production in microfluidic devices beyond mass transfer effects in order to develop novel processes.

7.6 ADOPTION OF MICROFLUIDICS BY INDUSTRY

There are many companies involved with microfluidics. Some producers fabricate and supply microfluidic chips; others are more involved in the R&D or sales of complete microfluidic systems. The activities of producers are diverse, including selling and customizing microfluidic applications, consulting, and even educating students. The users of microfluidic systems are from diverse fields such as the food- and chemical industries, pharmaceutical industries, and life sciences. In particular, point-of-care diagnostics and DNA sequencing utilities have grown a relatively large customer base.

In §1.1.4, we discussed why microfluidics is such an interesting technology. Our literature review indicated that the science and technology part of it are in constant development. The acceptance and actual use of microfluidics by producers and users, for whom researchers develop the technology, depends on more determinants than proven usefulness. The objective of this section is to indicate and discuss where problems come across regarding such acceptance and actual usage, and what determinants play a role in this. This information can facilitate collaboration between producers, users, and researchers, and stimulate industries to more investigate and study the potential of microfluidics.

The producers' attitudes towards acceptance of microfluidics by users are diverse. Some companies are passive, while others are actively involved in the process of attaining acceptance of microfluidics. Many companies are actively involved in initiatives such as Process on a Chip (PoaC), which bring the producers, users, and researchers together via, for instance, progress meetings, and symposia. Because microfluidics touches upon multiple disciplines, it requires inputs from various specialists. Hence, these initiatives are required for the technology and acceptance to develop and grow. For this to occur, trust in microfluidics is required. However, this trust is variable; some companies believe in microfluidics, while others do not. Even within a company, this attitude can change from time to time due to, for instance, changing boards. Such attitude changes can also result in decreased

financial inputs for research institutes and therefore slow developments down. In particular, microfluidics for production and downstream processing and acceptance thereof will need more time.

Many researchers and producers experience resistance, but also unwillingness for technology push innovation. Both parties frequently have a wish for a more customer (e.g. user) driven demand. On the other side, users often lack the detailed expertise on microfluidics. For instance, it is not straightforward to obtain expertise in using microfluidic devices, which makes it difficult to establish desired reactions. Moreover, many producers and users are even unable to provide a clear terminology of microfluidics. Much is thus unknown about microfluidics, and fully understanding the concept takes time. It is therefore difficult to have clear demands, to accept the technology, and to see the opportunities of microfluidics. Typically, users want to see more proofs of concept, more examples, and more calculations and estimations for larger scale applications (Pavlou 2009). It is only then that users of more conventional processing techniques may take further steps towards microfluidics.

Often, the perception is that costs are a major factor that either drives or limits the introduction of a technology as microfluidics. Of course, replacement of existing processes is inherently costly, but also the materials and production of microfluidic devices involves additional costs. A microfluidic device has relatively high costs per volume. This is also because such devices have a relatively low active volume of microstructures compared to their total volume. For these reasons, microfluidic devices should optimally use the available space. For analytical microfluidics, this is of less importance. However, for production and preparative purposes, such a system volume and total costs are major determinants. Besides, the economy of scale is a well-known concept that applies to many conventional reactors and equipment, but for microfluidic devices, such concepts may not hold. Often, users ask for startup and mass production costs because they are interested in the concept of larger volume production, but at the same time, they are aware of the

high costs involved with building larger – or more correctly more – microfluidic devices. Overall, it is difficult to actually predict what the (unexpected) costs of a large scale micro process engineered plant will be because there are relatively few comprehensive examples (Roberge et al. 2008).

The materials that producers of microfluidics use are commonly new to process engineers. Stainless steel or other metallic alloys are traditionally used and have a proven record. However, this is not the case for the new micro-processed materials such as glass, silica, and polymers. In addition, there is not yet any real standard for microfluidic devices regarding their sizes and macro-fluidic connections. Such standardization for compatibility with current systems is important for microfluidics to prosper. An advantage is that nowadays, much commercial equipment is available to operate the microfluidic devices.

In brief, successful innovation with microfluidics requires expertise in many fields such as microfabrication, microchemistry, and micro process engineering. By educating people on microfluidics, the willingness of users (e.g. industries) to adapt to this technology can increase. Skepticism of users towards this new technology can diminish when researchers and producers are able to demonstrate the true benefits of microfluidics. Initiatives such as PoaC prove to be essential for speeding up adoption of microfluidics by industry.

7.7 CONCLUSIONS

Microfluidics involves the exploitation of the phenomena that manifest themselves on microscale. This thesis shows that microscale applications can indeed offer unprecedented benefits. For instance, mass parallelization can on one hand reduce the time required for data acquisition and on the other hand tremendously increase device throughput. Furthermore, reduced diffusion times enable the application of mass diffusion separation in liquids in order to fractionate components, even those with comparable diffusivities. With optimized microchannel and membrane dimensions, this novel separation process can even compete with currently available separation technologies – with the advantage of negligible transmembrane pressures. In a subsequent study, we used such optimized dimensions and could achieve diffusion-based enrichment of components with membrane sieves of only 25 μm thick. Moreover, this technology enabled an unprecedented counter-current flow type for higher enrichment efficiency. The advantages of such a process include the general applicability to any diffusing component – regardless of its diffusivity or concentration.

A further benefit is that immobilized enzymes can synthesize components without diffusion limitation effects. We introduced the critical time parameter, which can be used to set conditions for enzymatic conversions without diffusion limitations in microreactors. Furthermore, we developed generic design guidelines that enable the restriction of design parameters, such as microchannel dimensions, to design spaces based on criteria such as the critical time, but also productivity, and pressure. Moreover, these design spaces are applicable to a single or a multiple of microfluidic devices.

In addition to the mentioned benefits, we discussed the importance of adoption of microfluidics. We found out that many determinants are involved in this including the multidisciplinarity of microfluidics, innovation type, costs per volume, unexpected costs, standardization, familiarity with materials, and networking

initiatives. Knowledge of these determinants is of utmost importance to reduce skepticism towards and stimulate adoption of microfluidics by industry.

Although researchers have abundantly studied microfluidics for analytical and sensory applications, microfluidics for preparative processes is still in its infancy. The aim of this thesis was to fill parts of that gap between these fields. With the presented research, engineers can better develop process intensifications by means of microfluidic devices, for which we showed that many opportunities lay ahead.

REFERENCES

Amador C, Gavriilidis A, Angeli P. 2004. Flow distribution in different microreactor scale-out geometries and the effect of manufacturing tolerances and channel blockage. Chemical Engineering Journal 101(1-3):379.

Arata HF, Rondelez Y, Noji H, Fujita H. 2005. Temperature alteration by an on-chip microheater to reveal enzymatic activity of β-galactosidase at high temperatures. Analytical Chemistry 77(15):4810-4814.

Aydogan N, Gurkan T, Yilmaz L. 1998. Effect of Operating Parameters on the Separation of Sugars by Nanofiltration. Separation Science and Technology 33(12):1767 - 1785.

Benedict M, Boas A. 1951. Separation of gas mixtures by mass diffusion. Chemical Engineering Progress 47:22.

Bird BR, Stewart WE, Lightfoot EN. 1960. Transport Phenomena.

Breure B, Peters EAJF, Kerkhof PJAM. 2008. Separation of azeotropic mixtures of alcohols and water with FricDiff. Separation and Purification Technology 62(2):349-362.

Brody JP, Yager P. 1997. Diffusion-based extraction in a microfabricated device. Sensors and Actuators, A: Physical 58:13-18.

Brody JP, Yager P, Goldstein RE, Austin RH. 1996. Biotechnology at low Reynolds numbers. Biophysical Journal 71(6):3430-3441.

Broek AP. 1993. Characterization of hemodialysis membranes: membrane structure and function: University of Twente.

Cavaille D, Combes D. 1995. Characterization of beta-galactosidase from Kluyveromyces lactis. Biotechnology and Applied Biochemistry 22(1):55-64.

Choi J-H, Fukushi K, Yamamoto K. 2007. A submerged nanofiltration membrane bioreactor for domestic wastewater treatment: the performance of cellulose acetate nanofiltration membranes for long-term operation. Separation and Purification Technology 52(3):470-477.

Chou C-F, Bakajin O, Turner SWP, Duke TAJ, Chan SS, Cox EC, Craighead HG, Austin RH. 1999. Sorting by diffusion: An asymmetric obstacle course for continuous molecular separation. PNAS 96(24):13762-13765.

Chovan T, Guttman A. 2002. Microfabricated devices in biotechnology and biochemical processing. Trends in Biotechnology 20(3):116.

Cichelli MT, Weatherford WDJ, Bowman JR. 1951. Sweep diffusion gas separation process. Part I. Chemical Engineering Progress 47:33.

Cohen CB, Chin-Dixon E, Jeong S, Nikiforov TT. 1999. A microchip-based enzyme assay for protein kinase A. Analytical Biochemistry 273:89-97.

Crittenden RG, Playne MJ. 1996. Production, properties and applications of food-grade oligosaccharides. Trends in Food Science & Technology 7(11):353-361.

de Jong J, Lammertink RGH, Wessling M. 2006. Membranes and microfluidics: a review. Lab on a Chip 6:1125-1139.

Deen WM. 1987. Hindered transport of large molecules in liquid-filled pores. AIChE Journal 33(9):1409-1425.

deMello AJ. 2006. Control and detection of chemical reactions in microfluidic systems. Nature 442:394-402.

Dickson RC, Dickson LR, Markin JS. 1979. Purification and properties of an inducible β-galactosidase isolated from the yeast Kluyveromyces lactis. Journal of Bacteriology 137(1):51-61.

Doran PM. 2000. Bioprocess Engineering Principles. London: Academic Press Limited.

Duffy DC, McDonald JC, Schueller OJA, Whitesides GM. 1998. Rapid prototyping of microfluidic systems in poly(dimethylsiloxane). Analytical Chemistry 70(23):4974-4984.

Ehrfeld W, Hessel V, Löwe H. 2000. Microreactors: New Technology for Modern Chemistry: Wiley-VCH. 288 p.

Einstein A. 1905. On the Motion of Small Particles Suspended in Liquids at Rest Required by the Molecular-Kinetic Theory of Heat. Annalen der Physik 17:549-560.

Feng YM, Chang XL, Wang WH, Ma RY. 2009. Separation of galacto-oligosaccharides mixture by nanofiltration. Journal of the Taiwan Institute of Chemical Engineers 40(3):326-332.

Fleming Glass KK, Longmire EK, Hubel A. 2008. Optimization of a microfluidic device for diffusion-based extraction of DMSO from a cell suspension. International Journal of Heat and Mass Transfer 51(23-24):5749-5757.

Friedrich CR, Vasile MJ. 1996. Development of the micromilling process for high-aspect-ratiomicrostructures. Journal of Microelectromechanical Systems 5(1):33-38.

Geboers M, Kerkhof P, Lipman P, Peters F. 2007. FricDiff: A novel separation concept. Separation and Purification Technology 56(1):47-52.

Gibson GR, Probert HM, Loo JV, Rastall RA, Roberfroid MB. 2004. Dietary modulation of the human colonic microbiota: updating the concept of prebiotics. Nutrition Research Reviews 17(02):259-275.

Gibson GR, Roberfroid MB. 1995. Dietary Modulation of the Human Colonic Microbiota: Introducing the Concept of Prebiotics. Journal of Nutrition 125(6):1401-1412.

Goulas AK, Grandison AS, Rastall RA. 2003. Fractionation of oligosaccharides by nanofiltration. Journal of the Science of Food and Agriculture 83(7):675-680.

Goulas AK, Kapasakalidis PG, Sinclair HR, Rastall RA, Grandison AS. 2002. Purification of oligosaccharides by nanofiltration. Journal of Membrane Science 209(1):321-335.

Guijt-van Duijn RA, Moerman R, Kroon A, van Dedem GWK, van den Doel R, van Vliet L, Young IT, Laugere F, Bossche A, Sarro P. 2003. Miniaturized analytical assays in biotechnology. Biotechnology Advances 21(5):431-444.

Hadd AG, Raymond DE, Halliwell JW, Jacobson SC, Ramsey JM. 1997. Microchip device for performing enzyme assays. Analytical Chemistry 69:3407-3412.

Haeberle S, Zengerle R. 2007. Microfluidic platforms for lab-on-a-chip applications. Lab on a Chip 7:1094-1110.

Harrison DJ, Fluri K, Seiler K, Fan Z, Effenhauser CS, Manz A. 1993. Micromachining a Miniaturized Capillary Electrophoresis-Based Chemical Analysis System on a Chip. Science 261(5123):895-897.

Hartman RL, Jensen KF. 2009. Microchemical systems for continuous-flow synthesis. Lab on a Chip 9(17):2495-2507.

Hertz GL; PHILIPS NV, assignee. 1924. Apparatus for separating gases from a mixture thereof. United States patent 1498097.

Hessel V, Löwe H. 2003a. Microchemical Engineering: Components, Plant Concepts User Acceptance - Part I. Chemical Engineering & Technology 26(1):13-24.

Hessel V, Löwe H. 2003b. Microchemical Engineering: Components, Plant Concepts, User Acceptance - Part II. Chemical Engineering & Technology 26(4):391-408.

Holl MR, Galambos P, Forster FK, Brody JP, Afromowitz MA, Yager P. 1996. Optimal design of a microfabricated diffusion based extraction device. Proceedings of the American Society of Mechanical Engineering:183-189.

Hornby WE, Lilly MD, Crook EM. 1968. Some changes in the reactivity of enzymes resulting from their chemical attachment to water-insoluble derivatives of cellulose. Biochemical Journal 107:669-674.

Horvath C, Sardi A, Solomon BA. 1972. Enzyme reactor tubes: effect of diffusion and slug flow. Physiological chemistry and physics 4(2):125-130.

Ismagilov RF, Stroock AD, Kenis PJA, Whitesides G. 2000. Experimental and theoretical scaling laws for transverse diffusive broadening in two-phase laminar flows in microchannels. Applied Physics Letters 76(17):2376-2378.

Jensen KF. 2001. Microreaction engineering - is small better? Chemical Engineering Science 56:293-303.

Kamholz AE, Weigl BH, Finlayson BA, Yager P. 1999. Quantitative Analysis of Molecular Interaction in a Microfluidic Channel: The T-Sensor. Analytical Chemistry 72(23):5340-5447.

Kanno K-i, Maeda H, Izumo S, Ikuno M, Takeshita K, Tashiro A, Fuji M. 2002. Rapid enzymatic transglycosylation and oligosaccharide synthesis in a microchip. Lab on a Chip 2(1):15-18.

Kerkhof PJAM. 1996. A modified Maxwell-Stefan model for transport through inert membranes: The binary friction model. Chemical Engineering Journal 64:319-343.

Keyes JJ, Pigford RL. 1957. Diffusion in a ternary gas system with application to gas separation. Chemical Engineering Science 6(4-5):215-226.

Kikutani Y, Hibara A, Uchiyama K, Hisamoto H, Tokeshi M, Kitamori T. 2002. Pile-up glass microreactor. Lab on a Chip 2:193-196.

Knitter R, Liauw MA. 2004. Ceramic microreactors for heterogeneously catalysed gas-phase reactions. Lab on a Chip 4(4):378-383.

Kockmann N, Engler M, Woias P. 2004. Theoretische und experimentelle untersuchungen der mischvorgänge in t-förmigen microreaktoren - Teil 3. Chemie Ingenieur Technik 76(12):1777-1783.

Kolfschoten RC, Janssen AEM, Boom RM. 2011. Mass diffusion based separation of sugars in a microfluidic contactor with nanofiltration membranes. Submitted for publication.

Kolmogorov AN. 1941. Local structure of turbulence in an incompressible liquid for ever large Reynolds numbers. Doklady Akademii Nauk SSSR 30(4):5.

Kralj JG, Sahoo HR, Jensen KF. 2007. Integrated continuous microfluidic liquid-liquid extraction. Lab on a Chip 7:256-263.

Kreulen H, Smolders CA, Versteeg GF, Van Swaaij WPM. 1993. Determination of mass transfer rates in wetted and non-wetted microporous membranes. Chemical Engineering Science 48(11):2093-2102.

Kreutzer MT, Kapteijn F, Moulijn JA, Heiszwolf JJ. 2005. Multiphase monolith reactors: Chemical reaction engineering of segmented flow in microchannels. Chemical Engineering Science 60(22):5895-5916.

Lee M-Y, Srinivasan A, Ku B, Dordick JS. 2003. Multienzyme catalysis in microfluidic biochips. Biotechnology and Bioengineeing 83(1):20-28.

Levich B. 1942. The Theory of Concentration Polarization. Acta Physico-Chimica Sinica U.R.S.S. 17:257-307.

Li W, Li J, Chen T, Chen C. 2004. Study on nanofiltration for purifying fructo-oligosaccharides: I. Operation modes. Journal of Membrane Science 245(1-2):123-129.

Lilly MD, Hornby WE. 1966. The kinetics of carboxymethylcellulose-ficin in packed beds. Biochemical Journal 100(3):718-723.

Liu L, Loh NH, Tay BY, Tor SB, Murakoshi Y, Maeda R. 2005. Mixing and characterisation of 316L stainless steel feedstock for micro powder injection molding. Materials Characterization 54(3):230-238.

Long WR; 1949. Apparaturs for obtaining x-ray diffraction patterns. USA.

Losey MW, Schmidt MA, Jensen KF. 2001. Microfabricated multiphase packed-bed reactors: Characterization of mass transfer and reactions. Industrial & Engineering Chemistry Research 40:2555-2562.

Luo C, Jiang L, Liang S, Ouyang Q, Ji H, Chen Y. 2009. High-throughput microfluidic system for monitoring diffusion-based monolayer yeast cell culture over long time periods. Biomedical Microdevices 11(5):981-986.

Mair DA, Rolandi M, Snauko M, Noroski R, Svec F, Frechet JMJ. 2007. Room-Temperature Bonding for Plastic High-Pressure Microfluidic Chips. Analytical Chemistry 79(13):5097-5102.

Manz A, Graber N, Widmer HM. 1990. Miniaturized total chemical analysis systems: A novel concept for chemical sensing. Sensors and Actuators B: Chemical 1(1-6):244-248.

Mao H, Yang T, Cremer PS. 2001. Design and Characterization of Immobilized Enzymes in Microfluidic Systems. Analytical Chemistry 74(2):379-385.

Mao HH, Yang TT, Cremer PSPS. 2002. A microfluidic device with a linear temperature gradient for parallel and combinatorial measurements. Journal of the American Chemical Society 124(16):4432-4435.

Maruyama TT, Uchida JJ-i, Ohkawa TT, Futami TT, Katayama KK, Nishizawa KK-i, Sotowa KK-i, Kubota FF, Kamiya NN, Goto MM. 2003. Enzymatic degradation of p-chlorophenol in a two-phase flow microchannel system. Lab on a Chip 3(4):308-312.

Mata C, Longmire E, McKenna D, Glass K, Hubel A. 2008. Experimental study of diffusion-based extraction from a cell suspension. Microfluidics and Nanofluidics 5(4):529-540.

Michaelis L, Menten ML. 1913. Kinetics of Invertase Action. Biochemische Zeitschrift 49.

Mulder M. 1996. Basic principles of membrane technology. Dordrecht: Kluwer Academic Publishers.

Pavlou F. 2009. Microreactor technology: Is the industry ready for it yet? Pharmaceutical Technology Europe 21(10).

Perry RH, Green DW. 1997. Perry's Chemical Engineers' Handbook. New York: McGraw-Hill.

Poiseuille JLM. 1847. Sur Ie mouvement des liquides de nature differente dans les tubes de tres petits diametres. Ann. Chim. Phys. 21:76-110.

Pontalier P-Y, Ismail A, Ghoul M. 1997. Mechanisms for the selective rejection of solutes in nanofiltration membranes. Separation and Purification Technology 12(2):175-181.

Pontalier P-Y, Ismail A, Ghoul M. 1999. Specific model for nanofiltration. Journal of Food Engineering 40(3):145-151.

Purcell EM. 1976. Life at low reynolds number. American Journal of Physics 45:3-11.

Ramsey JM. 1999. The burgeoning power of the shrinking laboratory. Nat Biotech 17(11):1061-1062.

Reyes DR, Iossifidis D, Auroux PA, Manz A. 2002. Micro Total Analysis Systems. 1. Introduction, Theory, and Technology. Analytical Chemistry 74(12):2623-2636.

Reynolds O. 1883. An Experimental Investigation of the Circumstances Which Determine Whether the Motion of Water Shall Be Direct or Sinuous, and of the Law of Resistance in Parallel Channels. Philosophical Transactions of the Royal Society of London 174:935-982.

Ristenpart WD, Wan J, Stone HA. 2008. Enzymatic Reactions in Microfluidic Devices: Michaelis-Menten Kinetics. Analytical Chemistry 80(9):3270-3276.

Roberfroid M. 2007. Prebiotics: The Concept Revisited. Journal of Nutrition 137(3):830S-837S.

Roberge DM, Zimmermann B, Rainone F, Gottsponer M, Eyholzer M, Kockmann N. 2008. Microreactor Technology and Continuous Processes in the Fine Chemical and Pharmaceutical Industry: Is the Revolution Underway? Organic Process Research & Development 12(5):905-910.

Salieb-Beugelaar GB, Dorfman KD, Berg Avd, Eijkel JCT. 2009. Electrophoretic separation of DNA in gels and nanostructures. Lab on a Chip 9(17):2508-2523.

Schwertz FA. 1947. Separation of Gases by Single and Double Diffusion. American Journal of Physics 15(1):31-36.

Selvi A, Breure B, Gross J, de Graauw J, Jansens PJ. 2007. Basic parameter study for the separation of a isopropanol-water mixture by using FricDiff technology. Chemical Engineering and Processing 46(9):810-817.

Sharp AK, Kay G, Lilly MD. 1969. The kinetics of beta-galactosidase attached to porous cellulose sheets. Biotechnology and Bioengineering 11:363-380.

Shuck FO, Toor HL. 1963. Separation of liquids by mass diffusion. AIChE Journal 9(4):442-447.

Song H, Ismagilov RF. 2003. Millisecond kinetics on a microfluidic chip using nanoliters of reagents. Journal of the American Chemical Society 125(47):14613-14619.

Spalding DB. 1954. Mass Transfer in Laminar Flow. Proceedings of the Royal Society of London, Series A: Mathematical and Physical Sciences 221(1144):78-99.

Srinivasan A, Wu X, Lee M-Y, Dordick JS. 2002. Microfluidic peroxidase biochip for polyphenol synthesis. Biotechnology and Bioengineeing 81(5):563-569.

Stepánek E, Kubícek M, Marek M, Adler PM. 1999. Optimal design and operation of a separating microreactor. Chemical Engineering Science 54(10):1493-1498.

Stitt EH. 2002. Alternative multiphase reactors for fine chemicals: A world beyond stirred tanks? Chemical Engineering Journal 90(1-2):47-60.

Swarts JW, Kolfschoten RC, Jansen MCAA, Janssen AEM, Boom RM. 2010. Effect of diffusion on enzyme activity in a microreactor. Chemical Engineering Journal 162(1):301-306.

Swarts JW, Vossenberg P, Meerman MH, Janssen AEM, Boom RM. 2008. Comparision of two-phase lipase catalyzed esterification on micro and bench scale. Biotechnology and Bioengineering 99(4):855-861.

Sweet RG, Cumming RC; 1968. Fluid droplet recorder with a plurality of jets patent 3373437.

Tanaka YY, Slyadnev MMN, Sato KK, Tokeshi MM, Kim HHB, Kitamori TT. 2001. Acceleration of an enzymatic reaction in a microchip. Analytical Sciences 17(7):809-810.

Thorsen T, Maerkl SJ, Quake SR. 2002. Microfluidic Large-Scale Integration. Science 298(5593):580-584.

Urban PL, Goodall DM, Bruce NC. 2006. Enzymatic microreactors in chemical analysis and kinetic studies. Biotechnology Advances 24:42-57.

van den Berg A. 1995. Micro Total Analysis Systems: Proceedings of the μTAS'94 Workshop. Twente.

Van der Bruggen B, Mänttäri M, Nyström M. 2008. Drawbacks of applying nanofiltration and how to avoid them: A review. Separation and Purification Technology 63(2):251-263.

Vegas R, Moure A, Domínguez H, Parajó JC, Álvarez JR, Luque S. 2006. Purification of oligosaccharides from rice husk autohydrolysis liquors by ultra- and nano-filtration. Desalination 199(1-3):541-543.

Wang J, Chatrathi MP, Tian B. 2001. Microseparation chips for performing multienzymatic dehydrogenase/oxicase assays: Simultaneous electrochemical measurement of ethanol and glucose. Analytical Chemistry 73(6):1296-1300.

Watts P, Wiles C, Haswell SJ, Pombo-Villar E, Styring P. 2001. The synthesis of peptides using micro reactors. Chemical Communications (Cambridge, United Kingdom)(11):990-991.

Wesseling H, Krishna R. 2000. Mass transfer in multicomponent mixtures. Delft: Delft University Press.

Whitesides GM. 2006. The origins and the future of microfluidics. Nature 442(7101):368.

Whitesides GM, Stroock AD. 2001. Flexible Methods for Microfluidics. Physics Today 54(6):42-48.

Whitman WG. 1923. The two-film theory of gas absorption. Chemical and Metallurgical Engineering 29:146-148.

Wijmans JG, Baker RW. 1995. The solution-diffusion model: a review. Journal of Membrane Science 107(1-2):1-21.

Wilke CR, Chang P. 1955. Correlation of diffusion coefficients in dilute solutions. AIChE Journal 1(2):264-270.

Williams PS, Levin S, Lenczycki T, Giddings JC. 1992. Continuous SPLITT fractionation based on a diffusion mechanism. Industrial & Engineering Chemistry Research 31(9):2172-2181.

Xia Y, Whitesides GM. 1998. Soft Lithography. Annual Review of Materials Science 28(1):153-184.

Xiang F, Lin Y, Wen J, Matson DW, Smith RD. 1999. An Integrated Microfabricated Device for Dual Microdialysis and On-Line ESI-Ion Trap Mass Spectrometry for Analysis of Complex Biological Samples. Analytical Chemistry 71(8):1485-1490.

Yue V, Kowal R, Neargarder L, Bond L, Muetterties A, Parsons R. 1994. Miniature field-flow fractionation system for analysis of blood cells. Clinical Chemistry 40(9):1810-1814.

Zhao DDS, Gomez FFA. 1998. Double enzyme-catalyzed microreactors using capillary electrophoresis. Electrophoresis 19(3):420-426.

Zheng BB, Ismagilov RFRF. 2005. A microfluidic approach for screening submicroliter volumes against multiple reagents by using preformed arrays of nanoliter plugs in a three-phase liquid/liquid/gas flow. Angewandte Chemie 44(17):2520-3.

SUMMARY

Microfluidic devices make precisely controlled processing of substances possible on a microliter level. The advantage is that, due to the small sizes, the driving forces for mass and heat transfer are high. The surface to volume ratios are also high, which can benefit many surface oriented processes. In addition, because of their small volumes, microfluidic devices reduce reagent consumption and risk of failure compared to larger counterparts. Furthermore, the parallelization of such devices can increase productivity while maintaining their characteristics. Overall, these advantageous properties give many opportunities for reaction and separation processes.

Although researchers have intensively studied microfluidics for analytical and sensory applications, microfluidics for preparative processes is still in its infancy. This thesis research involved exploring these processes for biocatalysis and bio-separations with microfluidic devices. The purpose of this thesis was to yield a better understanding of microfluidics for the preparative processes and larger-scale production. We therefore addressed subjects including microfluidic parallelization, membrane separation, biocatalysis, and design. The presented research is useful for further developing innovative process intensification by means of microfluidic devices.

Parallelization of microfluidic devices can facilitate the generation of more data or product in less time. In Chapter 2, we present a proof of concept of such a parallelization for obtaining information on reaction and separation kinetics. We assembled different microfluidic contactors into a single device in order to perform distinct experiments simultaneously. The concept of the parallelization was based on the decoupling of pressure drop from residence time. We demonstrated this by microfluidic membrane separations and determination of membrane properties. The reported device enabled a three times higher throughput compared to devices with a single separation region.

Processes such as chromatographic separation and nanofiltration can remove low molecular weight sugars from liquid mixtures of oligosaccharides. In Chapter 3, we present a novel separation process based on the concept of mass diffusion. Differences between diffusivities of the components drive such a separation, while membranes, in particular nanofiltration membranes, can enhance the separation. We demonstrate this by the use of a membrane microfluidic device for the separation of small molecular weight components. Our results show that mass diffusion separation in liquids is a feasible concept. With optimized microchannel and membrane dimensions, the presented separation process might compete with currently available separation technologies.

For diffusion-based processes, such as mass diffusion separation shown in Chapter 3, small diffusion distances – and thus thinner membranes – can reduce diffusion times significantly. In Chapter 4, we used a microfluidic contactor to contact liquid streams via such extremely thin membranes. We show that the presented concept can be useful for diffusion-based pre-concentration or downstream processes such as fractionation and enrichment. Our results indicate that also this method can yield a feasible process. Moreover, the technology is generally applicable to any diffusing component – regardless of its absolute diffusivity or concentration.

Fast mass transfer and low reagent consumption have made enzyme microreactors popular research tools. In Chapter 5, we used such a microreactor to study the effect of diffusion on enzyme activity. We found that the Michaelis-Menten kinetic parameters were similar at the microscale and bench scale. Our results show that with residence times below a few seconds, diffusion effects limited the reaction rate and therefore reduced the conversion per volume of enzyme microreactor. The critical residence time where this limitation occurred increased quadratically with channel width, increased with enzyme concentration, and decreased with substrate concentration. We concluded that in order to use an enzyme microreactor efficiently, such effects should be taken into account.

Many parameters such as the enzyme properties, operating conditions, and dimensions of the microreactor determine to what extent mass transfer restrictions affect the reaction rate and the productivity. The use of microchannels can indeed shorten the characteristic mass transfer time, as shown in Chapter 5, but may also affect the productivity of the microreactor. Chapter 6 provides the correlations between these parameters for coflow enzyme microreactors obeying Michaelis-Menten kinetics. These correlations outline the design space based on reduced mass transfer restrictions and maximum productivity respectively. The methodology that yields the design space provides a generic hands-on approach to optimally design coflow enzyme microreactors.

Microfluidics involves the exploitation of the phenomena that manifest themselves on microscale. This thesis shows that microscale applications can indeed offer unprecedented benefits. The discussion in Chapter 7 summarizes and reflects on the previous parts of this thesis. We conclude that it is important to explore and exploit other characteristics of continuous production in microfluidic devices beyond mass transfer effects in order to develop novel processes. In addition, we stress the importance of adoption of microfluidics, and show which determinants are involved in this. Knowledge of these determinants is of utmost importance to reduce skepticism towards and stimulate the adoption of microfluidics by industry.

SUMMARY IN DUTCH

Microfluide of microvloeistofsystemen maken het mogelijk om zeer kleine vloeistofstromen te behandelen. Het voordeel van werken op deze schaal is dat de drijvende krachten voor massa- en warmtetransport hoog zijn. Het typische oppervlak per volume-eenheid in deze systemen is ook groot. Veel processen die te maken hebben met oppervlakken kunnen daar baat bij hebben. Vanwege de kleine volumes consumeren microvloeistofsystemen relatief weinig reagentia en dragen ze een lager risico bij systeemfalen dan processen op grotere schaal. Door middel van parallellisering kan het productievolume van deze systemen verhoogd worden met behoud van hun karakteristieke dimensies en dus voordelen. In totaal is het duidelijk dat er veel mogelijk is met deze systemen voor reacties en scheidingen.

Hoewel microtechnologie uitgebreid is bestudeerd voor bijvoorbeeld analytische toepassingen, staat het gebruik voor de productie van grotere volumes nog in de kinderschoenen. Dit promotieonderzoek omvatte het verkennen van deze processen voor biokatalyse en bio-scheidingen met behulp van microvloeistofsystemen. Het doel was om een beter begrip te krijgen van dergelijke processen op microschaal met het oog de productie van grotere hoeveelheden. Daarom zijn onderwerpen als parallellisering, membraanscheiding, biokatalyse, en dimensionering onderzocht. De resultaten zijn bedoeld voor gebruik bij verdere procesintensivering met behulp van microvloeistofsystemen.

Het parallelliseren van microvloeistofsystemen kan een methode zijn om snel informatie over processen te verkrijgen. Zo tonen we in Hoofdstuk 2 een geparallelliseerd systeem dat hiervoor bedoeld is. Hiervoor hebben we verschillende microcontactoren in een enkel systeem geïntegreerd om verschillende experimenten tegelijktijdig te kunnen uitvoeren. Het concept van deze parallellisering is gebaseerd op het ontkoppelen van de drukval en de verblijftijd in het systeem. We demonstreren dit door middel van een membraanscheiding op microschaal waardoor we met succes enkele

membraaneigenschappen konden vaststellen. Het gepresenteerde systeem gaf een drie keer hogere doorvoer in vergelijking met microvloeistofsystemen die uit een enkele contactor bestaan.

Scheidingsprocessen zoals chromatografie en nanofiltratie kunnen suikers met een laag molecuulgewicht scheiden uit oplossingen van oligosachariden. In Hoofdstuk 3 presenteren we een nieuw scheidingsconcept gebaseerd op massadiffusie. Verschillen tussen de diffusiesnelheden van de componenten leiden tot deze scheiding. Membranen, meer specifiek nanofiltratiemembranen, kunnen de betreffende scheiding verbeteren, hetgeen is gedemonstreerd door middel van een membraan-microsysteem voor de scheiding van de genoemde suikers. De resultaten geven aan dat het concept potentieel heeft. Met geoptimaliseerde microkanaal- en membraandimensies kan het gepresenteerde concept naar verwachting concurreren met momenteel beschikbare scheidingsmethoden.

Kleine diffusieafstanden, en daarom dunnere membranen, kunnen de benodigde diffusietijden significant reduceren voor diffusie-gebaseerde processen, zoals de massa-diffusiescheiding van Hoofdstuk 3. In Hoofdstuk 4 is een microcontactor gebruikt om vloeistofstromen met elkaar in contact te brengen via een zeer dun membraan. Het concept blijkt waardevol te zijn voor diffusie gebaseerde verrijking en fractionering. Deze technologie is toepasbaar op elk vloeistofmengsel, onafhankelijk van de gerelateerde absolute diffusiviteiten of concentraties, zolang er maar een zeker verschil in diffusiesnelheden is.

Snel massatransport en een lage consumptie van reagentia hebben de enzym-microreactor populair gemaakt. In Hoofdstuk 5 hebben we een dergelijke microreactor gebruikt om de effecten van diffusie op de enzymactiviteit te bestuderen. Het bleek dat de kinetische parameters in het Michaelis-Menten model op microschaal nauwelijks afweken van de waarden gevonden op grotere schaal. Bij verblijftijden van enkele seconden belemmeren diffusie-effecten de reactie en reduceren daarmee de conversie per volume microreactor. De kritische verblijftijd waarbij deze limitering een rol gaat spelen is afhankelijk van het kwadraat van de

kanaalbreedte, van de enzymconcentratie, en neemt af als functie van de substraatconcentratie. Met deze effecten rekening dient gehouden te worden om de enzym-microreactor efficiënt te kunnen gebruiken.

Veel variabelen, waaronder de enzymeigenschappen, de reactie-omstandigheden, en de dimensies van de microreactor bepalen de mate waarin massatransport de reactiesnelheid en productiviteit kan beïnvloeden. Het gebruik van microkanalen kan inderdaad de tijd die nodig is voor massatransport reduceren. Hoofdstuk 6 toont de correlaties tussen deze variabelen voor enzym-microreactors die voldoen aan de Michaelis-Menten kinetiek. Deze correlaties geven richtlijnen voor een correct ontwerp van enzymatische microreactors dat de snelheid van massatransport afstemt op de reactiesnelheid, om een optimale productie te kunnen combineren met een zo klein mogelijk systeemvolume. Deze richtlijnen zijn algemeen toepasbaar voor enzymatische microreactors.

Microtechnologie maakt gebruik van de andere verhoudingen tussen verschijnselen op microschaal. Dit promotieonderzoek laat zien dat microtechnologie veel voordelen kan bieden, mits de systemen goed worden gedimensioneerd. De discussie in Hoofdstuk 7 vat de conclusies uit het proefschrift samen en biedt een reflectie op het werk. Om nieuwe en innovatieve processen te kunnen ontwerpen is het belangrijk om massatransport en andere karakteristieken, zoals reactiesnelheden geïntegreerd te beschouwen. Daarnaast is het belangrijk is de industrie bereid is om een dergelijke nieuwe technologie te omarmen. Daarvoor is een inventarisatie gemaakt van de factoren die hierbij een rol spelen. Goede kennis daarvan is erg belangrijk voor de uiteindelijke implementatie van microtechnologie voor preparatieve doeleinden.

PUBLICATIONS

Kolfschoten RC, Janssen AEM, Boom RM. 2007. Towards high-throughput experimentation in a membrane microreactor. The 7th Netherlands Process Technology Symposium, Veldhoven.

Kolfschoten RC, Janssen AEM, Boom RM. 2009. High-throughput separation in a microfluidic device with multiple contacting regions. New Biotechnology 25(Supplement 1):S164-S164.

Kolfschoten RC, Janssen AEM, Boom RM. 2010. Mass diffusion based separation of sugars in a microfluidic contactor with nanofiltration membranes. Submitted for publication.

Kolfschoten RC, Janssen AEM, Boom RM. Diffusion-based membrane separation in a microfluidic contactor. Will be submitted for publication.

Kolfschoten RC, Swarts JW, Janssen AEM, Boom RM. 2010. Guidelines for optimal design of enzyme microreactors. Submitted for publication.

Kolfschoten RC, Janssen AEM, Boom RM. 2010. Design of enzyme microreactors for sustainable production. Proceedings of Innovation for Sustainable Production, Brugge.

Swarts JW, Kolfschoten RC, Jansen MCAA, Janssen AEM, Boom RM. 2010. Effect of diffusion on enzyme activity in a microreactor. Chemical Engineering Journal 162(1):301-306.

Zhang Z, Boyle PM, Kolfschoten RC, Boccazzi P, Sinskey AJ, Jensen KF. 2006. Evaporation-driven pH and glucose feeding control in a polymer-based, instrumented micro bioreactor for bioprocess developments. Proceedings of Micro Total Analysis Systems, Tokyo.

The research described in this thesis was carried out within the Dutch research initiative “Process on a Chip” (PoaC), part of the framework Advanced Chemical Technologies for Sustainability (ACTS), and financially supported by the Dutch organization for scientific research (NWO).

The research described in Chapter 5 was co-financed by the EU program INTERREG IIIA of the EU-region Rijn-Waal and by the ministries of Economic Affairs of the Netherlands and Nordrhein-Westfalen.

Financial support from Wageningen University for printing this thesis is gratefully acknowledged.